Low Level Task Execution, Programming and Control for Jigs, Fixtures and Equipment

By

Erlank Slabbert

Submitted in fulfilment of the academic requirements for Masters of Science in Mechanical Engineering, College of Agriculture, Engineering and Science,
University of KwaZulu-Natal
Durban
South Africa

Supervisor: Prof Glen Bright

Co-Supervisor: Dr Anthony Walker

October 2019

Preface

The research contained in this thesis was completed by the candidate while based in the Discipline of Mechanical Engineering of the College of Agriculture, Engineering and Science, University of KwaZulu-Natal, Howard College, South Africa. The research was financially supported by the Blue Sky Research Grant.

The contents of this work have not been submitted in any form to another university, except where the work of others is acknowledged in the text, the results reported are due to investigations by the candidate.

Signed: Prof Glen Bright

Date: 23rd Octoberr 2019

Declaration 1: Plagiarism

I Erlank Slabbert declare that,

i. The research reported in this dissertation/thesis, except where otherwise indicated, is my original work.
ii. This dissertation/thesis has not been submitted for any degree or examination at any other university.
iii. This dissertation/thesis does not contain other persons' data, pictures, graphs or other information, unless otherwise specifically acknowledged as being sourced from other persons.
iv. This dissertation/thesis does not contain other persons' writing, unless specifically acknowledged as being sourced from other researchers. Where other written sources have been quoted, then:
    a. their words have been re-written but the general information attributed to them has been referenced;
    b. Where their exact words have been used, their writing has been placed inside quotation marks, and referenced.
v. Where I have reproduced a publication of which I am a co-author or editor, I have indicated in detail which part of the publication was actually written by myself alone and have fully referenced such publications.
vi. This dissertation/thesis does not contain text, graphics or tables copied and pasted form the Internet, unless specifically acknowledged, and the source being in the dissertation/thesis and in the Reference sections.

Signed:

……

Mr Erlank Slabbert

As the Candidate's Supervisor I agree/do not agree to the submission of this thesis.

Signed:

…….

Prof Glen Bright

Declaration 2: Publications

1 Slabbert E.*, Bright G., Walker A., “Low Level Task Execution, Programing and Control for Jigs, Fixtures and Equipment” Coma ’16 International Conference on Competitive Manufacturing, Stellenbosch, 2016.

2 Slabbert E.*, Bright G., Walker A., “Modal Analysis of Machining Processess on an Automated Flexible Fixture for a Reconfigurable Manufacturing System” International Conference on Mechatronics and machine Vision in Practice, Aukland, 2017.

3 Slabbert E.*, Bright G., Walker A., “Modal response of a symmetric Workpiece for control System Development of an Automated Flexible Fixture in a Flexible Manufacturing System” International Conference on Control and Automation, Anchorage, 2018.

*Primary author

Signed:

……...

Mr Erlank Slabbert

Abstract

Modelling of the vibrational characteristics of a symmetric and asymmetric part for differing fixturing setups was performed in SolidWorks. Aluminium was selected for the part material. Mesh independency was reached at a mesh size of 1.5 mm and 370000 cells. The results revealed a strong correlation between fixturing setup and vibrational response, attributed to the corresponding stiffness of each fixture setup.

The two simulated parts were CNC machined from aluminium and used in experimental testing to validate the simulation results. The experimental testing was performed using an NI DAQ, 25000HZ accelerometer and NI impact hammer. A strict methodology was used to ensure consistent and comparable results. The testing results showed a high amount of dampening in the system, the trends however were still apparent and corroborated the simulation results.

A methodology for fixture setup optimization and operation order optimization was developed based on the natural frequency results.

Aknowledgements

The author would like to thank his supervisors, Prof Glen Bright and Dr Anthony Walker, for their ongoing support and guidance. Without their direction and guidance this research would not have been possible. Thanks must also be given to the Blue-Sky research grant for funding this research. Lastly, the author would like to acknowledge his parents, Andre and Vanessa Slabbert, for their ongoing support during my studies at the university of Kwa-Zulu natal, without them this work would not have been possible.

Table of Contents

List of Tables

List of Figures

Nomenclature

symbols	Description	Units
a_e	Radial depth of cut	mm
a_p	Axial depth of cut	mm
A	Area	m
b	Chip width	mm
c	Damping co-efficient	Kg/s^{-1}
C	Substitution	
f	Chatter frequency	Hz
f_t	Tooth frequency	Hz
f_x	x-direction force component	N
f_y	y-direction force component	N
f_z	z-direction force component	N
k	Cutting force co-efficient	
n	Lobe number	
N	Spindle speed	s^{-1}
r	Cutter radius	m
r_b	Dimensionless Ratio between b and b_{min}	
R	Tool path radius	m

Greek	Description	Units
ζ	Damping co-efficient ratio	
ς	Ratio of the damping co-eff. to the critical damping co-eff.	
ϕ	Radial immersion angle	$Deg.$

Subscripts	Description
A	Axial
ex	Exit
min	Minimum
R	Radial
st	Start
T	Tangential

Abbreviations	Description
ADOC	Axial depth of cut
ABS	Acrylonitrile butadiene styrene
AFFS	Automated flexible fixturing system
CCT	Conservative congruence transform
CAD	Computer aided drawing
CNC	Computer controlled cutting
COM	Centre of mass
COV	Centre of volume
CSM	Clamping surface mount
FEA	Finite element analysis
FEM	Finite element method
FMS	Flexible manufacturing system
IR	Industrial robots
LCA	Load cell clamp assembly
NIDAQ	National instruments data acquisition
MIF	Machining input frequency
RDOC	Radial depth of cut
RPM	Revolutions per minute
SLD	Stability lobe diagram

Chapter 1: Introduction

Product customization is becoming an increasing demand by modern consumers, with customers desiring products with more utilitarian, uniqueness and self-expressiveness value [1]. This customer demand for mass customization has been a driving force behind further developments of flexible manufacturing systems (FMS) [2] and reconfigurable manufacturing systems (RMS). In FMS the plant uses process flexibility to accommodate smaller production batches, whereas in RMS the plant changes its layout for each new product cycle [3]. Manufacturing technologies have a long way to go before mass customization is feasible. In order to make mass customization achievable, the manufacturing process must be made as efficient as possible, to reduce production costs such as time, human resource and material wastage. In current mass production, fixtures generally create the bottle neck in the production cycle [4] and are thus a large time-cost to production. The automated flexible fixture system (AFFS) was developed to reduce the time wastage caused by fixtures. The AFFS is a robotic reconfigurable fixture that can accommodate a large variety of part geometries and make change overs automatically. The AFFS allows for greater flexibility in a manufacturing environment for facilitating mass customization.

In machining, one of the greatest limiting factors is chatter. Chatter is an unwanted phenomenon involving escalating vibration during machining that leaves a poor surface finish. The freshly cut surface contains characteristic wavy lines, resulting in poor precision and accuracy [5]. Current research for chatter prevention and control has been focused on cutting tool technologies, process dampening technologies and adjusting cutting parameters to achieve chatter-free machining. Research into the effect of fixturing on chatter has been minimal. The development of the AFFS has provided a platform for investigating the effect that fixturing has on the vibrational characteristics of the machining system and thus the formation of chatter.

1.1 Dissertation outline

An introduction to the research is put forward in chapter 1. This includes an overview of the factories of the future research and the current state of modern manufacturing with relation to FMS. This chapter also defines the AFFS and its role in the factories of the future research. Finally, the aim and objectives of the research are defined, and the design methodology is discussed.

Chapter 2 outlines the literature reviewed for this research. Chatter and its causes in end milling are discussed, followed by a machining model. A history of modelling chatter, analytically and experimentally, is provided, followed by an overview of stability lobe diagrams. The chapter concludes with a consideration of alternative chatter control methods

to adjusting cutting conditions and stiffening cutting tools, and research involving Finite Element Method (FEM) simulations of the harmonics of machining systems.

Chapter 3 introduces a symmetrical and asymmetrical part for the modal response simulations. Fixturing set-ups are defined for both parts. Simulation parameters for mesh, fixturing and material are outlined. The methodology and procedure followed for the simulation of the modal response is presented.

Chapter 4 presents the simulated modal response data. Mesh Independence is discussed, followed by the modal displacement diagrams. The simulation data is presented in both table and graph form to highlight the various trends in the relationship between fixturing, part geometry and modal response. The implications of the simulation data with reference to adjusting the fixturing for optimum frequency response is discussed.

Chapter 5 presents the physical testing of the modal response to validate the simulation findings. The chapter begins with an outline of the experimental setup, including the parts analysed, load cell assembly and the data acquisition hardware. The methodology and procedure used in testing is put forward. The results are presented in graph form, and the modal frequencies are extrapolated from the graphs. The causes of errors in the data capture and response of the system is discussed.

Chapter 6 discusses the implications of the experimental results and the trends revealed by the simulations in chapter 2. The relationship of deflection and centre of mass with the harmonic response trends are analysed. A methodology for fixture optimization, using expert systems, is proposed. The shortfalls of the AFF is examined, and improvements are suggested for future work. The AFFS contribution to industry 4.0 is discussed.

Chapter 7 provides a conclusion to the dissertation. The aims and objectives of the research are addressed, and the research results are outlined. Future work, consisting of improving the AFFS and measuring the vibration response during machining in both a chatter induced and chatter free environment, is proposed.

1.2 Overview of the Automated Flexible Fixture

This section introduces the AFFS, its basic features, and its role in the factories of the future research. A more detailed analysis of the AFFS is provided in chapter 2.

The AFFS consists of a gripper bed for locating the workpiece, and two 3-degree of freedom (DOF) pin matrix clamps. The Pin matrix clamps were designed to mould around the workpiece to facilitate a variety of workpiece geometries. The gripper bed, or 2-finger parallel gripper locator as labelled in figure 1.1, is mounted to a workpiece positioning mechanism that

provides two degrees of rotational freedom. The clamps are mounted to lead screw actuators that are driven by stepper motors. All the AFFS components are mounted to a single baseplate.

The full assembly of the AFFS is given in figure 1.1. The figure shows an isometric view of a CAD model of the AFFS, with labels of the main components. In the image the steppers motors are illustrated in black. The pin matrix clamp positioning assembly consists of one stepper motor controlling vertical actuation, one stepper motor providing breadth wise actuation, and two stepper motors controlling length wise actuation.

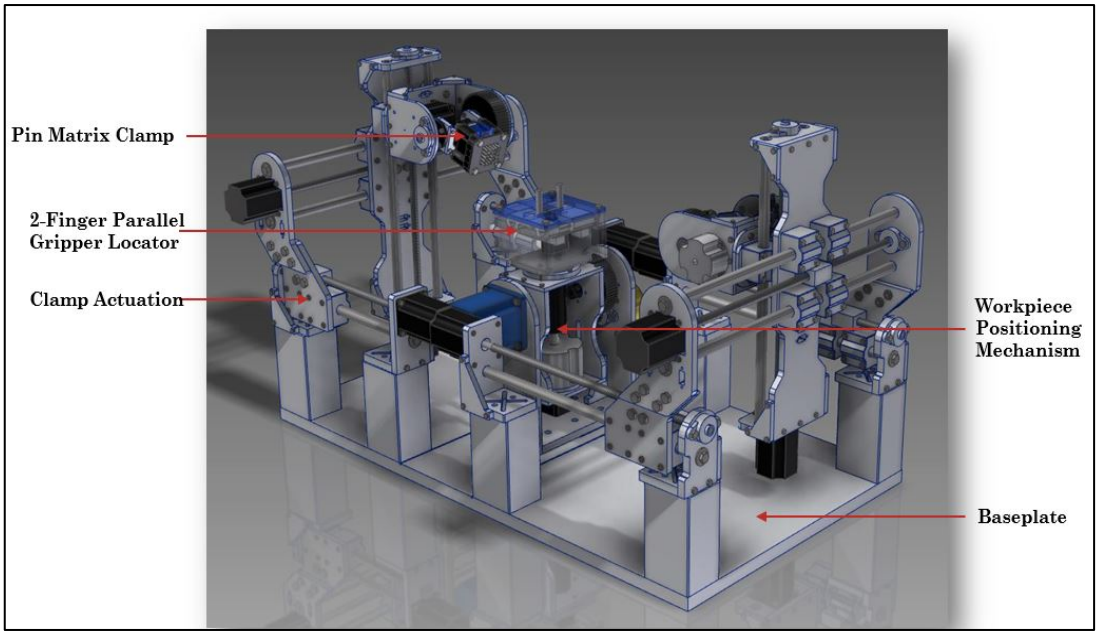

Figure 1.1 The Automated Flexible Fixturing System

The flexibility inherent in the design of the AFFS allows for a large variety of fixturing setups for a single part. The heterogeneity of fixture setups in the AFFS necessitates the selection of the optimum fixturing setup(s) for the part. The optimum fixture setup is the one that minimizes the time the part spends in the AFFS, setup time, machining time and the fixturing time. The setup time is the time it takes to remove a finished part from the AFFS and locate the new workpiece. The fixturing time is the time required to move the fixture into its final clamped position, including any repositioning of the fixture during the machining process. Machining time is dependent on the cutting parameters of the cutting machine. The set-up time is assumed constant. A fixturing setup that will allow for the shortest combination of fixturing and machining time can be defined as the optimum setup.

The fixturing setup may play a significant role in the vibrational response of the AFFS and thus affect chatter formation during machining. Thus, the fixture time as well as the machining time may be dependent on the fixturing setup.

1.3 Research Aim and Objectives

The aim of the research was to develop a methodology for chatter control based on fixture optimization. The research objectives were the following:

- Complete a literature review on vibration and the causes of chatter, as well as current work in chatter reduction.
- Conceptualize a theoretical part to be analysed
- Perform FEA simulations on the theoretical part to determine its harmonic response
- Analyse the FEA results to determine the relationship between fixturing and harmonic response, as well as part geometry and harmonic response
- Validate the simulation results through experimental testing of the part in the AFFS
- Develop a methodology for fixture setup optimization

In summary, the dissertation aimed to provide research into the merit of using fixturing as the means of improving the vibrational response of a fixture-part system, specifically in the context of the AFFS.

1.4 Research Contribution

The contribution of this research was a methodology for fixture setup generation and optimization based on the static harmonic response of the fixture-part system. The simulated and experimental results revealed the relationship between fixture setup and the resulting vibrational characteristics of the system. The literature review revealed that one of the causes of secondary chatter were the vibrations of the part being machined; thus, chatter can be suppressed by decreasing the static vibrations of the part-fixture system using the fixture setup generation mythology proposed by this research. The primary impact of this research is to make flexible fixturing systems more feasible in a reconfigurable manufacturing environment. The vibrational results were obtained through the simulation and experimentation of a novel part geometry that highlights the effects of symmetry and fixture position on vibration. An innovative solution to fixture setup generation is proposed, in the form of an expert system.

1.5 Chapter Summary

Chapter 1 introduced the AFFS as a technology developed to accommodate mass customisation. It defined the AFFS and its features, and introduced the proposal for chatter control using fixturing. It outlined the aims and objectives of the research, principally that of chatter reduction through optimizing fixture setup, and offered a solution to them in the form of an analysis of a control part in the AFFS. A summary and brief description of the chapters in this thesis was provided.

Chapter 2: Literature review

2.1 Chapter Introduction

Chapter 2 focuses on chatter and its causes. Investigates the vibrational phenomena in milling and their relationship to chatter. Causes of chatter in milling operations are discussed. The models predicting cutting forces in machining, and the conditions for stability as well as regenerative vibration, are investigated. Stability lobe diagrams, a result of both analytical models and experimental methods, are reviewed. In conclusion, current work in modelling the physical structures of the machine tool system are laid out.

2.2 Vibrations

The vibrations that occur in machining operations can be classified as one of three types; free vibration, forced vibration and self-excited vibration[6]. Free vibration is the natural harmonic vibration of a system, such as the vibration in a guitar string or tuning fork. shows. Figure 2.1 presents a model of a free vibration system. The dampening of the system (c) reduces the displacement of the vibration over time to zero.

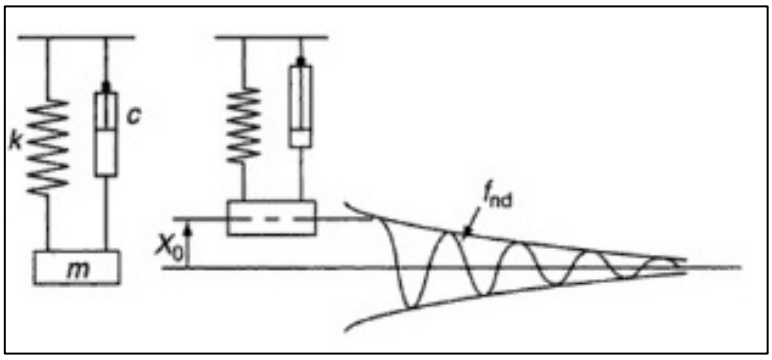

Figure 2.1 Free vibration model[7]

Forced vibrations occur when a periodic force acts on a system. The force results in a periodic vibration in the system, illustrated in figure 2.2 by a sin wave of amplitude A, proportional to the frequency of the applied force. An example of a forced vibration is the vibration in a rotating system due to an imbalance in the system, such as an unbalanced shaft. In machining the forced vibration is caused by the cutting tools and occurs at the frequency of spindle speed and tool teeth setup. The expression for this forced vibration is:

$$Frequency = \frac{RPM}{60} x\ (no.of\ teeth) \tag{2.1}$$

Thus, a three-tooth stack up running at 6000 rpm will cause forced vibrations at a frequency of 300 Hz.

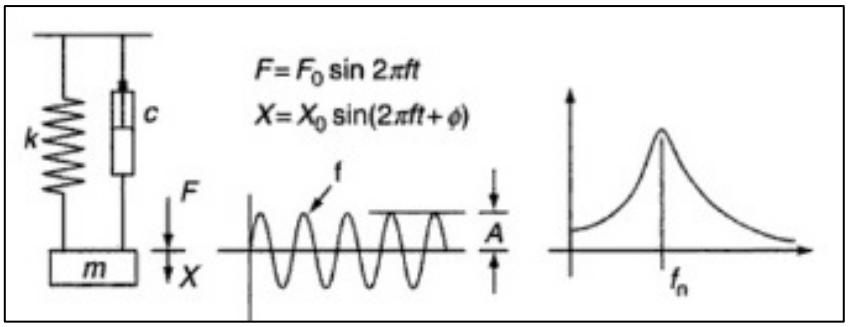

Figure 2.2 Forced vibration model[7]

Self-excited vibration, in machining, occurs when the forces in the system cause regenerative vibration due to the feedback of those forces in the system. An example of this type of vibration is the case where, during machining, the grooves from a previous tool path coincide with the next path of the cutting tool causing an escalating vibration in the system due to this feedback between the cut surface and cutting tool. This type of vibration is known as chatter. Figure 2.3 illustrates the feedback loop of regeneration and the resulting vibrational response.

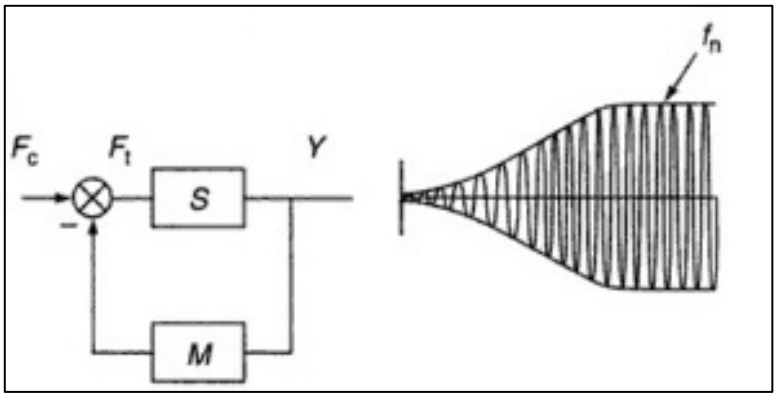

Figure 2.3 Self excited vibration model[7]

2.3 Chatter

Chatter in machining is a major limiting phenomenon for modern manufacturing. Chatter leads to poor surface finishes, decreased machining accuracy[8], accelerated wear in cutting tools, machines and bearings, and it limits production rates[7]. Chatter can occur in milling, turning, grinding and drilling operations. Chatter leads to inaccuracies in machining, excessive noise, higher energy consumption, poor surface finish, accelerated machine and tool wear and lower production rates (material removal rates). Thus, the methods of eliminating chatter from machining have been an important area of research in modern manufacturing.

Chatter is a resonant vibration phenomenon that causes distinct groove patterns in the machined surface of the workpiece[9]. It is identifiable both by the surface patterns and the loud distinct noise it produces[10]. It occurs during machining due to the vibration of the machine setup or workpiece. Figure 2.4 shows the machining marks on a workpiece for both

stable and unstable cutting conditions. The grooves in the lower machine paths is evidence of chatter.

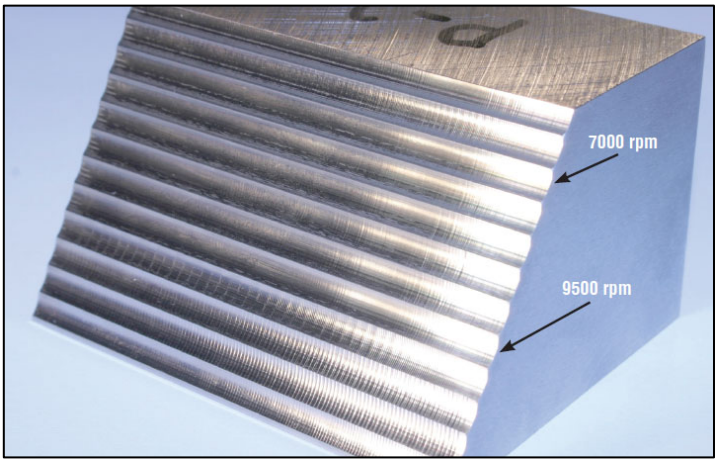

Figure 2.4 Chatter marks [9]

2.3.1 Causes of Chatter

There are two main modes of chatter, primary chatter and secondary chatter [11]. Primary chatter is the root cause of chatter, where the in initial waviness in the surface of the cutting piece is formed. Secondary chatter is the observable phenomenon of regenerative vibrations causes by the interaction of the cutting tool with the grooves caused by the primary chatter.

2.3.1.1 Primary Chatter

Primary chatter is a direct result of the chip formation process. One suggested origin of primary chatter is the effect of dry friction combined with intermittent contact between the cutting tool and workpiece[11]. As the cutting tool experiences variable shear stresses in the chip-formation process, the frictional forces on the cutting tool increase causing deflections that lead to regenerative vibrations. An investigation by Mohammad et al shows, through Finite Element Model (FEM) analysis, that heat generation in the cutting zone during the chip formation process can affect the occurrence of chatter[12]. A relationship between the width of cut with its corresponding thermal effects, and cutting stability was established through simulated results.

Mode coupling chatter falls under primary chatter as it occurs without any regeneration[13]. It occurs when the mass of the system vibrates at different phases and amplitudes in two degrees of freedom of the system[14]. Mode coupling chatter is prevalent in low stiffness systems, where low frequency vibrations occur.

2.3.1.2 Secondary Chatter

There are two types of secondary chatter that occur in machining due to self-excited vibrations; tool chatter and work piece chatter[9]. For tool chatter the cutting tool and machine harmonic vibration being transmitted to the workpiece causes the chatter. In workpiece chatter the workpiece harmonic response initiates the regenerative vibrations. This harmonic response occurs when the forced vibrations from the cutting tool equals the natural harmonic of the workpiece causing large displacements due to the cutting forces building the vibration. These large displacements of the workpiece cause the first uneven groove on the materials surface that starts the regenerative chatter process.

Klaver[15] from Okuma America states that an improperly secured part can cause chatter inducing vibrations. Kennametal[16] suggests that reworking a fixture to better hold the workpiece can reduce chatter.

2.4 Cutting Force Models

To further understand the formation of chatter and to build a foundation for analytical chatter prediction models, a model of the cutting forces and dynamics of a cutting tool in a milling operation is summarised in this section.

Cutting force models are the foundation to which machine chatter models are build. They also serve as a basis for the selection of machining parameters [17] such as feed rate and spindle speed [18]. This section serves to give insight into the forces and dynamics involved in machining processes. The models that proceed were developed by Wu et al [19] and are based on end milling .Wu's research focuses on two primary cutting force models for end milling: linear and circular.

2.4.1 Linear Milling Processes

Linear milling processes involve cutting along a straight-line path. The feed rate at every point along the tool path remains constant, and is equal to the feed rate *f*. Figure 2.5 illustrates the co-ordinate system for linear milling, where $O_w\ X_w\ Y_w\ Z_w$ is a fixed position on the workpiece, and $O_c\ X_c\ Y_c\ Z_c$ is fixed to the cutting tools centre and moves in the $X_w\ Y_w$ plane. Co-ordinate vector X_c is oriented towards the feed direction, and Y_c is perpendicular to X_c pointing away from the cut surface.

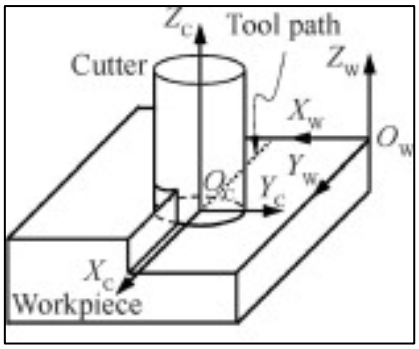

Figure 2.5 Linear milling process [19]

The angle that the cutting tool tooth makes with the edge of the workpiece is defined as ϕ. Figure 2.6 shows the cross-sectional view of the cutting tool. The radius of the cutter is r, and the feed direction or tool path is denoted by the arrow f.

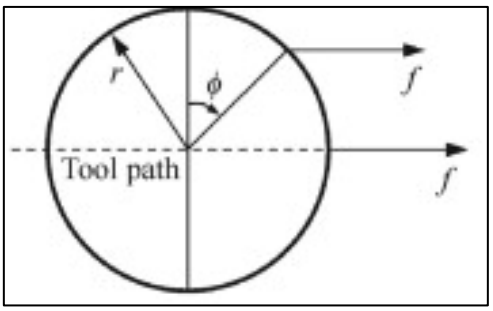

Figure 2.6 Linear milling cross-section[19]

2.4.2 Circular Milling Processes

Circular milling involves cutting along an arc of some radius *R*. Similar to the linear milling process. Figure 2.7 illustrates the co-ordinate system for circular milling, where $O_w\ X_w\ Y_w\ Z_w$ is a fixed position on the workpiece, and $O_c\ X_c\ Y_c\ Z_c$ is fixed to the cutting tools centre and moves in the $X_w\ Y_w$ plane. Co-ordinate vector X_c is oriented towards the instantaneous feed direction, and Y_c is positioned perpendicular to the tools path.

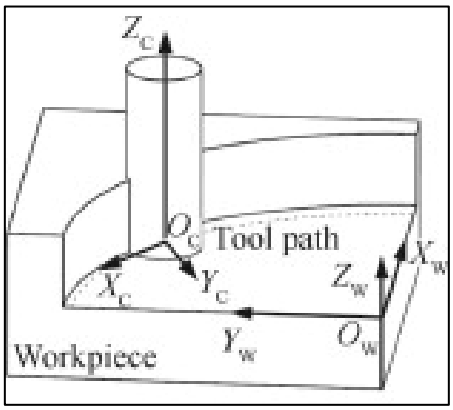

Figure 2.7 Circular milling process [19]

Figure 2.8 shows the cross-sectional view of the cutting tool. As in the linear model, the angle that the cutting tool tooth makes with the edge of the workpiece is defined as ϕ. The radius of the cutter is r, the radius of the tool path is R. The feed rates around the leading face of the cutter varies about its circumference relative to the radius of the tool path and the distance from the centroid of the cutter.

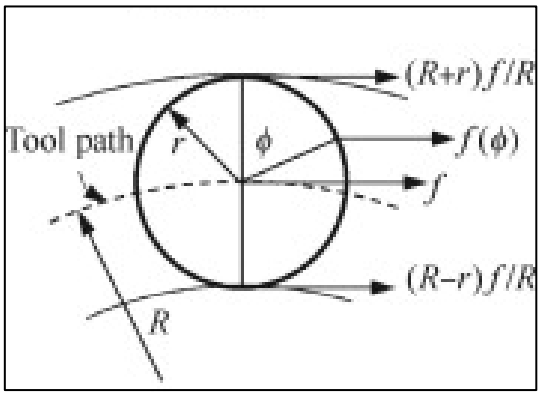

Figure 2.8 Circular milling cross-section[19]

The expressions for the cutting force coefficients developed by Wu et al made use of the mechanistic model given by Altintas and Lee [20] where, to calculate the total cutting force, the cutting flute was divided into a finite number of differential elements, and each elements force component integrated numerically.

This resulted in the following expressions for the force coefficients:

$$K_T = \left(\frac{2\pi}{f_z N A_1}\right)\left(\frac{C_3 Fx - (C_2 - C_1)Fy}{{C_3}^2 + (C_2 - C_1)^2}\right) \tag{2.2}$$

$$K_R = \varsigma\left(\frac{A_2((C_2 - C_1)Fx + C_3 Fy)}{{C_3}^2 + (C_2 - C_1)^2}\right) - \frac{A_3 Fz}{C_4} \tag{2.3}$$

$$K_R = \varsigma\left(\frac{A_2((C_2 - C_1)Fx + C_3 Fy)}{{C_3}^2 + (C_2 - C_1)^2}\right) - \frac{A_3 Fz}{C_4} \tag{2.4}$$

$$K_A = \varsigma\left(\frac{A_3((C_2 - C_1)Fx + C_3 Fy)}{{C_3}^2 + (C_2 - C_1)^2}\right) + \frac{A_2 Fz}{C_4} \tag{2.5}$$

$$Where\ \varsigma = \frac{2\pi}{f_z N\left({A_2}^2 + {A_3}^2\right)},$$

$$C_1 = \frac{1}{2}(\phi)\Big|_{\phi_{st}}^{\phi_{ex}},\ C_2 = \frac{1}{4}(\sin(2\phi)\Big|_{\phi_{st}}^{\phi_{ex}},\ C_3 = \frac{1}{4}(\cos(2\phi)\Big|_{\phi_{st}}^{\phi_{ex}},\ C_4 = (\cos(\phi)\Big|_{\phi_{st}}^{\phi_{ex}}$$

$$And\ A_1 = \int_{z_1}^{z_2} dz\ ,\ A_2 = \int_{z_1}^{z_2} \sin k(z)dz\ ,\ and\ A_3 = \int_{z_1}^{z_2} \cos k(z)dz$$

K_T , K_R , and K_A are the cutting force coefficients in the tangential (X_c), radial (Y_c) and axial (Z_c) directions, of the cutting tool, respectively. The angles ϕ_{ex} and ϕ_{st} are the exit and start radial immersion angles.

The force coefficients are constants in the machining process and thus, once they have been established, can be used to determine the cutting forces involved in machining operations of varying operational parameters. These equations for both linear and circular milling cutting forces were validated by Wu et al through experimental data.

2.4.3 Chatter prediction model for milling processes

Several analytical models have been proposed

One of the earliest models of chatter in orthogonal cutting is by Tlusty and Polacek [21] who derived stability laws identifying the chatter free axial depth of cut as a function of the structural dynamics of workpiece and cutting tool system. Tobias and Hanna [22] developed a mathematical theory for nonlinear chatter, providing an explanation for the stages at which chatter develops, by modelling the cutting tool structure as a single degree of freedom system with its corresponding nonlinear stiffness characteristics, and the cutting force being represented in terms of the chip thickness. Tobias and Shi later build upon this model showing that in cases where the cutting force characteristics are non-linear, stabile machining can be achieved through increasing the mean chip thickness of the cut [23]. Tlusty and Ismail used computer simulations to analyse chatter in milling, greatly improving accuracy over the then present methods of calculating stability [24]. A general mathematical model for predicting the limit of the axial depth of cut for chatter free milling was later presented by Minis et al [25]. In 1995 Altinas and Budak introduced a new analytical method for predicting stability lobes in milling [26]. They later improved upon this analytical model, removing the need for time domain simulations to determine chatter free axial and radial depths of cuts [27]. They then went on to develop an analytical method for predicting stability for variable pitch cutters, using cutting parameters such as cutting constants and number of teeth as inputs for the stability expression [28].

Some more relatively recent work on modelling chatter include work by Davies et al [29] on predicting stability for low radial immersion milling, Budaks' work on an analytical method

for increasing stability for milling cutters with non-constant pitch [30], and Budak and Tekelis research on analytical methods for optimizing chatter free end milling[31].

2.5 Stability Lobe Diagrams

The stability lobe diagram (SLD) is a tool used to determine parameters for stable cutting conditions. The most common SLD for milling operations relates the axial depth of cut (ADOC) to the spindle speed. Both axial and radial depth of cut (RDOC) are presented in figure 2.9. The ADOC is denoted by a_p and the RDOC by a_e.

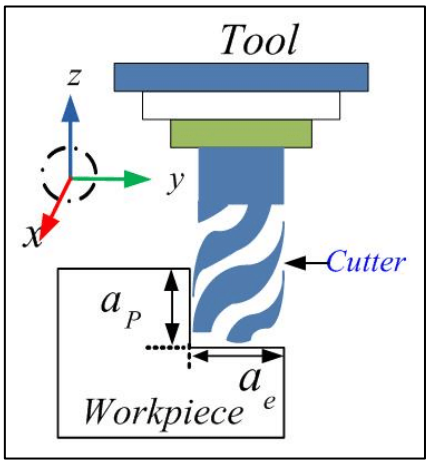

Figure 2.9 Axial and radial depth of cut [32]

The SLD's are characterised by the lobe shape of the curve, which designates the boundary between stable and unstable cutting conditions. The features of a SLD are illustrated in figure 2.10. The ADOC is plotted on the y-axis, and the spindle speed in rpm is plotted on the x-axis. The unstable region where chatter occurs is the area above the plotted curve. All combinations of spindle speed and axial depth that fall below the curve will result in stable chatter-free machining.

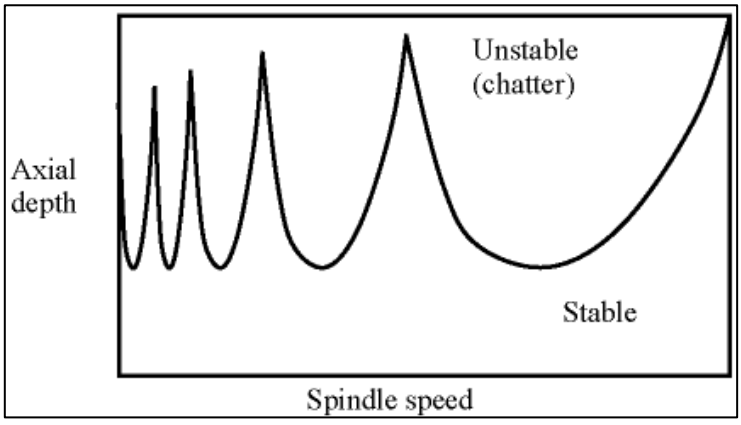

Figure 2.10 Stability lobe diagram [31]

Stability lobe diagrams are also affected by the RDOC, or radial immersion. A deeper radial cut will result in smaller stability zones compared with that of a shallower radial cut. Figure 2.11 illustrates the effect radial immersion has on the characteristic curve by comparing 3 scenarios for the same cutting tool system, showing the decrease in size of the stability zones with an increase in the percentage radial immersion.

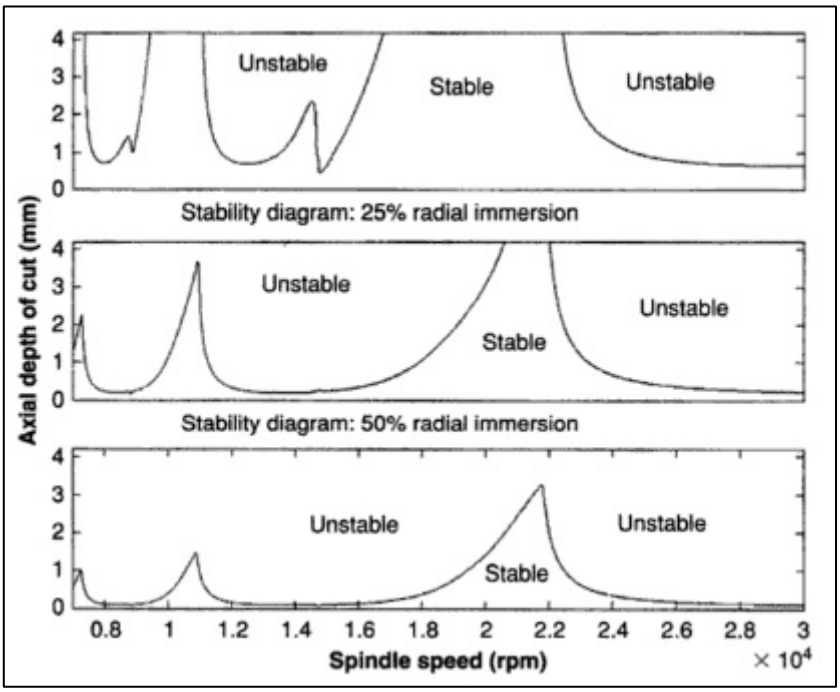

Figure 2.11 Stability lobe diagrams for differing axial depth of cut[7]

SLD's are created from the governing equations for machine chatter. These are formulated from the equations of vibration, chip width and regenerative vibration. The two equations needed for creating SLD's are equation 2.6 for the dimensionless chip width ratio (r_b), and equation 2.7 expressing the relationship between chatter frequency f, tooth frequency f_t and the lobe number n [33].

$$\frac{b}{b_{min}} = \frac{(1-r^2)^2 + (2\zeta r)^2}{-4\zeta(1+\zeta)(1-r^2)} = r_b \tag{2.6}$$

$$\frac{f}{f_t} = \frac{r}{r_t} = n + \frac{1}{2} + \frac{1}{\pi}\tan^{-1}\frac{-2\zeta r}{1-r^2} \tag{2.7}$$

In equations (2.6 and (2.7:

ζ = Ratio of the damping co-efficient to the critical damping co-efficient

c = Damping co-efficient

b = The desired chip width

b_{min} = The minimum chip width for stable cutting conditions

r_b = Dimensionless Ratio between b and b_{min}

n = Lobe number (Number of surface grooves between each consecutive cutter tooth)

From equations 2.6 and 2.7 we can find the chip width b, and the spindle speed N, using $b = b_{min}.r_b$ and $N = f_t.60/n.t$ These can be used to create a SLD, with chip width plotted on the y-axis against spindle speed on the x-axis. The proceeding graph, illustrated in figure 2.12, shows the curves plotted for chip width against spindle speed for different lobe numbers, with each lobe number plotted in a different colour. The upper border, highlighted in red, is where the lobes intersect, and are trimmed off for the final SLD, as all points above the upper border are unstable. The lower border, highlighted in green, demarcates the area of stable cutting conditions relevant to all lobe numbers.

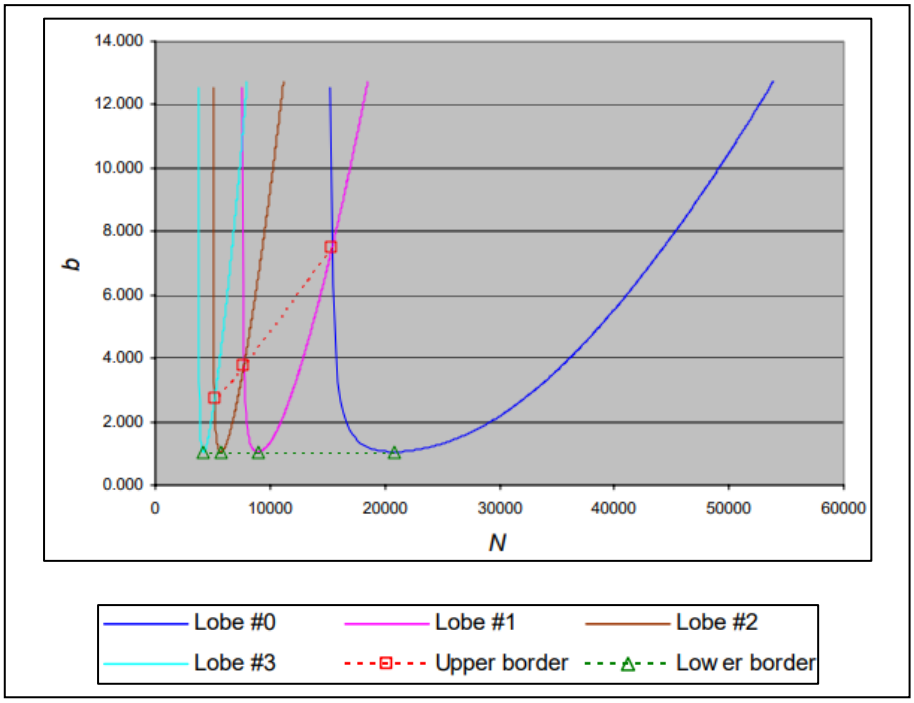

Figure 2.12 Stability Lobe Diagram of b plotted against N

The SLD can be divided into three differing regions of stability: Unconditionally unstable, conditionally stable, and unconditionally stable. The upper region above the upper border line is the area of unconditional instability. All points in this area between any two adjacent lobes are unstable. Conversely, all points below the lower border are unconditionally stable. The points that lie between the upper and lower borders are conditionally stable, where the points in this zone are stable below the lobe lines and unstable above them.

2.6 Modal Analysis for Harmonic Response of Systems

Modal analysis can be used to determine the harmonic response of a system. Modal analysis can be performed as a computer simulation using FEM analysis, calculated analytically, or derived from the physical testing of the vibrational response of the system. Analytical and simulation results must be validated through physical testing of the system, for example Wan et al uses operational modal analysis from chatter-free milling tests to validate the process damping of the system [34].

Several other researchers made use of FEM simulation in conjunction with experimental testing to determine the vibrational response of different milling systems for chatter vibration reduction. To reduce surface roughness in end milling, Gaidys et al [35] investigate superimposing high frequency vibrations onto the tool lead during machining. Their FEM model of the cutting tool is adjusted until the model parameters generate results consistent with the experimental findings. A study in FEM by Gaikwad [36] is used to validate analytical models developed for end mills for both static and dynamic response. The static analysis yields the tool deflection, while the mode shapes are determined by the dynamic analysis. Research by Uhlmann [37] used measurements collected during micro-milling to develop an FEM simulation of the loaded micro end mill, which in turn was used to create an innovative tool design. A methodology for simulating the cutting process in flat end milling was developed by Ozel and Altan [38], where chip flow, cutting forces, tool stresses and temperatures were obtained using finite element analysis (FEA) with acceptable accuracy in comparison to the dry machining experiments performed.

2.7 Alternative Methods for Chatter Control

Adjusting factors other than cutting parameters for chatter control has been researched for several types of machining operations, in an effort to improve machining efficiency without sacrificing cutting speeds. Several researchers have used transient stiffness designs to adjust the dampening properties of the machining system. A two-link robotic arm design was developed by Abdullah et al, whereby the joint stiffness is varied in synchronization with the spindle speed to control chatter[39]. Guo et al found that in a robotic boring process the robot itself caused the forced vibrations in the system initiating chatter. A dampening pressure foot was used to dampen the vibrations of the robot and control chatter[40].

2.8 Industrial Robots and Chatter Reduction

Machining robots is a technology aimed at improving the flexibility of a manufacturing environment due to their kinematic abilities and relative low cost compared to traditional CNC machines. Machining robots also offer the advantage of increased working area and allowed

workpiece geometry [41] over CNC milling machines. For robotic milling systems however, the stiffness of the robot is highly posture dependant [42] and impacts the accuracy of the machining process. The predisposed low stiffness of the robots [43] puts them at risk of high levels of vibration [44], making them susceptible to poor dimensional accuracy and chatter occurrence. The proceeding researchers developed strategies to improve and optimize industrial robots (IRs) performance in machining operations.

Lejun et al proposed a conservative congruence transform (CCT) stiffness model for a robotic milling system to avoid the occurrence of chatter [14]. Their stiffness model adjusted the robot tool path, based on its stiffness properties, to ensure that the cutting conditions remained stable. Vosniakos and Matsas improved upon the stiffness a robotic milling system though placement optimisation, using genetic algorithms, of the robot itself [45]. By selecting the correct initial position of the robot, a reduction in its range of necessary joint torques, to perform the machining operation, was achieved. Similarly to Vosinakos, Guo et al developed a model to increase the stiffness of a robot for machining applications [46]. They achieved this through maximizing a performance index based on robot posture stiffness. Xiong et al similarly used performance indexes to optimize posture of a 5-axis milling robot [47].Lin et al combined these two principles in their research by optimizing the posture of a machining robot and then extrapolating from this the optimum initial placement of the workpiece [42].

2.9 Chapter Summary

Chapter 2 presented information on the modes of chatter formation. It was found that chatter is generated through either the deflection in the tool due to cutting conditions, or the harmonic vibrations of the tool or workpiece. A machining model and stability lobe model was introduced, as well as the research on the development of analytical models for chatter prediction. The chapter concludes with a summary of the research done in harmonic response FEA simulations for end milling, and work performed in chatter reduction by using parameters other than cutting tool technologies and machining conditions to achieve stability.

Chapter 3: Modal Response Simulations

3.1 Chapter Introduction

This chapter details the simulation methodology used to determine the characteristic response of the system to various fixturing scenarios. The parts that were used in the harmonics testing are introduced, as well as the fixturing positions chosen for analysis. The simulation aims, objectives and procedure are laid out.

3.2 Simulation Aims and Objectives

The aim of the simulations was to determine the natural frequencies for a theoretical part under fixturing constraints, highlighting the effects fixturing and material removal have on the natural frequency of a part. The objectives of the simulations were the following:

- Select suitable part for simulation
- Determine fixture setups for part
- Achieve mesh independence in modal simulations

3.3 Parts for Modal Simulation

The selection of suitable parts for testing was a fundamental aspect of the research. The type of part chosen would largely determine the outcome of the testing results. Thus, the methodology of selecting parts for the simulations and experimental testing focused on keeping the research tractable and bounded

3.3.1 Part Geometry

The aim of the simulation is directly related to the part to be simulated, and can be split into two aspects:

- The role that part geometry plays on natural frequency
- The effect of fixturing position on the natural frequency on a part with a specific geometry

The parts to be used in the simulations need to have sufficient geometric variety to facilitate investigating the effect of the geometry on natural frequency, as well as the order of material removal. The parts geometry also needed to provide sufficient area for fixturing as well as allowing for a variety of unique fixturing positions. The following are constraints related to these requirements as well as the AFFS geometry:

- Parts must fit within the surface area of the fixture bed, to maximize the rigidity of the fixturing setups

- Part geometry must allow space for the locator pin holes
- The side surfaces of the part are reserved for fixturing, with machining on the top surface only
- Parts will be machined from billet material, to give higher resolution to the effects of material removal

Billet shapes considered for the part were those of the rectangular, square and cylindrical part family. The rectangular billet shape was chosen as it would allow 'flat' fixture surfaces to be used, and simplify the selection of fixturing setups. A rectangular billet better facilitates asymmetric features compared to square and cylindrical billets. It also provides more unique fixturing possibilities.

3.3.1.1 Part 1

Part 1 is a rectangular part with symmetric features machined on its upper surface at right angles to the plane of the upper surface. The machined features consist of two rectangular countersunk bores with filets on the corners, and four holes cut around the centre bores, shown in figure 3.1. The two central bores represent the bulk of the material removal, compared to the four circumferential holes.

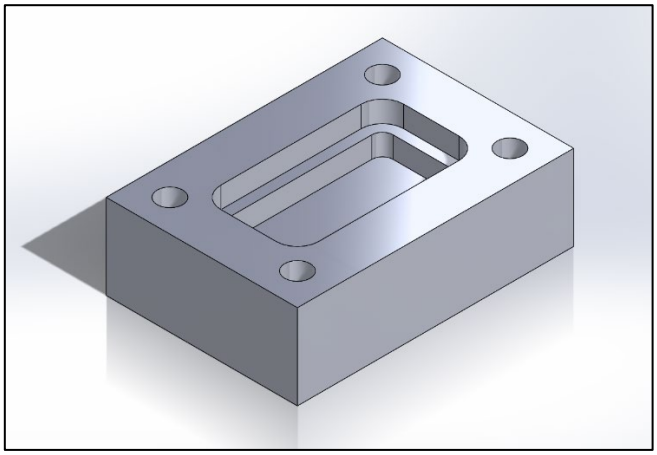

Figure 3.1 Part 1

The stages of machining for part 1 follow a natural progression from the billet to the finished part, seen in figure 3.2.The stages in machining will be referred to as operations 0 through 6, labelled in the figure as (a) through (g) respectively. Operation 0 is the billet, operations 1 and 2 are the counter sunk bores, and operations 3 to 6 are the circumferential holes.

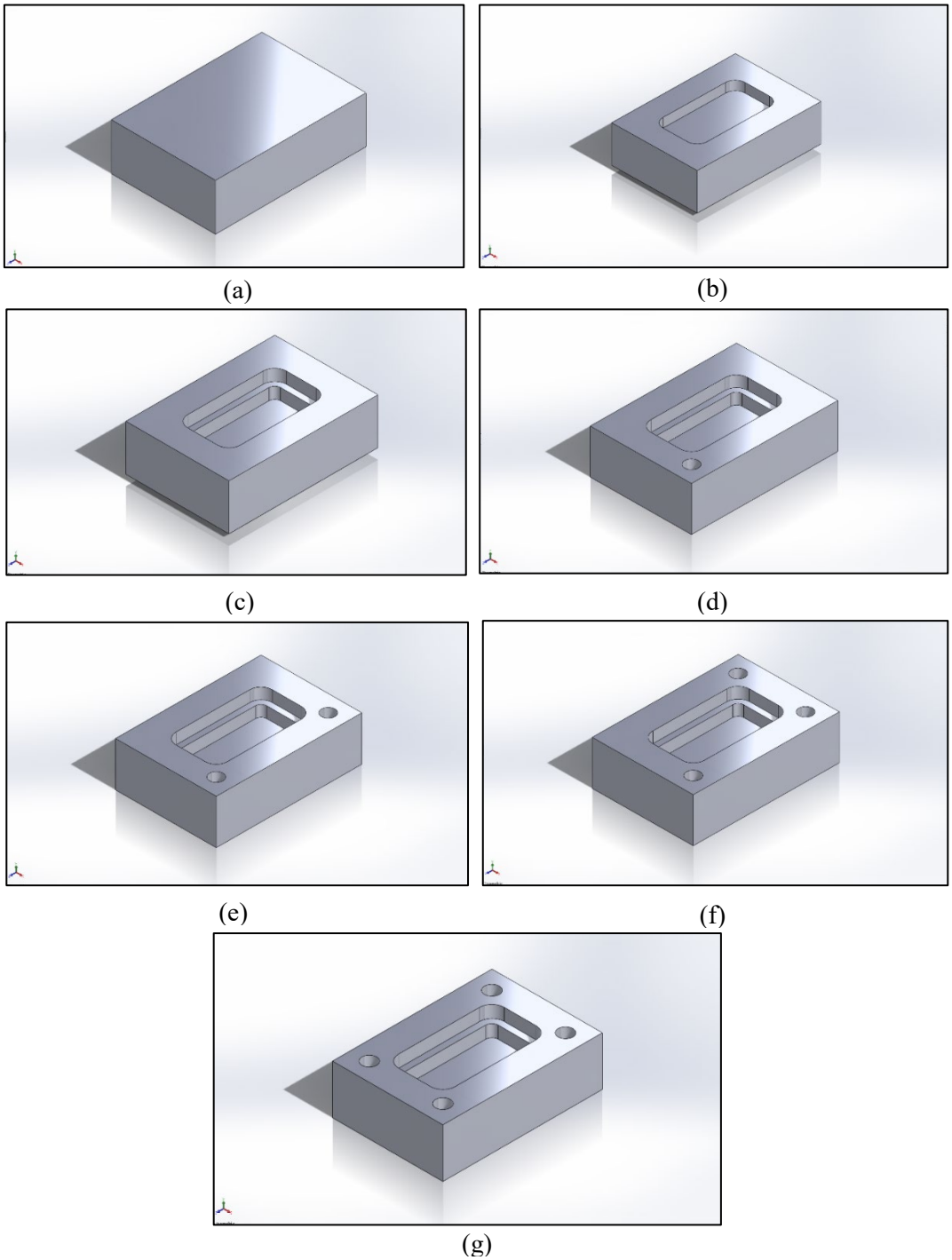

Figure 3.2 Operations 0 to 6 for Part 1

3.3.1.2 Part 2

Part 2 is cut from the same billet size as part 1. The geometric features of part two are also the same as part 1, except that their positioning has been changed to create asymmetry about the two horizontal axis. The features consist of two counter sunk bores in one corner of the billet, with three holes cut around the circumference of the bores, seen in figure 3.3. The asymmetric nature of part 2 is vital in determining the effect that moving a geometric feature has on the natural frequency of the system. The natural frequency response of part 1 will be used for comparison with part 2.

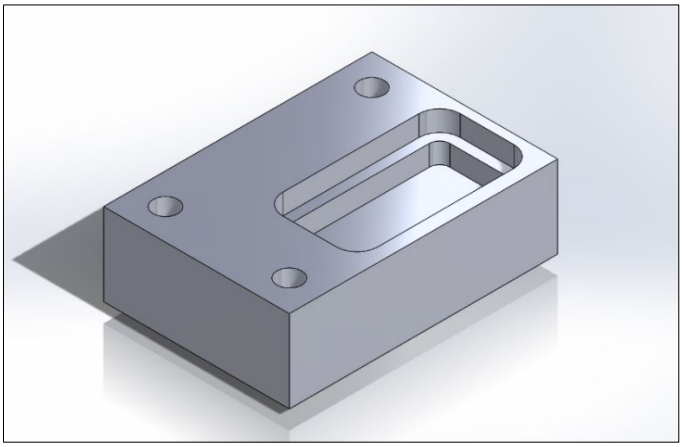

Figure 3.3 Part 2

The stages of machining for part 2 follow a natural progression from the billet to the finished part, seen in figure 3.4. The stages in machining will be referred to as operations 0 through 5, labelled in the figure as (a) through (f) respectively. Operation 0 is the billet, operations 1 and 2 are the counter sunk bores, and operations 3 to 6 are the circumferential holes.

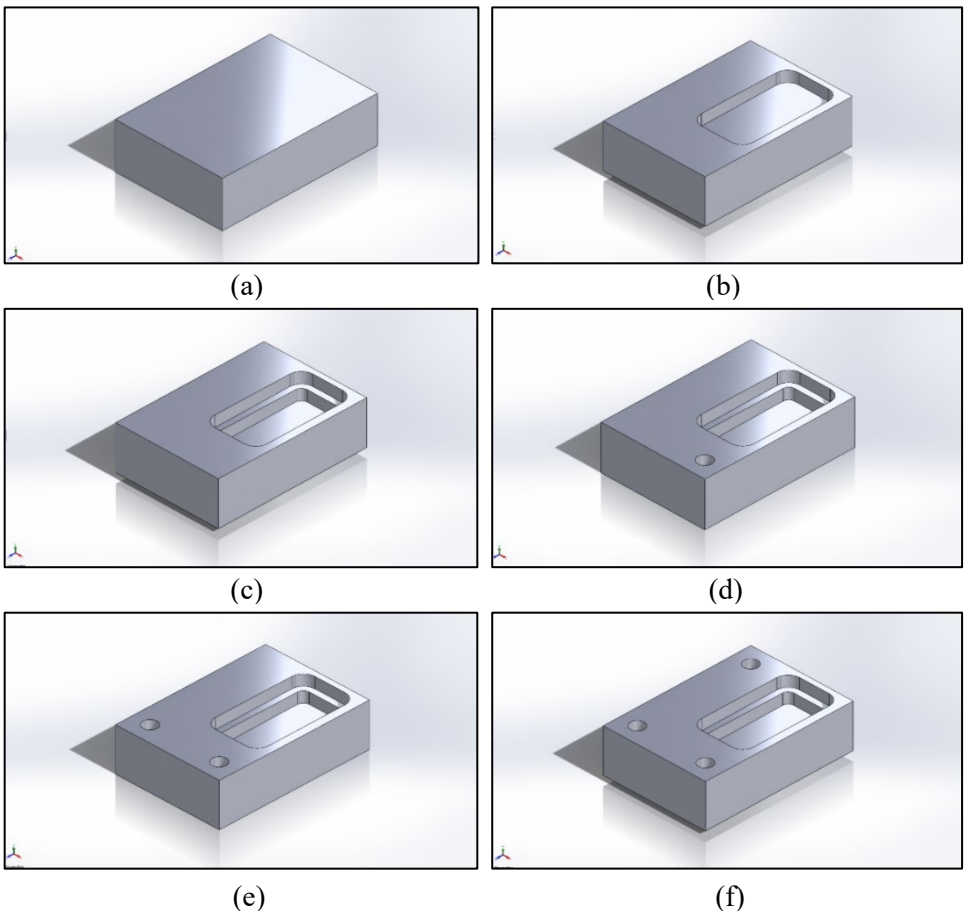

Figure 3.4 Operations 0 to 5 for Part 2

3.3.2 Part Material

The effect of material choice on the natural frequency was not an objective of this research, although it is known that the mechanical properties of materials influence free vibration and modal shape [48]. The material chosen was aluminium, based on its availability to the Author. The aluminium alloy used in the simulations and experiments was Aluminium 6082 with a Young Modulus of 71 GPa, Ultimate Tensile Strength of 330 MPa and a Yield Strength of 280 MPa.

3.4 The Automated Flexible Fixturing System

The anatomy of the AFFS was the first constraint on part size as well as fixturing positions. The aim of the AFFS was to prove the concept of a reconfigurable robotic fixture, though not necessarily to create a final product. This fact combined with budget constraints resulted in many of the components being built using the cheapest materials possible including fabrication in plastic using 3-d printing. This resulted in a working conceptual fixture with several rigidity flaws. The rigidity of the AFFS effected the experimental testing results and is discussed in detail in chapter 4.

Figure 3.5 illustrates a CAD model of the final assembly of the AFFS. The AFFS consisted of the following main components: The base plate, clamping arms tilting mechanism, pin matrix clamp, locator bed, stepper motors, electromagnetic brakes, lead screws, guide arms. The locator bed and the clamping arms actuation system is mounted to the base plate. The clamping arm actuation is achieved through a lead screw actuation system driven by stepper motors, with guide arms to add rigidity.

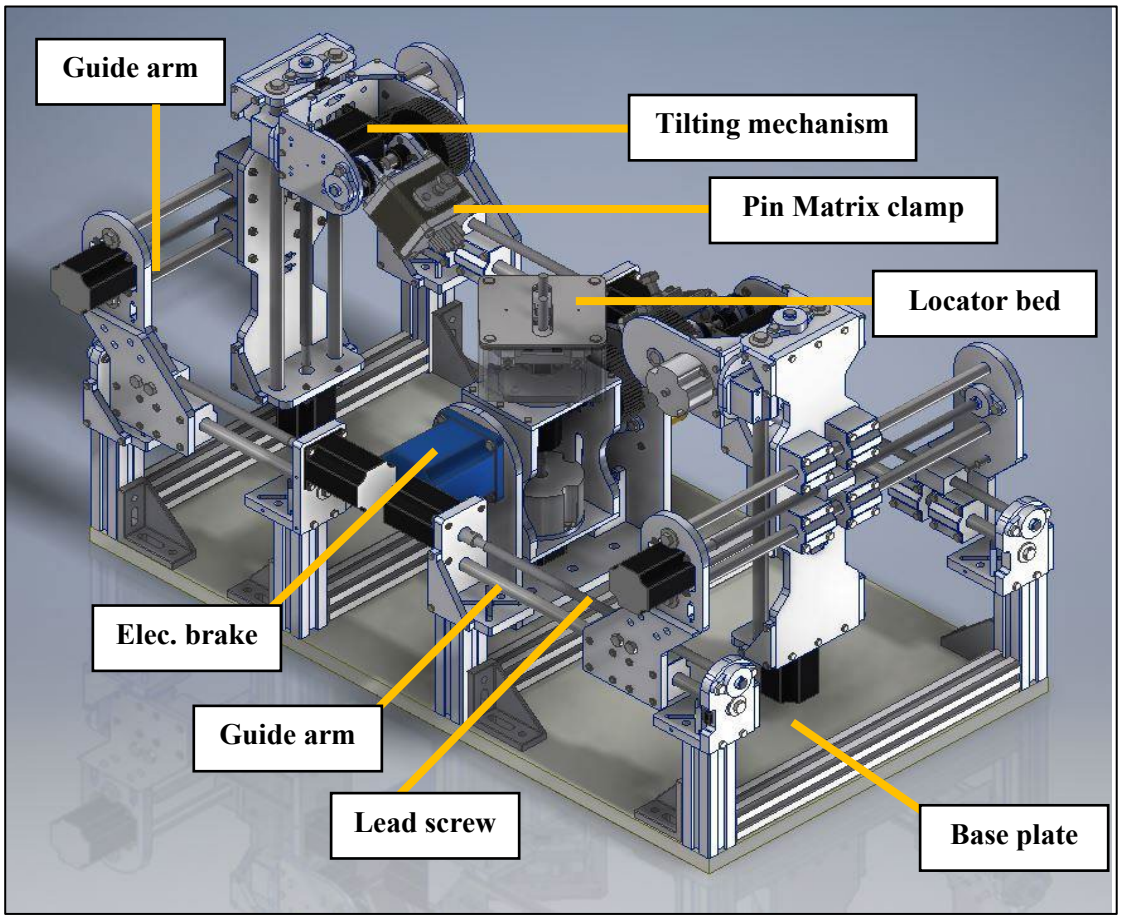

Figure 3.5 CAD model of the Automated Flexible Fixture System components with components labelled

The X-Y plane, illustrated in figure 3.6, is the horizontal plane parallel to the ground. The z axis is the vertical axis, perpendicular to the ground. The positioning of the co-ordinate system relative to the components of the AFFS will be used as reference for the other figures illustrating individual components and assemblies.

The clamping arms are constrained to move linearly along the X, Y and Z axis. The length of the x, y and z travel of the arms is 250 mm, 200 mm and 250 mm respectively, illustrated in figure 3.6. The distance from the bed to the upper most clamping arm position along the Z axis is 150 mm. The distance along the x axis between the clamping surfaces of the two arms is 170 mm. Thus, the AFFS can facilitate parts smaller than the $170x250x100$ cubic millimetres of volume between the fixture surfaces.

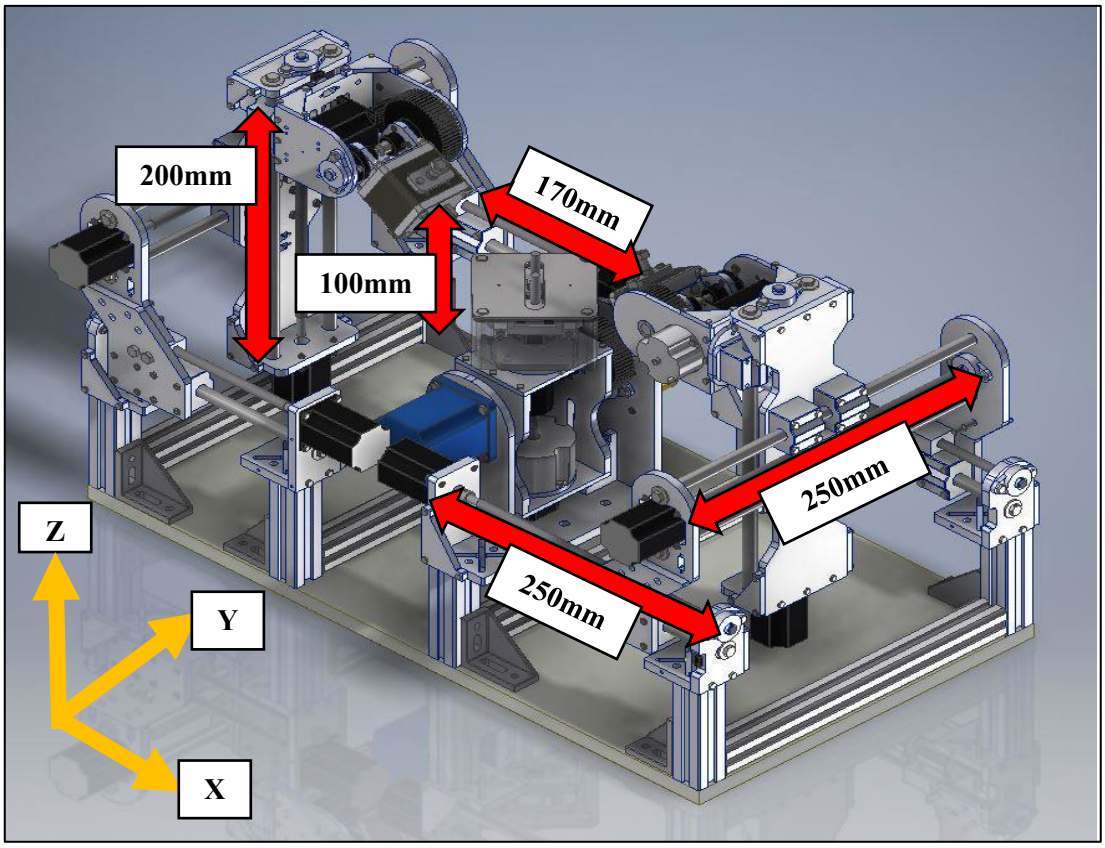

Figure 3.6 CAD model of the Flexible Fixturing System with co-ordinate system and dimensions

3.4.1 Locator Bed or 2-Finger Parallel Gripper

The purpose of the locator bed is to provide a platform for the part to rest on, as well as locating the part to a known position. Figure 3.7 shows the bed and its locating pins. The locator bed is a two-finger parallel gripper, consisting of two locating pins that actuate linearly, moving towards or away from each other. The locating pins have a variable gap size of 14 – 38 mm. The linear motion allows the locator to accommodate workpieces with varying feature gap sizes and locations. The workpieces are required to have pre-machined 2-point parallel

features for the location process. The pins exert a gripping force on the part to fix its location while the clamping arms move into position. The grip from the pins also holds the part in place during rotation of the bed. The locator beds internal parts were made mostly from 3-d printed parts in acrylonitrile butadiene styrene (ABS) plastic. The actuator is driven by 2 continuous stepper motors, one for each pin. The beds external structure is a stock ABS enclosure, with a fabricated aluminium sheet to strengthen and add rigidity to the top surface.

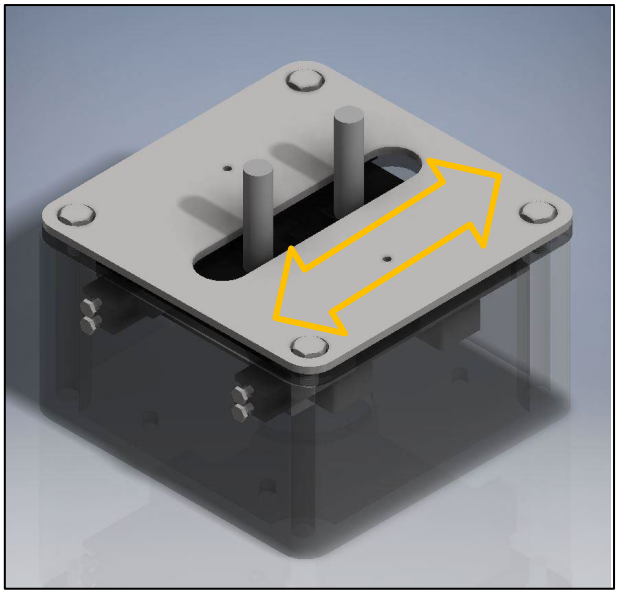

Figure 3.7 Locator bed gripper pins

The locator bed is mounted to a workpiece positioning mechanism, made up of two rotational actuators. The rotational actuators consist of aluminium chassis that are driven by geared stepper motors. Rotational locking is achieved using geared electromagnetic brakes. The inner actuator allows the bed to be rotated about the Z-axis, and the outer allows the bed to be roatated abut the Y-axis. The Z-axis rotation enables the clamp arms to fixture the workpiece along its length or breadth for cubic parts, or any arbitrary angle desired. The Y-axis roation orientates the workpiece in either the home position, illustrated in figure 3.8, for machining on the ‘top’ surface, or tilts the workpiece to allow machining on the ‘side’ surfaces.

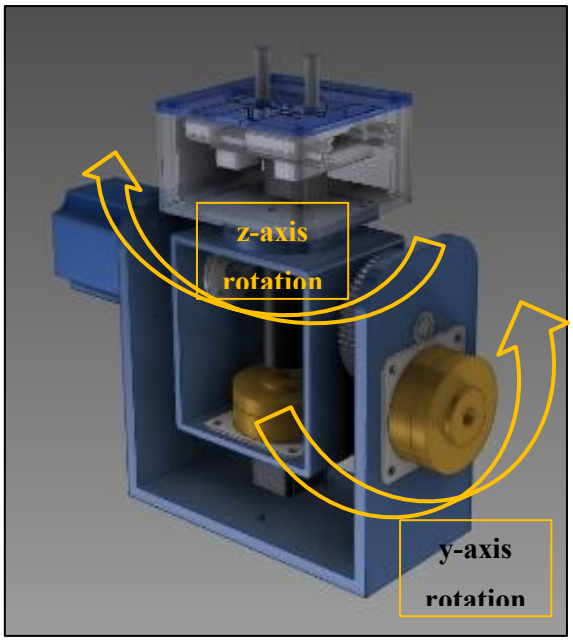

Figure 3.8 Fixture bed degrees of freedom

3.4.2 Pin Matrix Clamping Arms

The clamping arms consists of the pin matrix clamps and the tilting mechanism, illustrated in figure 3.10. The purpose of the pin matrix clamp is to mould around features in order to provide the optimum surface contact for a variety of possible geometries. It consists of a pin field, where each pin is able to move independently of the others. The pins are spring loaded, and are constrained to move linearly inwards and outwards of the body of the pin matrix. The pins are fastened in place using a friction plate that is driven by a micro servo motor, illustrated in figure 3.9. The entire pin matrix is 3-d printed from ABS with the exception of the pins, and friction plate.

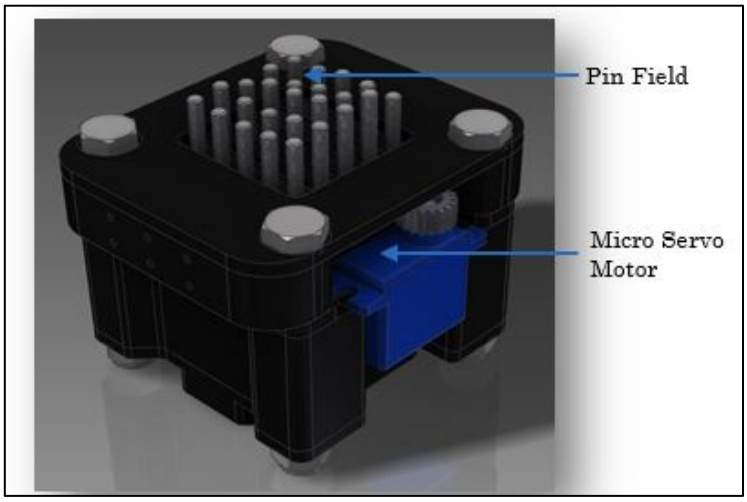

Figure 3.9 Pin matrix

The pin matrix tilting mechanism is driven by a geared stepper motor and held in place by an electromagnetic brake. The tilting mechanism rotates about the y-axis, shown in figure 3.10. The tilting bracket was assembled from aluminium segments. The rotation allows the clamping force to be applied perpendicular to a surface, angled 'downwards' towards the locating bed or at any angle relevant to the workpiece geometry.

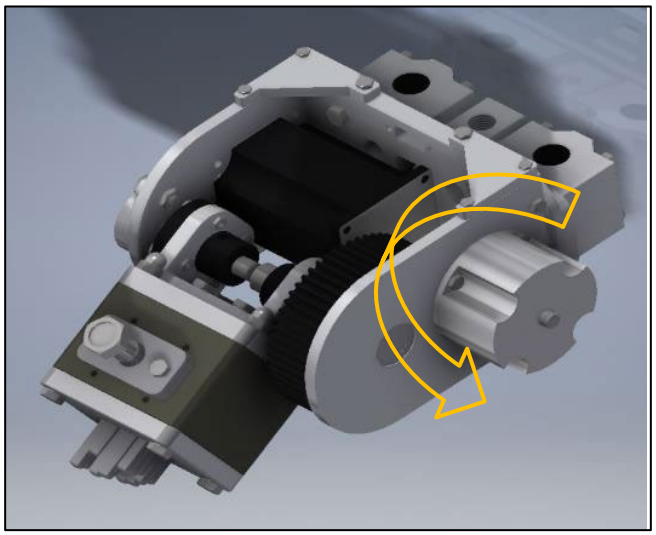

Figure 3.10 Pin matrix clamp adjustability

3.5 Fixturing Variations

The area between the clamping arm and the workpiece will be referred to as the fixture surface. The forces acting on the fixture surfaces must balance each other out as well as hold the workpiece in place without allowing any movement. The number of clamping arms limits the possible fixturing positions. The AFFS has two clamping arms, and thus they will be positioned in-line with each other on opposite sides of the workpiece for all fixture setups.

3.5.1 Final Fixturing Strategies

Each of the fixture setups for the simulations need to be positioned such that it provides a unique result for the frequency response. When the clamping arms are in-line with each other, the fixture surfaces can be positioned anywhere along the length or breadth of the workpiece. The areas for fixturing will be limited to three positions along both the length and breadth of the workpiece. These positions are the centroid of the length and breadth sides, and the extreme ends of the length and breadth sides.

3.5.1.1 Part 1 Fixturing

Two of the fixturing setups for part 1 operation 6 are seen in figure 3.11. The workpiece has been fixtured with the fixture surfaces along its breadth. Image (a) shows the fixture surface at the breadth-centre position, while image (b) shows the fixture surface at the breadth-side

position. The name of each fixture setup describes the location of the two fixture surfaces along the sides of the workpiece.

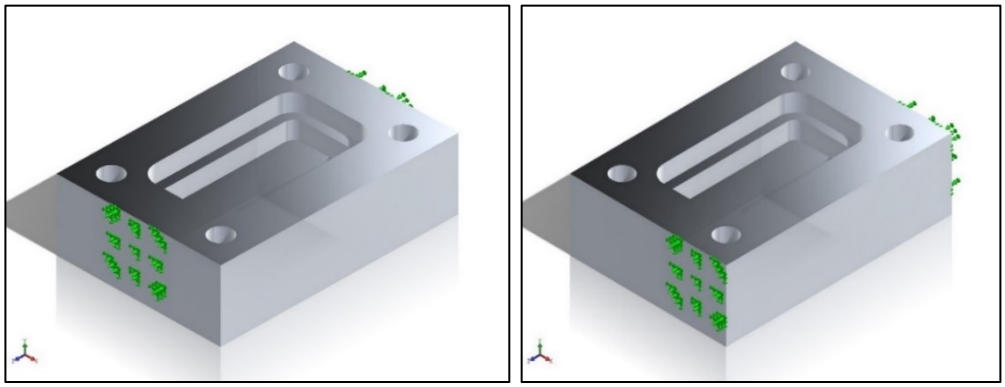

(a) (b)

Figure 3.11 (a) Breadth-centre and (b) breadth-side fixturing for part 1

The final two fixturing positions for part 1 operation 6 are shown in figure 3.12. Image (a) of Figure 3.12 shows the length-centre fixture setup, and image (b) shows the length-side fixture setup. Part 1 operation 6 has geometric features that are symmetric about the horizontal centrelines on its upper surface, and thus has only 4 unique fixture setups.

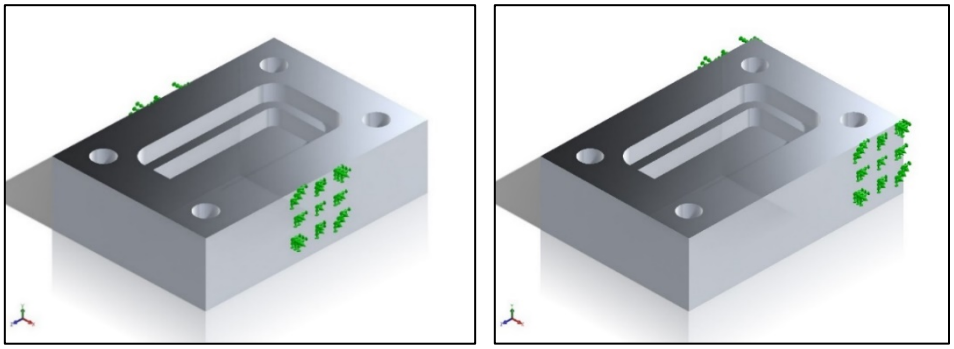

(a) (b)

Figure 3.12 (a) Length-centre and (b) length-side fixturing for part 1

3.5.1.2 Part 2 Fixturing

Part 2 operation 1 has an asymmetric geometry about its horizontal centrelines on its upper surface. Due to the positions of the main bore all the stages of machining are asymmetric. figure 3.13 shows the fixturing positions on the breadth surface of part 2. Image (a) shows the breadth-centre fixture position, image (b) depicts the breadth-side-a fixture position and image (c) depicts the breadth-side-b fixture setup. The breadth-side-a setup is positioned away from the centre of mass (COM), whereas the breadth-side-b fixture setup is positioned closer to the COM.

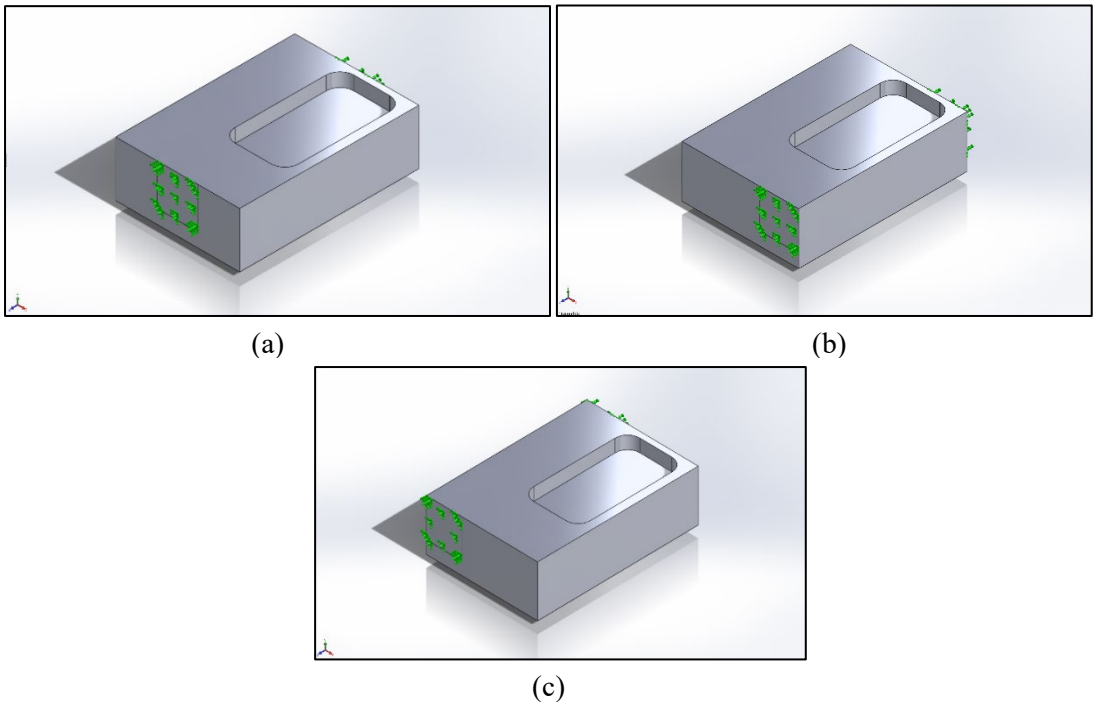

Figure 3.13 (a) Breadth-centre, (b) breadth-side-a and (c) breadth-side-b fixturing for part 2 op. 1

The fixture positions along the length of part 2 for operation 1 are shown in Figure 3.14. Image (a) shows the length-centre fixture position, image (b) depicts the length-side-a fixture position and image (c) depicts the length-side-b fixture setup. The length-side-a setup is positioned away from the COM, whereas the length-side-b fixture setup is positioned closer to the COM.

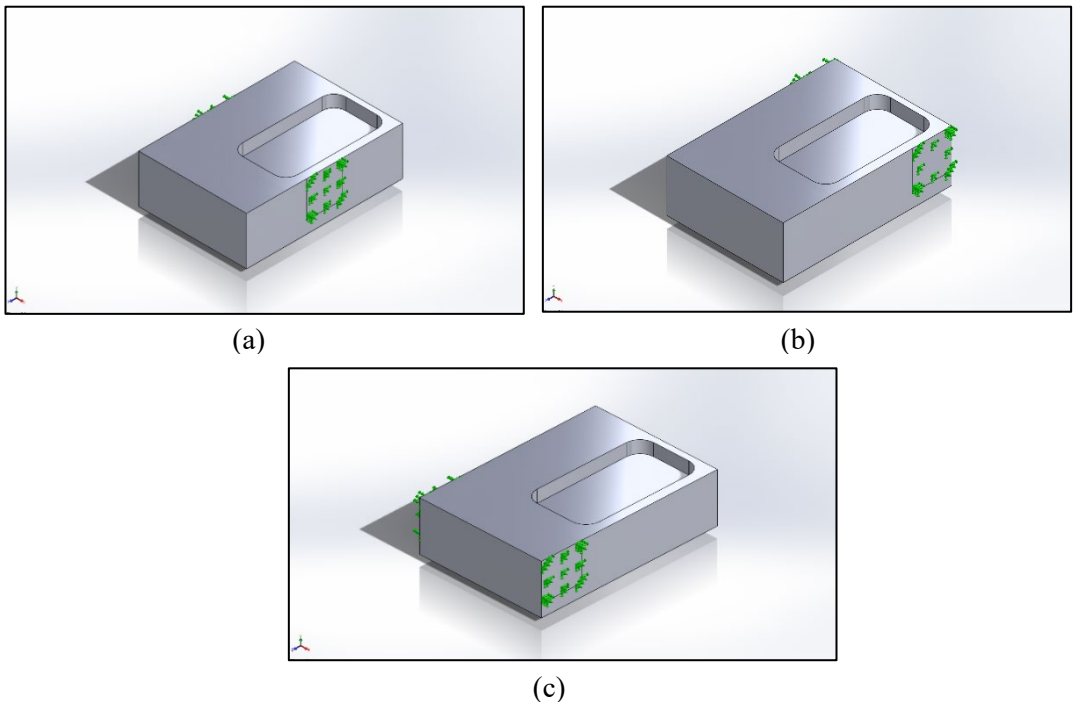

Figure 3.14 (a) Length-centre, (b) length-side-A and (c) length-side-B fixturing for part 2 operation 1

3.5.2 Simulation Fixturing Properties

The dampening effect of the AFFS on the part was an important consideration in determining the fixture properties for the simulation. The dampening properties of the AFFS were unknown and could not be determined through simulation of the AFFS due to its complexity. The fixture surfaces were chosen to be set as fixed, which sets the dampening forces to zero and does not allow for any motion of the fixed surface. This fixture type yielded the maximum possible frequency response of the workpiece for a given fixture setup.

Determining the dampening properties of the AFFS requires an iterative approach where the dampening properties of the workpiece fixture constraints are adjusted in each simulated until the frequency response matches those of the experimental results. The expert systems for fixture optimization were based on vibration testing rather than simulation, thus the dampening properties of the AFFS were not required.

3.6 Mesh

SolidWorks high quality mesh type was used to mesh the workpiece models. This mesh type uses 3D tetrahedral elements, consisting of 10 nodes, for all solid components. This mesh model does require more computational power than other simpler meshes, but is able to represent curved boundaries with more accuracy which makes it suitable for the workpiece geometry.

Figure 3.15 shows the final volume mesh for part 1 operation 1. The optimal mesh size was determined, through iteration, as 1.5 mm corresponding to 370000 cells, illustrated in Figure 4.1 on page 31. The image of the mesh shows minimal cell warpage, including the cells in areas of particular concern such as the corners and around the curved edges of the solid.

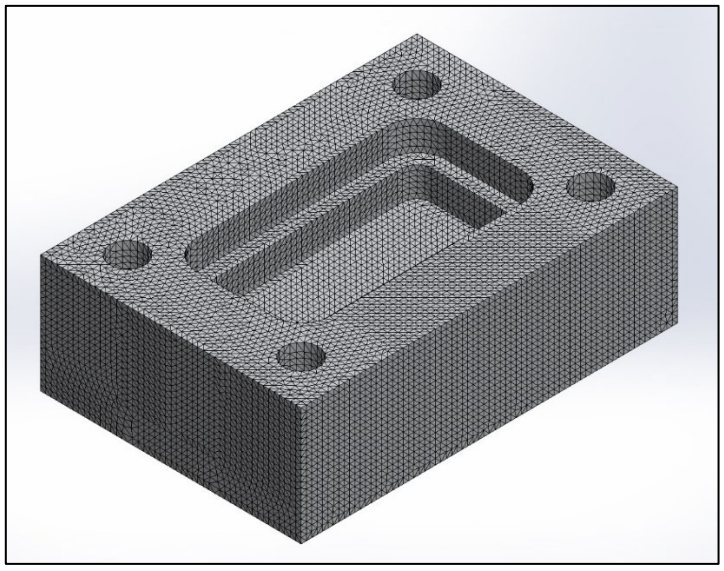

Figure 3.15 Mesh for part 1 operation 1

3.7 Simulation Procedure

The following procedure was followed for each simulation:

- Open the part file in SolidWorks
- Create a sketch on the side wall surface of the part
- Draw the area of the fixture surface in the relevant position
- Create a spit line feature from sketch
- Start a new frequency analysis simulation
- Apply fixed geometry to the fixturing area, or split line feature
- Select the part material as aluminium 6082
- Select the mesh option
- Specify mesh type and size
- Create a surface mesh
- After meshing is completed check mesh for geometric errors
- Run the frequency simulation
- Export the simulation data as a MS word file

In the procedure, a split line feature was created from the sketch of the fixture surface. The split line feature converts a closed sketch that has been drawn on the part to a surface that can be constrained as a fixture or have a load applied to it.

3.8 Chapter Summary

Chapter 3 introduces the simulation aims and objectives. The two parts that were chosen for the modal simulations, a symmetrical and non-symmetrical part, were presented. The fixturing capabilities of the AFFS were discussed and fixture setups were developed. The mesh parameters and material selection were given, as well as the simulation procedure to be followed.

Chapter 4: Simulation Results

4.1 Chapter Introduction

Chapter 4 presents the simulation results for part 1 and part 2. It focuses on the harmonic frequencies and briefly discusses the displacement results. The results are presented in table form to illustrate the maximum frequencies, as well as in graph form. The frequency graphs highlight the effect of material removal on the harmonic vibrations for each fixture setup. Simulations regarding the rearrangement of operation order are also presented.

4.2 Mesh Independence

Determining mesh independence ensured the accuracy of the simulation results. The mesh size and quality were directly related to the accuracy of the simulations, but came at a computational cost. At a certain point a large increase in computational cost lead to a very small improvement in simulation accuracy. Thus, a balance between accuracy and computational time had to be achieved. A mesh independence plot was used to visualize the relationship between the mesh density, representative of the computational cost, and the results for the harmonic frequency.

The graph in figure 4.1 shows the mesh independence plot. Five simulations are plotted, each run with decreasing mesh sizes, represented by the nodes on the graph. The decrease in mesh size correlates to an increase in the mesh cell count. The x-axis of the graph shows the cell count; the y-axis represents the corresponding frequency result of the simulation for that cell count.

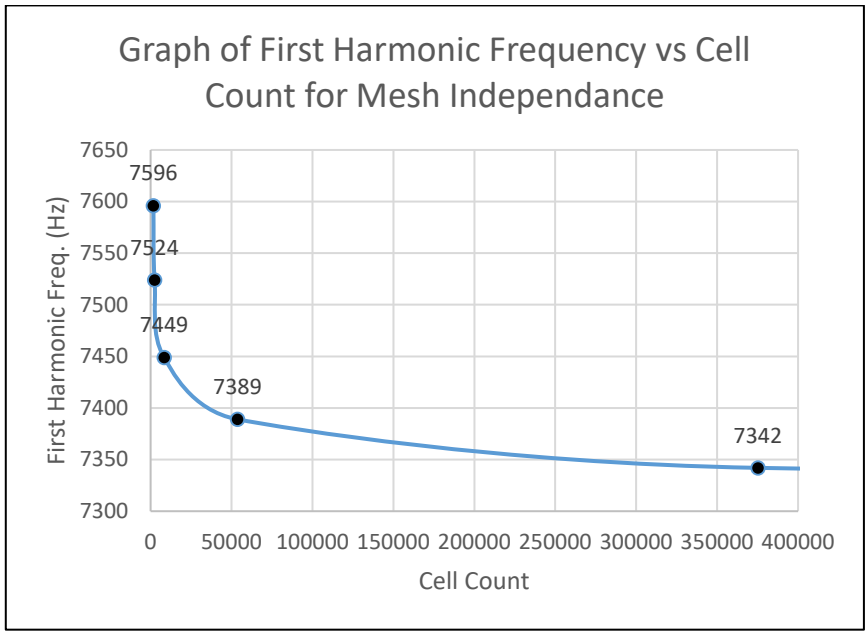

Figure 4.1 Mesh independency for part 1 operation 1

For the first 3 simulations a relatively small change in cell count resulted in a substantial change in harmonic frequency. Between the point on the graph of approximately 51000 and 370000 cells, simulation 4 and 5, the curve begins to asymptotically approach 7340 Hz. The cell counts of 51000 and 370000 correspond to mesh sizes of 3 mm and 1.5 mm respectively. The last node, at 37000 cells, represents the point where mesh independence is reached. All the modal simulations were thus performed with a mesh size of 1.5 mm.

4.3 Modal Displacement Results

Figure 4.2 (a) illustrates the displacement results for the first mode of vibration of part 1 operation 1. The CAD model is represented with a colour scheme that reflects the amount of deflection, blue representing no deflection gradating to red for maximum deflection. Image (b) illustrates the fourth harmonic shape of part 1 operation 6.

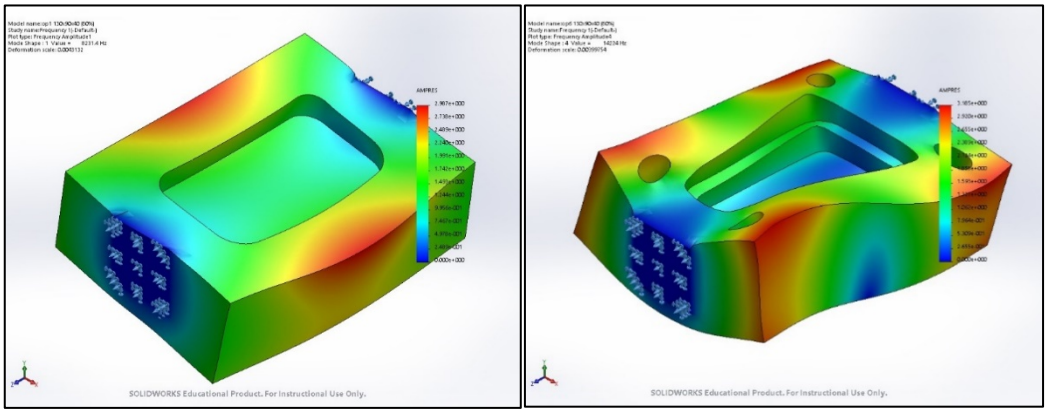

(a) (b)

Figure 4.2 (a) First harmonic shape for part 1 operation 1 (b) Fourth harmonic shape for part 1 operation 4

The blue areas on the models in both image (a) and (b) represent anti-nodes, while the red areas represent nodes. Image (a) has 2 nodes and 2 anti-nodes, while image (b) has 4 nodes and 4 anti-nodes. These results for the workpiece deflection were used to determine the positioning of the accelerometer for experimental testing. The nodal areas where maximum deflection occurs are the optimum position for the accelerometer to record the vibration frequency.

4.4 Harmonic Frequencies of Part 1

This section presents all the simulation results for natural frequency in both table and graph form, for part 1.

4.4.1 Results in Table Form

Table 4.1 shows the first 5 modal frequencies for part 1 for all operations and fixture setups. The results are placed in descending operation order, starting from the billet (operation 0) at the head of the list and ending at operation 6. The table facilitates quick comparisons of the natural frequencies of each fixture setup for each operation.

The following are observations on the modal highest frequencies for each operation:

- For the base part the fixture setup that produces the highest frequency response for modes 1 and 2 is length-centre. The best response for modes 3, 4 and 5 is breadth-centre
- For operation 1 length-centre produces the highest frequencies for mode 1, followed breadth-centre for modes 2 to 5
- For operations 2 length-centre fixturing produces the highest frequencies for mode 1, followed breadth-centre for modes 2 and 3, length-side for mode 4, and breadth-centre for modes 5 and 6
- For operation 3 length-centre produces the highest frequencies for mode 1, followed breadth-centre for modes 2 to 5
- For operation 4 and 5 length-centre fixturing produces the highest frequencies for mode 1, followed breadth-centre for modes 2 and 3, length-side-1 for mode 4, and breadth-centre for modes 5 and 6
- For operation 6 length-centre fixturing produces the highest frequencies for mode 1, followed breadth-centre for modes 2 to 5

The fixture setup that provides the highest natural frequencies for the majority of the modal frequencies for the operations is the breadth-centre fixture setup.

Table 4.1 Modal Frequencies for Part 1 for all Fixturing Setups

	Part 1	Mode 1	Mode 2	Mode 3	Mode 4	Mode 5
Billet (op.0)	Breadth centre	8166	12454	15260	16150	17802
	breadth side	7618	11109	13232	13883	17629
	Length centre	10586	12217	12391	12533	16371
	length side	6925	10035	13022	14652	17267
Operation 1	Breadth centre	8231	11505	13589	15069	18319
	breadth side	7342	9670	12635	13854	15934
	Length centre	10283	10508	11187	11267	16206
	Length side	6048	9368	12740	13734	17420
Operation 2	breadth centre	8150	10159	12413	14243	18259
	breadth side	6972	8509	11677	13594	15073
	Length centre	9616	9753	10527	10561	16073
	length side	5469	8530	12430	12738	16515
Operation 3	Breadth centre	8114	10113	12462	14238	18271
	Breadth side a	6912	8464	11453	13568	15049
	Breadth side b	6996	8655	11664	13732	15183
	Length centre	9644	9831	10523	10744	16125
	Length side a	5550	8625	12539	12667	16592
	Length side b	5453	8508	12386	12720	16494
Operation 4	Breadth centre	8080	10066	12511	14236	18282
	Breadth side a	6943	8608	11439	13708	15156
	Breadth side b	6943	8608	11438	13710	15155
	Length centre	9762	9841	10664	10774	16174
	Length side a	5637	8719	12579	12665	16666
	Length side b	5443	8490	12344	12701	16472
Operation 5	Breadth centre	8042	10018	12545	14225	18293
	Breadth side a	6968	8756	11425	13852	15258
	Breadth side b	6882	8565	11222	13681	15132
	Length centre	9776	9989	10677	10888	16242
	Length side a	5624	8702	12558	12628	16645
	Length side b	5522	8585	12454	12626	16547
Operation 6	Breadth centre	8009	9971	12607	14224	18312
	Breadth side	6913	8711	11212	13829	15232
	Length centre	9954	9990	10740	10939	16303
	Length side	5609	8683	12541	12576	16622

4.4.2 Results in Graph Form

The table results are represented in this section in graph form. The results have been graphed to better illustrate the relationship between the machining operations and the corresponding frequency change for a given mode of vibration. This illustrates the effect of material removal or geometry change on the natural frequency.

4.4.2.1 First Harmonic

The first harmonic for breadth centre fixturing, seen in figure 4.3, starts at 8166 Hz for the billet and increases to 8231 Hz after machining the first rectangular cut. The second cut brings the frequency down to 8150 Hz. The four holes bring the frequency down to 8009 in a linearly proportional manner.

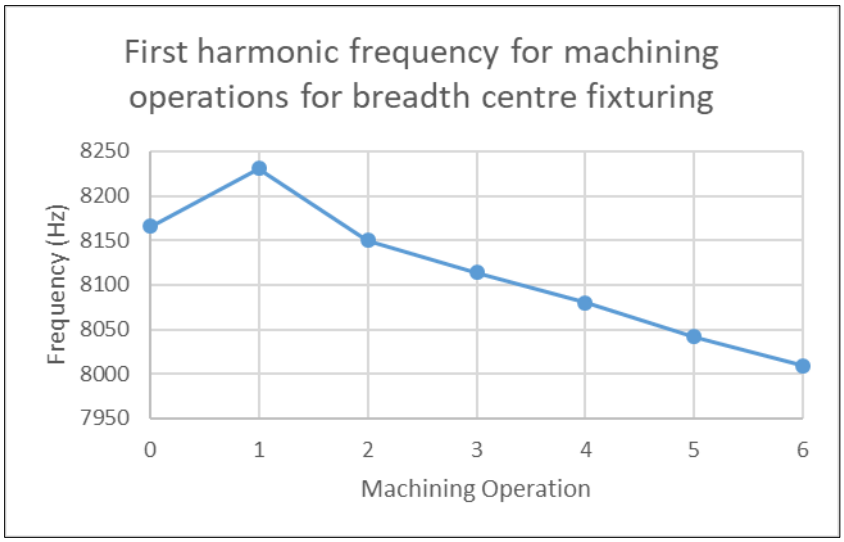

Figure 4.3 Natural Frequencies for Machining Operations for Breadth Centre Fixturing of Part 1

The first harmonic for breadth side fixturing, seen in figure 4.4, starts at 7618 Hz and decreases through 7342 Hz for the first cut to 6972 Hz for the second. The first hole decreases the frequency to 6912 Hz, followed by an increase to linearly to 6968 Hz for holes 2 and 3. The last hole corresponds to a frequency of 6913 Hz. The length side 2 fixturing, applicable to the asymmetric operations 3 to 5, is shown in blue. The harmonic of operation 3 for breadth side 2 fixturing is 6996 Hz, it then drops linearly to 6882 Hz for operation 5.

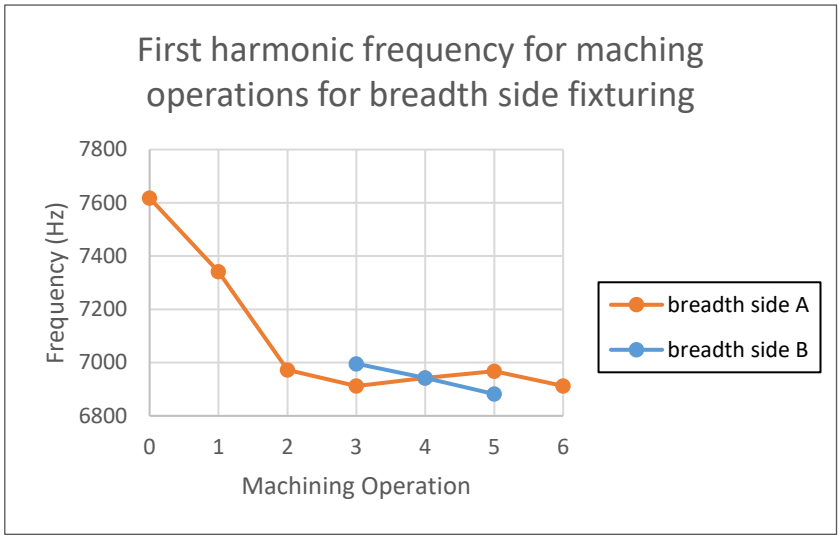

Figure 4.4 Natural Frequencies for Machining Operations for Breadth Side Fixturing of Part 1

The first harmonic for length centre fixturing, seen in figure 4.5, starts at 10586 Hz for the billet. It then decreases through 10283 Hz for cut 1 to 9616 Hz for cut 2. Thereafter it increases in a linear fashion to 9954 Hz through the machining of the four holes.

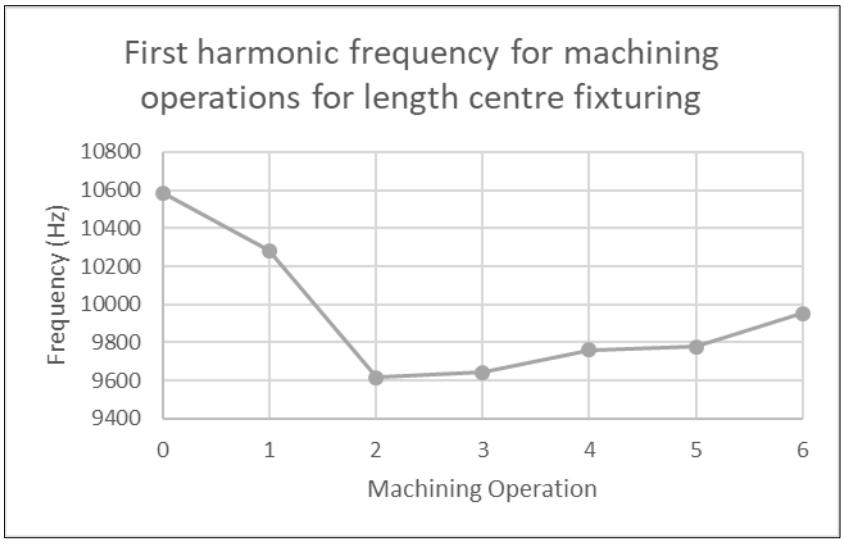

Figure 4.5 Natural Frequencies for Machining Operations for Length Centre Fixturing of Part 1

The first harmonic for length side fixturing, shown in figure 4.6, starts at 6925 Hz for the billet. It then decreases linearly through 6048 Hz to 5469 Hz for operation 2. The first two holes each increase the harmonic frequency until it reaches 5637 Hz. It then decreases to 5624 Hz for operation 5 and ends at 5609 Hz for operation 6. The length side 2 operation, shown in blue, starts at operation 3 with a frequency of 5453 Hz which decreases slightly to 5443 Hz and finally increases to 5522 Hz.

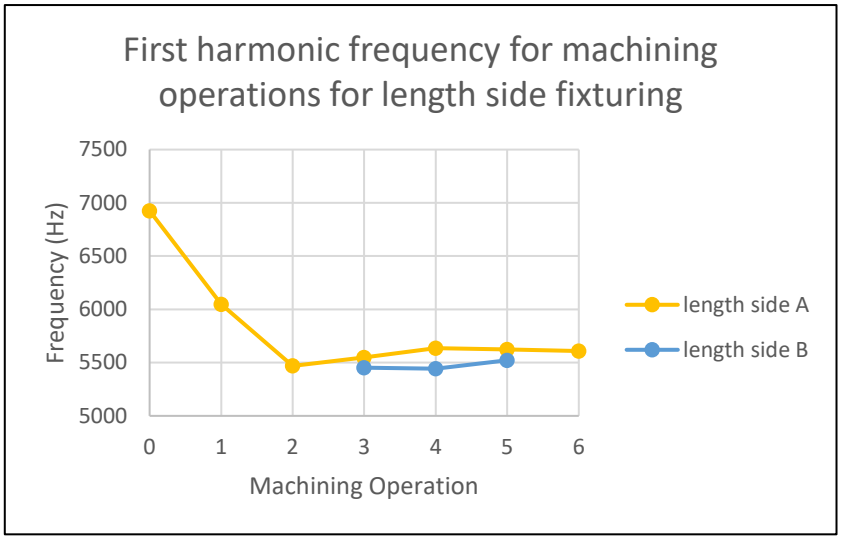

Figure 4.6 Natural Frequencies for Machining Operations for Length Side Fixturing of Part 1

4.4.2.2 Second Harmonic

The second harmonic for breadth centre fixturing, shown in figure 4.7, starts at 12454 Hz for the billet and decreases linearly to the second operation at 8150 Hz. The four holes each decrease the frequency slightly to a final harmonic of 9971 Hz at operation 6.

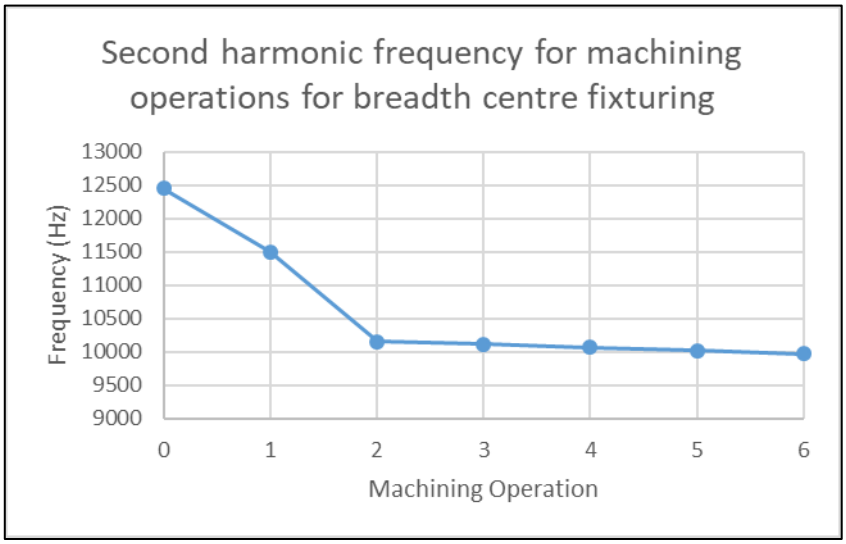

Figure 4.7 Natural Frequencies for Machining Operations for Breadth Centre Fixturing of Part 1

The second harmonic frequency for breadth side fixturing, shown in figure 4.8, starts at 11109 Hz for the billet and then decreases linearly to 8509 Hz. It then increases for each hole cut until it reaches 8771 Hz at operation 6. The breadth side 2 fixturing, shown in blue, starts at 8655 Hz for operation 3. It then decreases through 8608 Hz to 8565 Hz for operation 5.

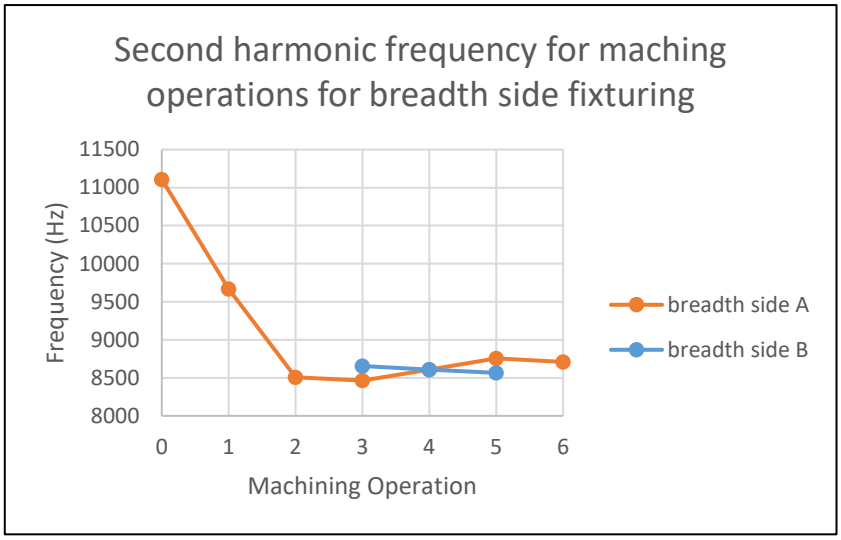

Figure 4.8 Natural Frequencies for Machining Operations for Breadth Side Fixturing of Part 1

The second harmonic for length centre fixturing, seen in figure 4.9, starts at 12217 Hz and decreases though 10508 Hz to 9753 Hz for operation 2. It then increases with each hole cut until it reaches 9990 Hz at operation 6.

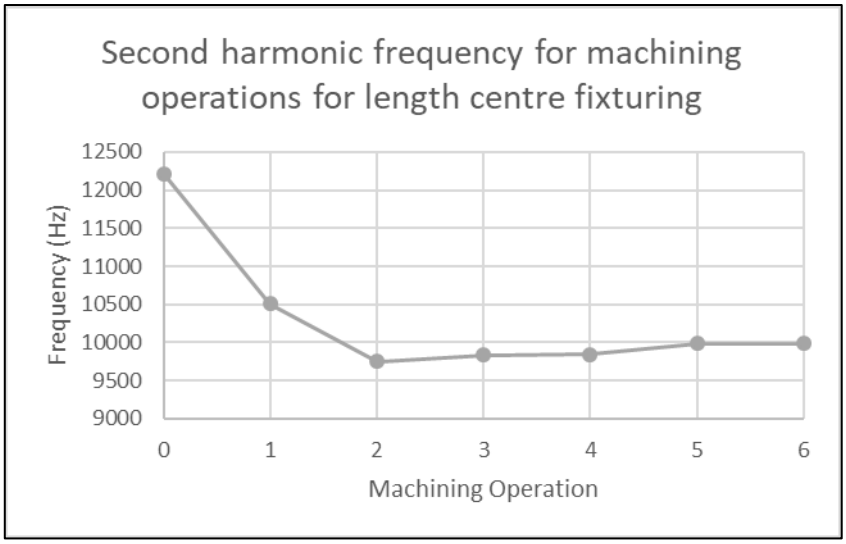

Figure 4.9 Natural Frequencies for Machining Operations for Length Centre Fixturing of Part 1

The second harmonic for length side fixturing, seen in figure 4.10,starts at 10035 Hz and then decreases to 9368 Hz for cut 1 and 8530 for cut 2. The frequency increases to 8702 Hz after the third cut hole. The last hole cut increases the frequency to 9990 Hz. The length side 2 fixturing, shown in blue, starts at 8508 Hz for operation 3 and increases to 8585 Hz for operation 5.

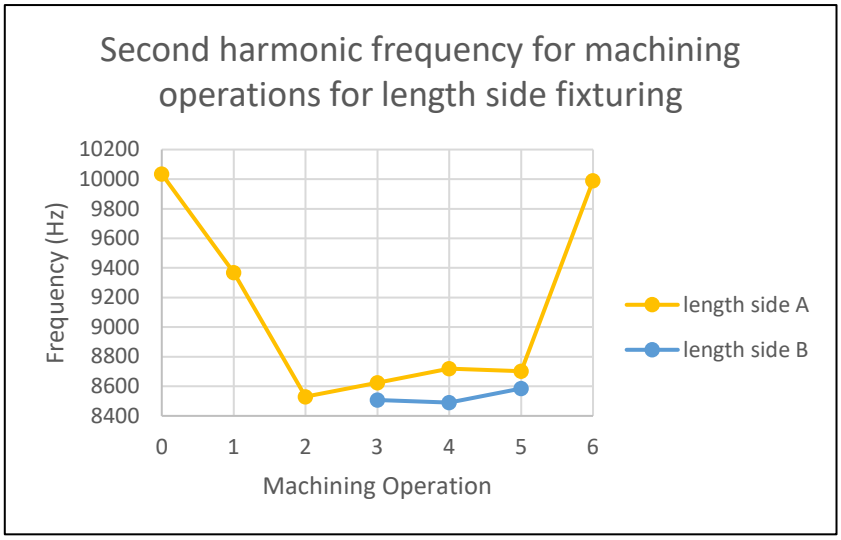

Figure 4.10 Natural Frequencies for Machining Operations for Length Side Fixturing of Part 1

4.4.2.3 Third Harmonic

The Third harmonic for breadth centre fixturing, shown in figure 4.11, starts at 15260 Hz. It then decreases through 13589 Hz to 12413 Hz at operation 2. The four holes increase the frequency to a final state of 12607 Hz.

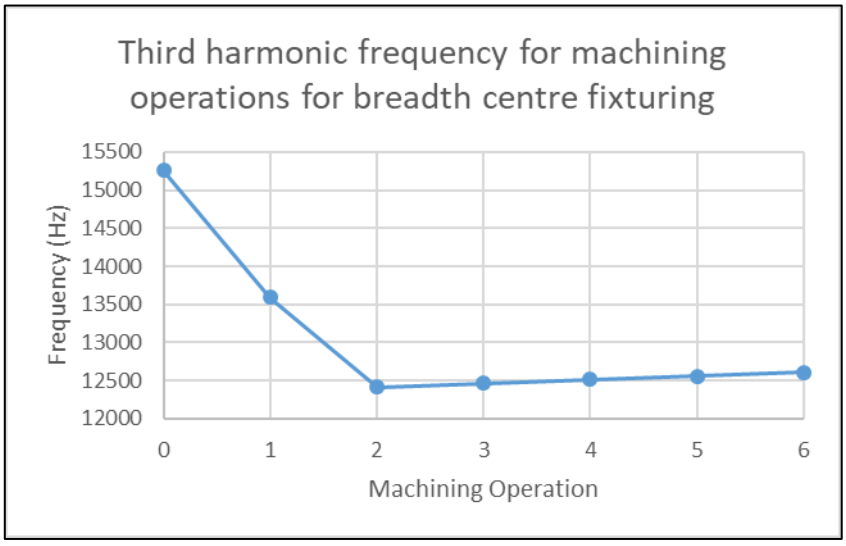

Figure 4.11 Natural Frequencies for Machining Operations for Breadth Centre Fixturing of Part 1

The third harmonic frequency for breadth side fixturing, shown in figure 4.12, starts at 13232 Hz for the billet. It then decreases through 12635 Hz to 11677 for operation 2. The four holes each decrease the frequency until it reaches 11212 Hz for operation 6. The breadth side 2 fixturing, shown in blue, starts at 11664 Hz for cut 3. It then decreases to a final frequency of 11222 Hz for cut 5.

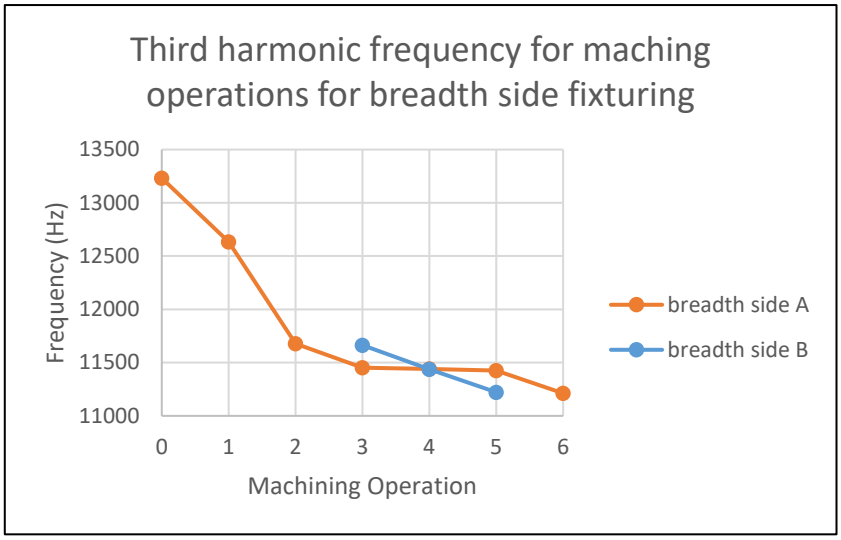

Figure 4.12 Natural Frequencies for Machining Operations for Breadth Side Fixturing of Part 1

The third harmonic frequency for length centre fixturing, shown in figure 4.13, starts at 12391 Hz for the billet. It then decreases through 11187 Hz to 10527 Hz for operation 2. It then increases, as the four holes are cut, to a final frequency of 10740 Hz.

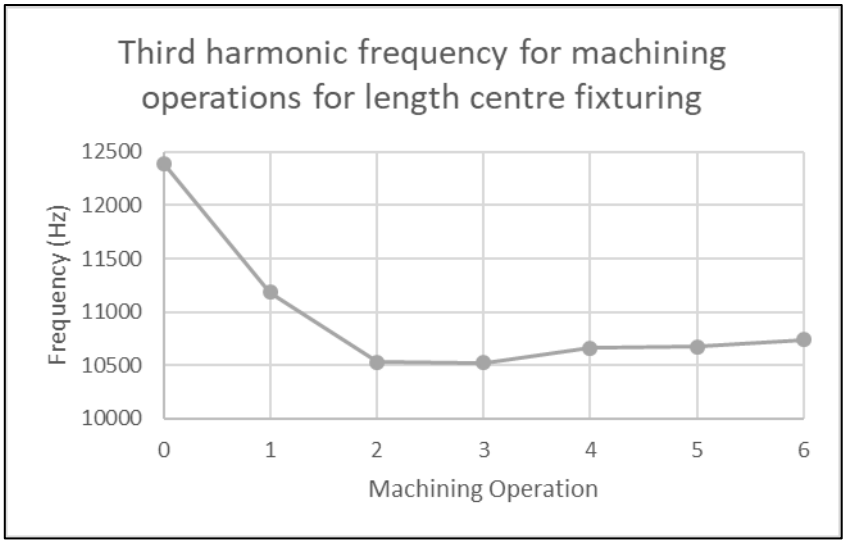

Figure 4.13 Natural Frequencies for Machining Operations for Length Centre Fixturing of Part 1

The third harmonic frequency for length side fixturing, shown in figure 4.14, starts at 13022 Hz for the billet. It then decreases linearly to 12430 Hz for operation 2. The first 2 holes cut bring the frequency up to 12579 Hz. The last two holes decrease the frequency to 12541 Hz at operation 6. The length side 2 fixturing, shown in blue, starts at 12386 Hz. It then decreases to 12344 Hz followed by an increase to 12454 Hz for operation 5.

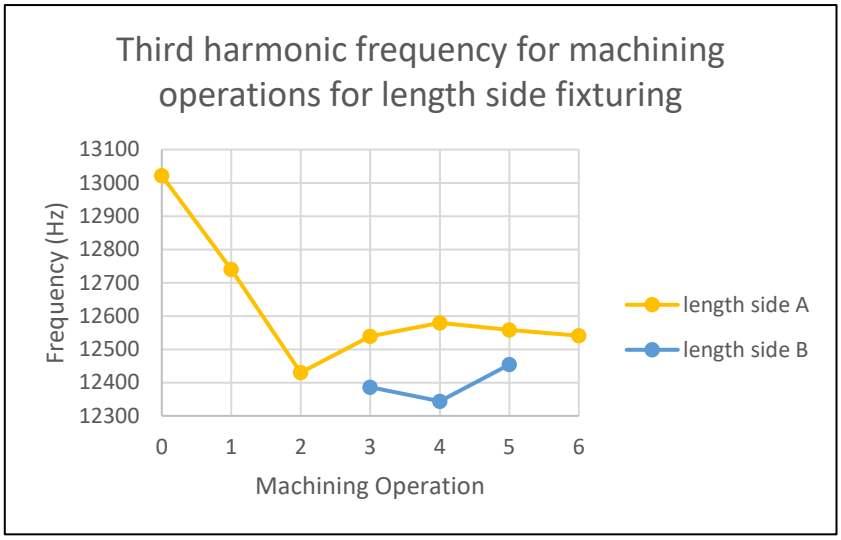

Figure 4.14 Natural Frequencies for Machining Operations for Length Side Fixturing of Part 1

4.4.2.4 Fourth Harmonic

The fourth harmonic frequency for breadth centre fixturing, shown in figure 4.15, starts at 16150 Hz for the billet. It then decreases to 14243 Hz for operation 2. The four holes decease the frequency to a final state of 12576 Hz at operation 6.

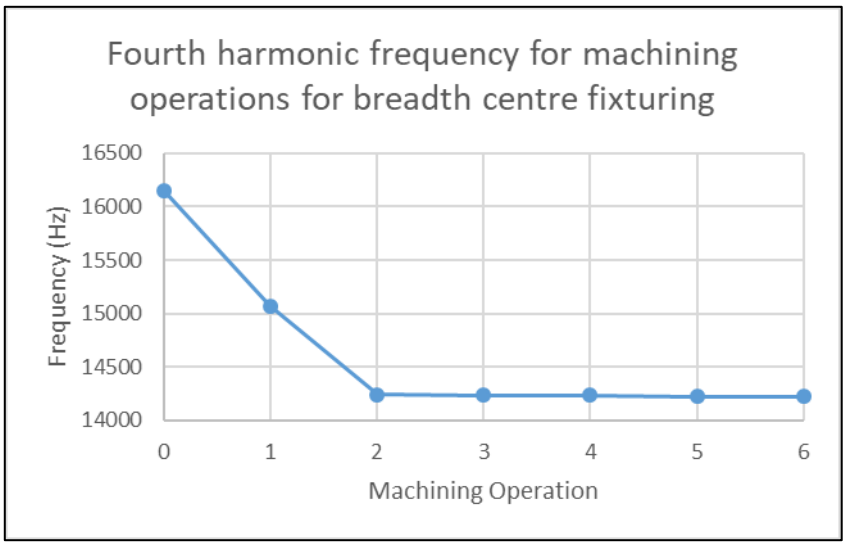

Figure 4.15 Natural Frequencies for Machining Operations for Breadth Centre Fixturing of Part 1

The fourth harmonic frequency for breadth side fixturing, shown in figure 4.16, starts at 13883 Hz for the billet. It then decreases through 13854 Hz to 13594 Hz. The first hole cut decreases the frequency to 13568 Hz. The frequency is increased linearly to 13852 Hz for operation 5, and decreases to a final frequency of 13829 Hz. The breadth side 2 fixturing, seen in blue, starts at 13732 Hz for operation 3. It then decreases through 13710 Hz to a final of 13681 Hz.

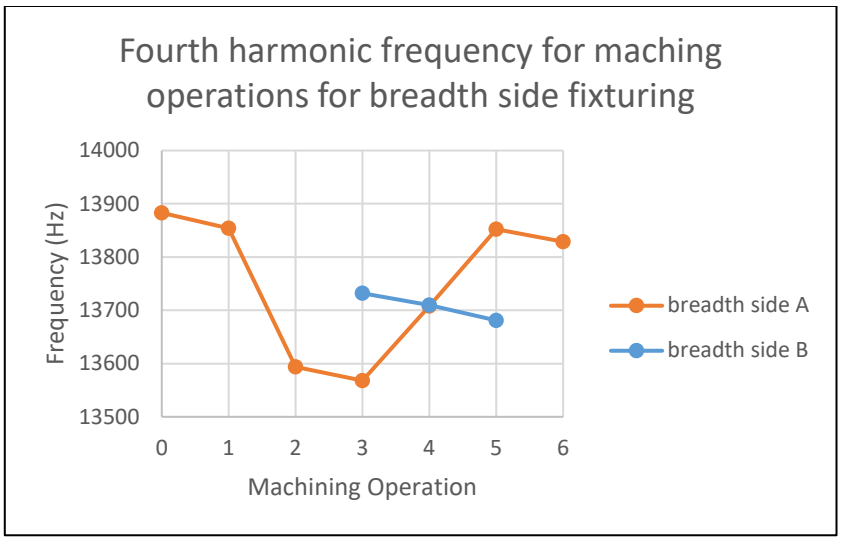

Figure 4.16 Natural Frequencies for Machining Operations for Breadth Side Fixturing of Part 1

The fourth harmonic frequency for length centre fixturing, shown in figure 4.17, starts at 12533 for the billet. It then decreases through 11267 Hz to 10561 Hz for operation 2. The four holes each increase the frequency to a final state of 10939 Hz for operation 6.

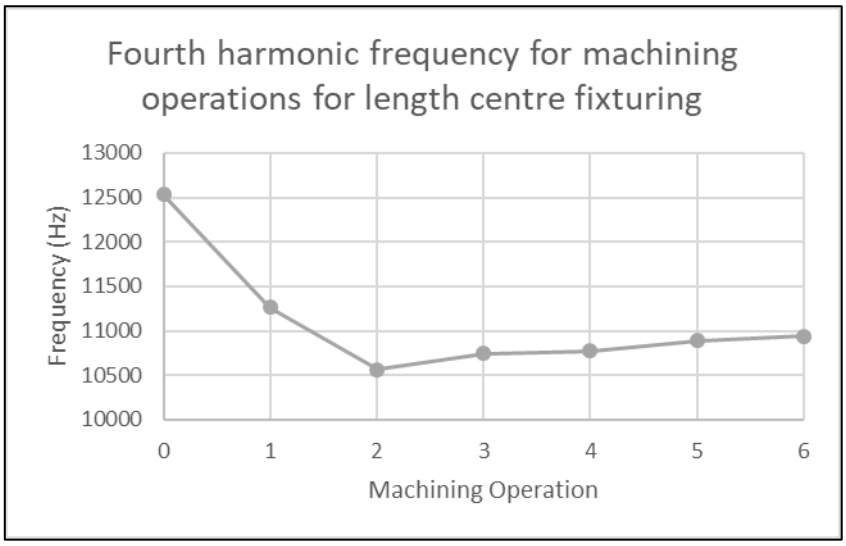

Figure 4.17 Natural Frequencies for Machining Operations for Length Centre Fixturing of Part 1

The fourth harmonic frequency for length side fixturing, shown in figure 4.18, starts at 14652 Hz for the billet. It then decreases to 12738 Hz after operation 1 and 2. The four holes cut decreases the frequency further to 12576 Hz. The length side 2 fixturing, shown in blue, starts at 12386 Hz. It then decreases though 12701 Hz to 12626 Hz at operation 5.

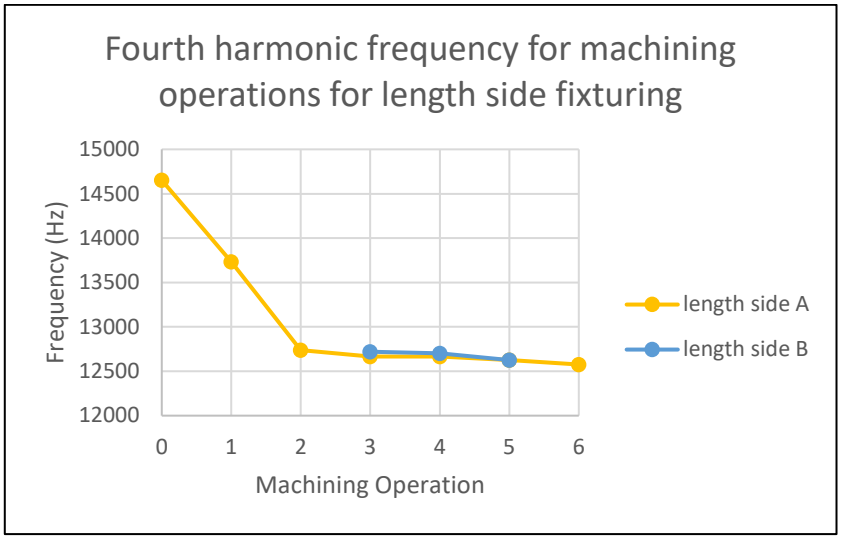

Figure 4.18 Natural Frequencies for Machining Operations for Length Side Fixturing of Part 1

4.4.2.5 Fifth Harmonic

The fifth harmonic for breadth centre fixturing, shown in figure 4.19, starts at 17802 Hz. It then increases to 18319 Hz for operation 1, and decreases slightly to 18259 For operation 2. The four holes cut increase the frequency to a final of 18312 Hz.

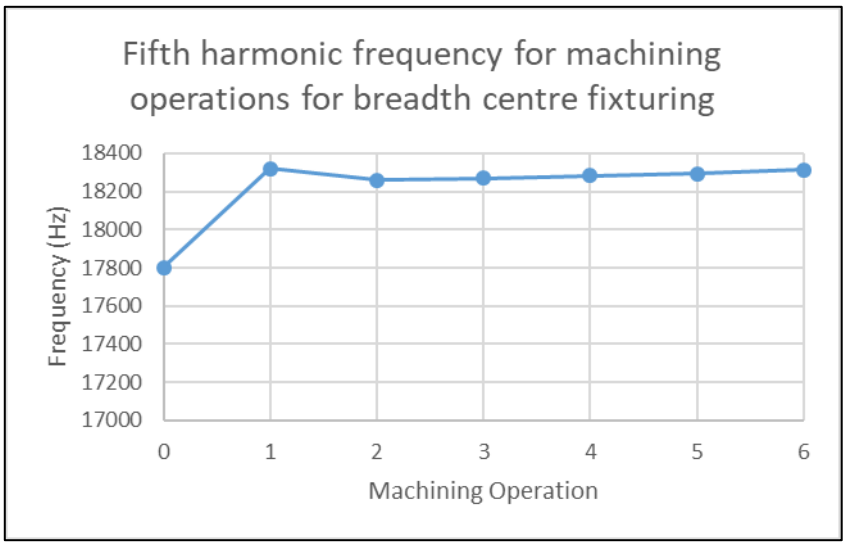

Figure 4.19 Natural Frequencies for Machining Operations for Breadth Centre Fixturing of Part 1

The fifth harmonic frequency for breadth side fixturing, shown in figure 4.20, starts at 17629 Hz for the billet. It then decreases to 15934 Hz for operation 1 and 15073 Hz for operation 2. The four holes cut increase the frequency to 15232 Hz at operation 6. The breadth side 2 fixturing, shown in blue, starts at 15183 Hz for operation 3. It decreases to 15156 Hz for operation 4 and finally 15132 for operation 5.

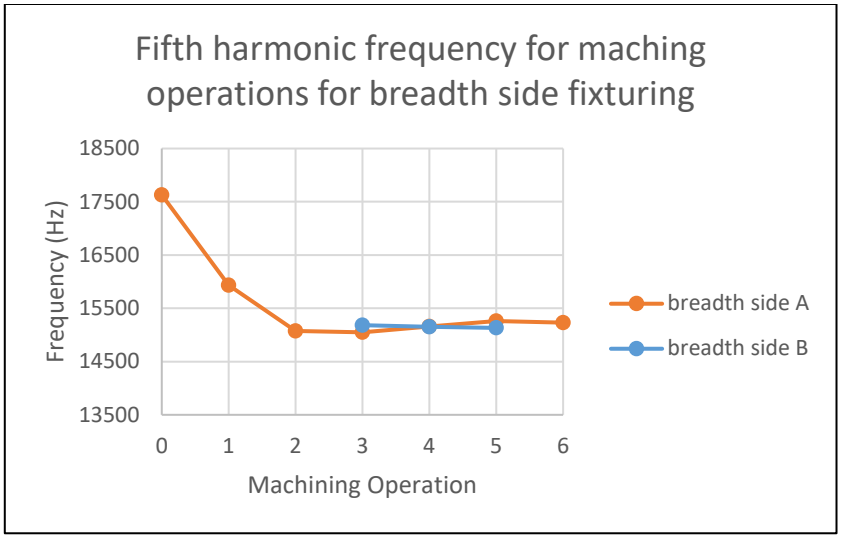

Figure 4.20 Natural Frequencies for Machining Operations for Breadth Side Fixturing of Part 1

The fifth harmonic for length centre fixturing, shown in figure 4.21, starts at 16371 Hz for the billet, and then decreases linearly to 16073. The four holes each increase the frequency until it reaches 16303 Hz at operation 6.

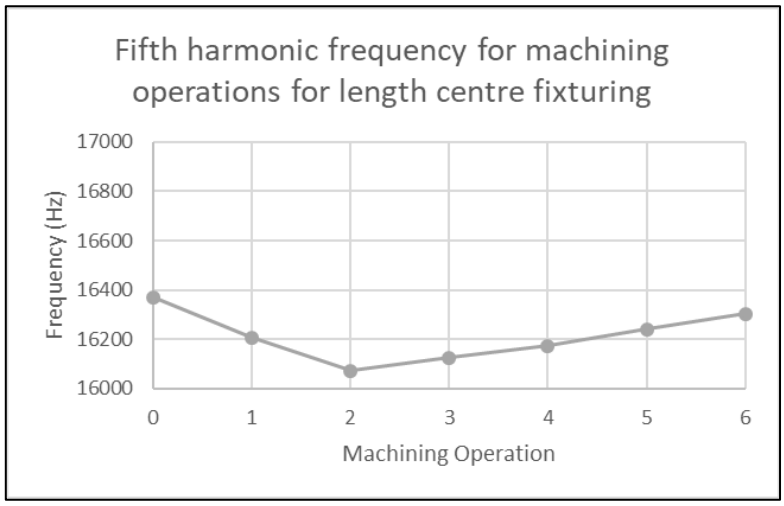

Figure 4.21 Natural Frequencies for Machining Operations for Length Centre Fixturing of Part 1

The fifth harmonic for length side fixturing, shown in figure 4.22, starts at 17267 Hz for the billet. It then increases to 17420 Hz for operation 1. Operation 2 bring the frequency down to 16515 Hz. The first two holes cut increase the frequency to 16666 Hz at operation 4. The frequency then decreases to 16622 Hz. The length side 2 fixturing, shown in blue, starts at 16494 Hz for operation 3. It decreases to 16472 Hz and then increases to 16547 at operation 5.

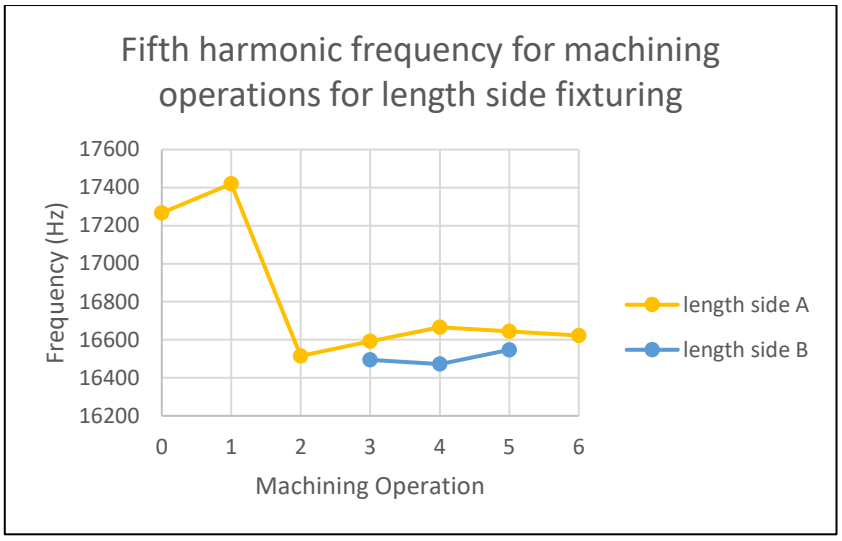

Figure 4.22 Natural Frequencies for Machining Operations for Length Side Fixturing of Part 1

4.5 Harmonic Frequencies of Part 2

4.5.1 Results in Table Form

Table 4.3 shows the modal frequencies for part 2 for all operation and fixture setups. The data is placed in order of operation starting from the billet at the head of the list down to operation 5. The table facilitates comparisons between the modal frequency and fixture setup for each operation.

For the billet, the fixture setup that produces the best frequency response for the first two modes is length-centre, the best response is for modes 3 to 5 is breadth-centre. For each mode, the order of order of best to worst response is different. For the lowest mode the differences are greater in size than for some of the higher modes.

Table 4.2 Modal Frequencies for Part 1 for all Fixturing Setups

	Part 2	Mode 1	Mode 2	Mode 3	Mode 4	Mode 5
Billet (op. 1)	Breadth centre	8166	12454	15260	16150	17802
	Breadth side	7618	11109	13232	13883	17629
	Length centre	10586	12217	12391	12533	16371
	Length side	6925	10035	13022	14652	17267
Operation 1	Breadth centre	8107	11725	13814	15382	18270
	Breadth side 1	7132	9993	12914	13563	16715
	Breadth side 2	7562	9975	12678	13989	15690
	Length centre	10250	10956	11535	11679	16243
	Length side 1	6192	9553	12580	13974	17374
	Length side 2	6440	9612	13061	13970	17310
Operation 2	Breadth centre	7980	10404	12424	14860	17951
	Breadth side 1	6754	9217	12182	13309	16150
	Breadth side 2	7263	8572	11944	13825	14531
	Length centre	9354	10275	10884	11313	16125
	Length side 1	5750	9169	12116	13515	17152
	Length side 2	5887	8515	12696	13001	15607
Operation 3	Breadth centre	7928	10380	12460	15006	17968
	Breadth side 1	6808	9377	12182	13440	16197
	Breadth side 2	7215	8560	11717	13805	14499
	Length centre	9548	10259	10936	11333	16160
	Length side 1	5736	9148	12059	13494	16972
	Length side 2	5994	8620	12682	13173	15567
Operation 4	Breadth centre	7897	10363	12458	15098	17967
	Breadth side 1	6843	9505	12188	13580	16301
	Breadth side 2	7112	8509	11586	13773	14463
	Length centre	9584	10279	10930	11563	16237
	Length side 1	5815	9244	12144	13514	17079
	Length side 2	5979	8600	12662	13128	15528
Operation 5	Breadth centre	7872	10339	12472	15080	17999
	Breadth side 1	6747	9443	12018	13545	16273
	Breadth side 2	7156	8603	11581	13925	14631
	Length centre	9585	10340	11116	11628	16326
	Length side 1	5885	9413	12282	13511	17136
	Length side 2	5968	8587	12644	13099	15499

4.5.2 Results in Graph Form

4.5.2.1 First Harmonic

The first harmonic for breadth-centre fixturing, shown in figure 4.23, starts at 8166 Hz for the billet. It then decreases though 8107 Hz at operation 1 to 7980 Hz for operation 2. The three holes bring the frequency down to 7872 Hz.

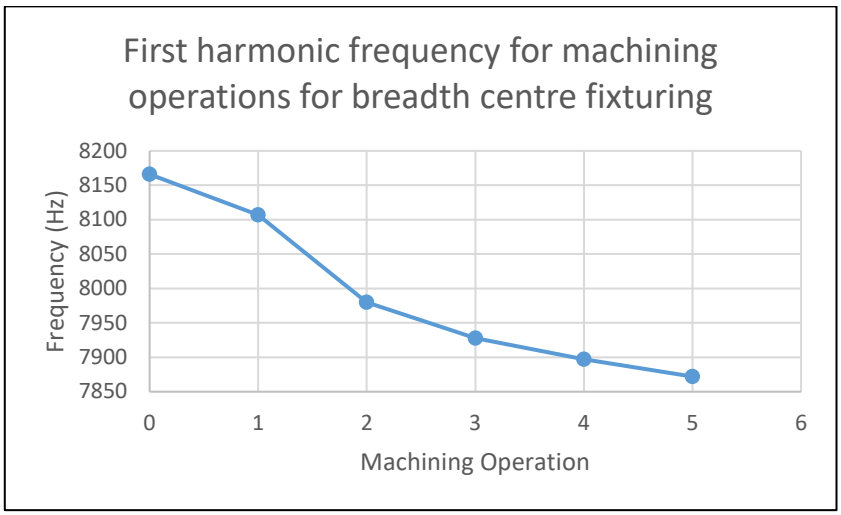

Figure 4.23 Natural Frequencies for Machining operations for Breadth Centre Fixturing of Part 2

The first harmonic frequency for breadth-side fixturing, shown in figure 4.24, has a billet frequency of 7618 Hz. The breadth-side-A fixturing, shown in blue, starts at 7132 Hz for operation 1. It then decreases to 6754 Hz for operation 2, increases though operation 3 to 6843 Hz for operation 4, and ends at 6747 Hz for operation 5. Breadth-side-B fixturing, shown in orange, starts at 7562 Hz for operation 1. It then decreases through 7263 Hz at operation 2 to 7112 Hz for operation 4, and increases to 7156 Hz at operation 5.

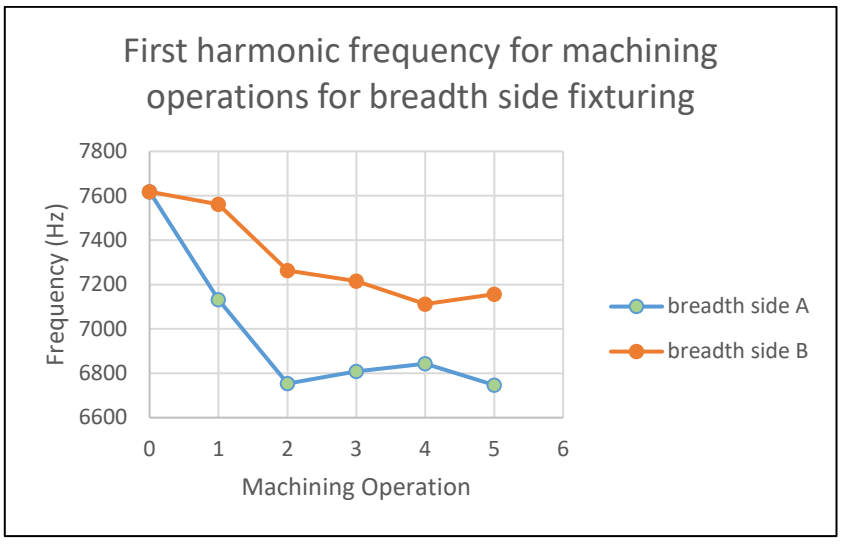

Figure 4.24 Natural Frequencies for Machining operations for Breadth side Fixturing of part 2

The first harmonic frequency for length-centre fixturing, shown in figure 4.25, starts at 10586 Hz for the billet. It then decreases through 10250 Hz for operation 1, to 9354 Hz for operation 2. The three holes increase the frequency to 9585 Hz.

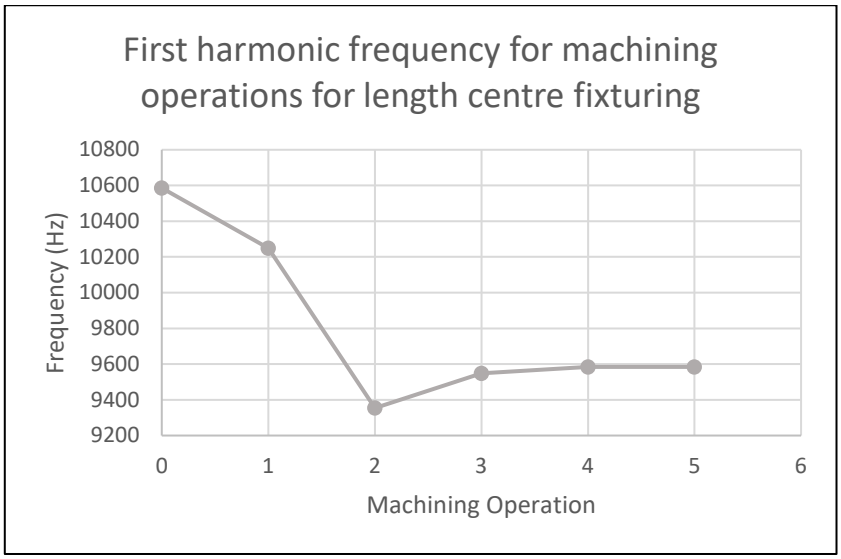

Figure 4.25 Natural Frequencies for Machining Operations for Length Centre Fixturing of Part 2

The first harmonic frequency for length-side fixturing, shown in figure 4.26, has a billet frequency of 6925 Hz. The length-side-A fixturing, shown in blue, starts at 6192 Hz for operation 1. It then decreases to 5450 Hz for operation 2 and increases to 5968 Hz for operation 5. Length-side-B fixturing, shown in orange, starts at 6440 Hz for operation 1. It then decreases to 5887 Hz at operation 2. It then increases to 5994 Hz for operation 3, and decreases to a final frequency of 5885 Hz for operation 5.

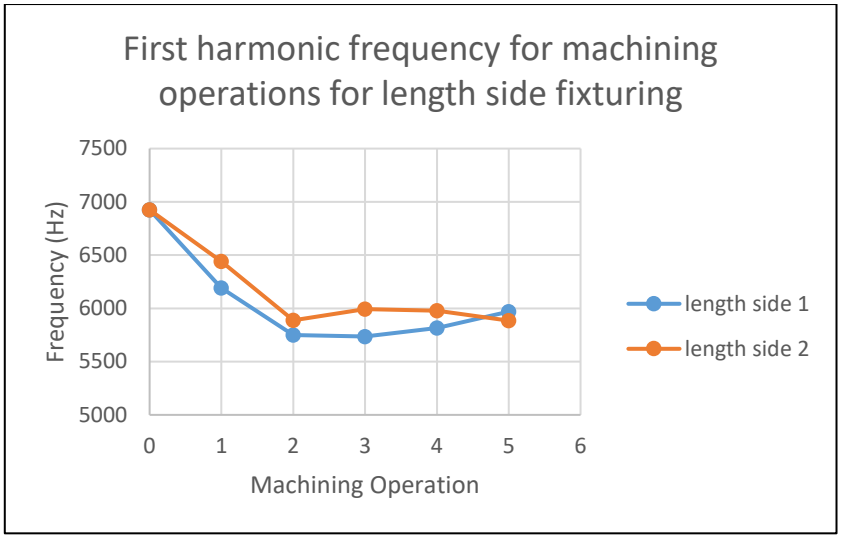

Figure 4.26 Natural Frequencies for Machining Operations for Length Side Fixturing of Part 2

4.5.2.2 Second Harmonic

The second harmonic frequency for breadth-centre fixturing, shown in figure 4.27, starts at 12454 Hz for the billet. It then decreases through 11725 Hz at operation 1 to 10404 Hz at operation 2. The three holes decrease the frequency to 10339 Hz.

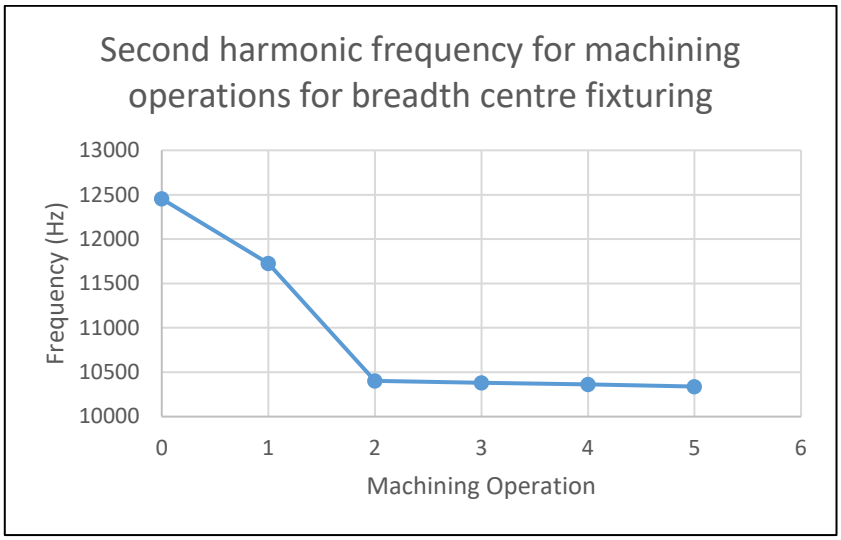

Figure 4.27 Natural Frequencies for Machining Operations for Breadth Centre Fixturing of Part 2

The second harmonic for breadth-side fixturing, shown in figure 4.28, results in a billet frequency 11109 Hz. The breadth-side-A fixturing, shown in blue, starts at 9993 Hz for operation 1, and then decreases to 9217 Hz for operation 2. Operation 4 increases the frequency to 9505 Hz, after which it decreases to 9443 Hz at operation 5. Breadth-side-B fixturing, shown in orange, starts at 9975 Hz for operation 1. It then decreases to 8572 Hz at operation 2, and increases to 8603 Hz for operation 5.

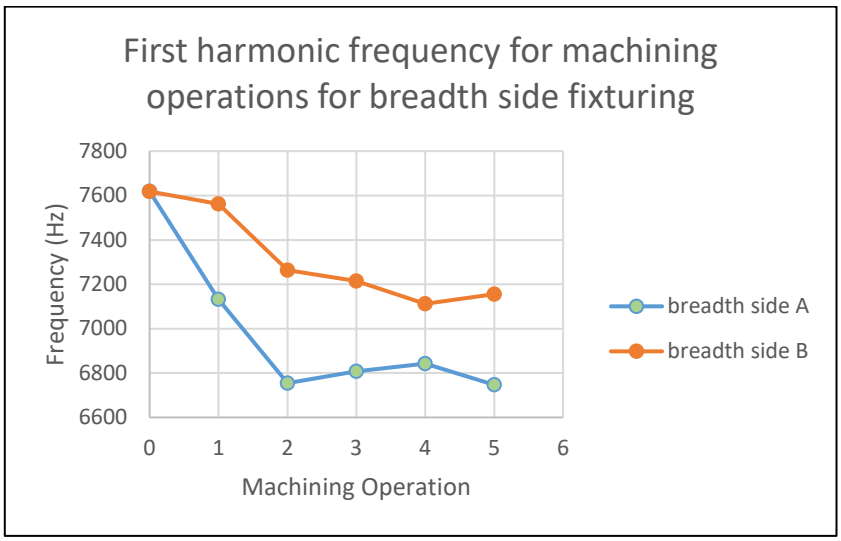

Figure 4.28 Natural Frequencies for Machining Operations for Breadth side Fixturing of part 2

The second harmonic for length-centre fixturing, shown in figure 4.29, starts at 12217 Hz for the billet. It then decreases through 10956 Hz for operation 1, to 10275 Hz for operation 2. The three holes cut increase the frequency slightly to 10340 Hz at operation 5.

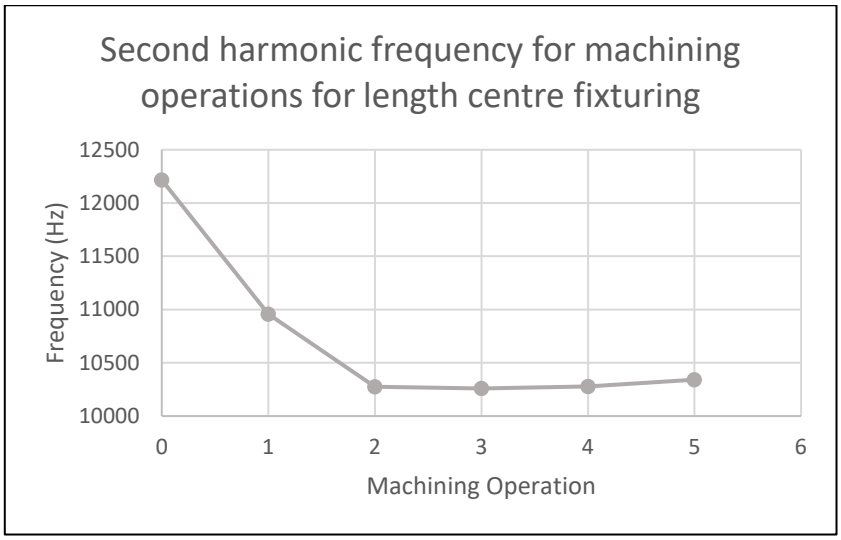

Figure 4.29 Natural Frequencies for Machining Operations for Length Centre Fixturing of Part 2

The second harmonic frequency for length-side fixturing, shown in figure 4.30, starts at 10035 Hz for the billet. The length-side-A fixturing, shown in blue, starts at 9553 Hz for operation 1. It then decreases through 9169 Hz for operation 2, and increases to 9244 Hz for operation 5. Operation 5 bring the frequency down to 8587 Hz. Length-side-B fixturing, shown in orange, starts at 9612 Hz for operation 1. It then decreases to 8515 Hz at operation 2, and increases to 9413 Hz for operation 5.

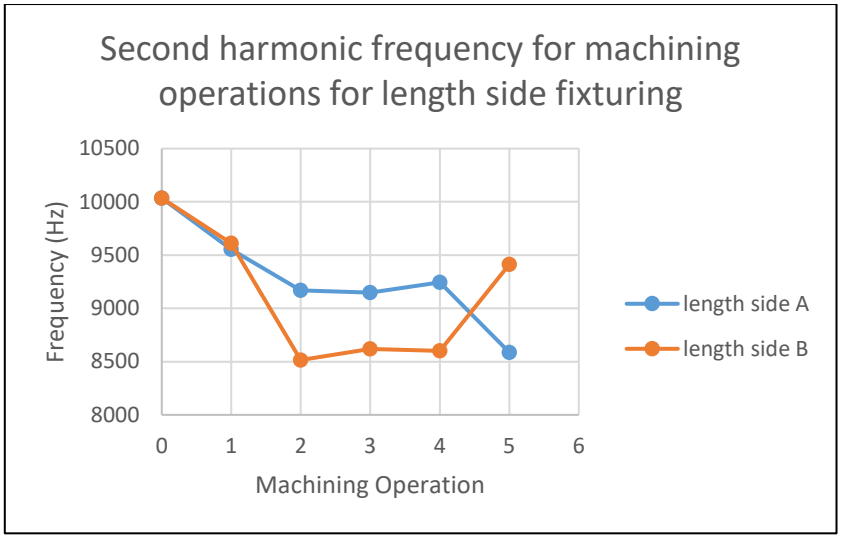

Figure 4.30 Natural Frequencies for Machining Operations for Length Side Fixturing of Part 2

4.5.2.3 Third Harmonic

The third harmonic frequency for breadth-centre fixturing, shown in figure 4.31, starts at 15260 Hz for the billet. It then decreases linearly to 12424 Hz at operation 2. The three holes cut increase the frequency slightly to 12472 Hz at operation 5.

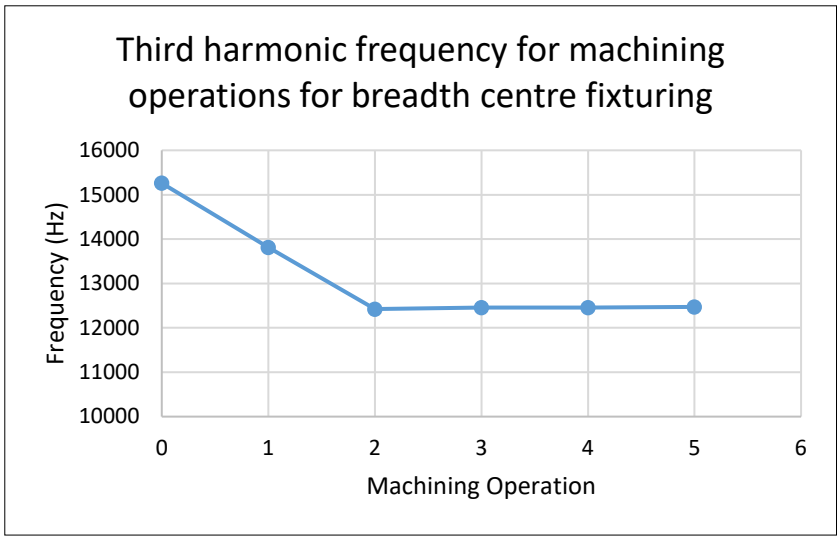

Figure 4.31 Natural Frequencies for Machining Operations for Breadth Centre Fixturing of Part 2

The third harmonic frequency for breadth-side fixturing, shown in figure 4.32, starts at 13232 Hz for the billet. The breadth-side-A fixturing, shown in blue, starts at 12914 Hz for operation 1. It then decreases to 12182 Hz for operation 2 and ends at 12018 Hz for operation 5. Breadth-side-B fixturing, shown in orange, starts at 12678 Hz for operation 1. It then decreases through 11944 Hz at operation 2 to 11581 Hz for operation 5.

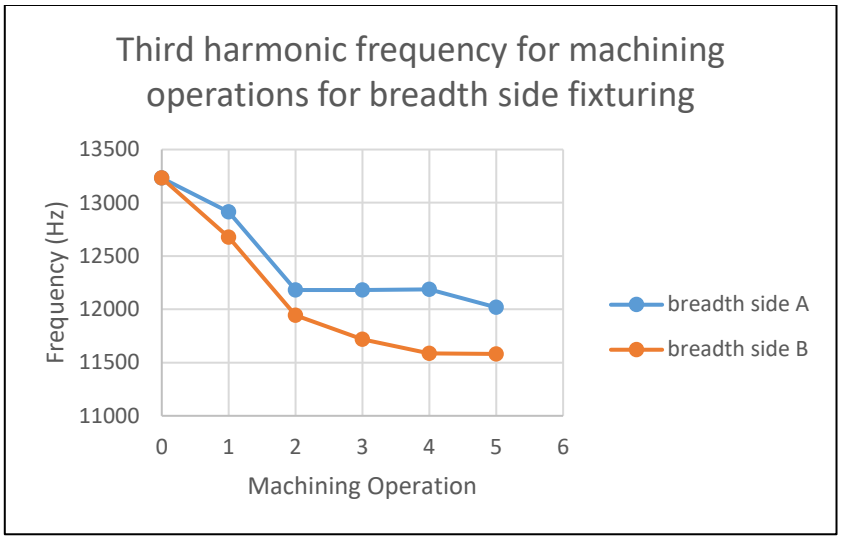

Figure 4.32 Natural Frequencies for Machining Operations for Breadth side Fixturing of part 2

The third harmonic frequency for length-centre fixturing, shown in figure 4.33, starts at 12391 Hz for the billet. It then decreases though 11535 Hz for operation 1, to 10884 Hz for operation 2. The three holes cut increase the frequency to 11116 Hz at operation 5.

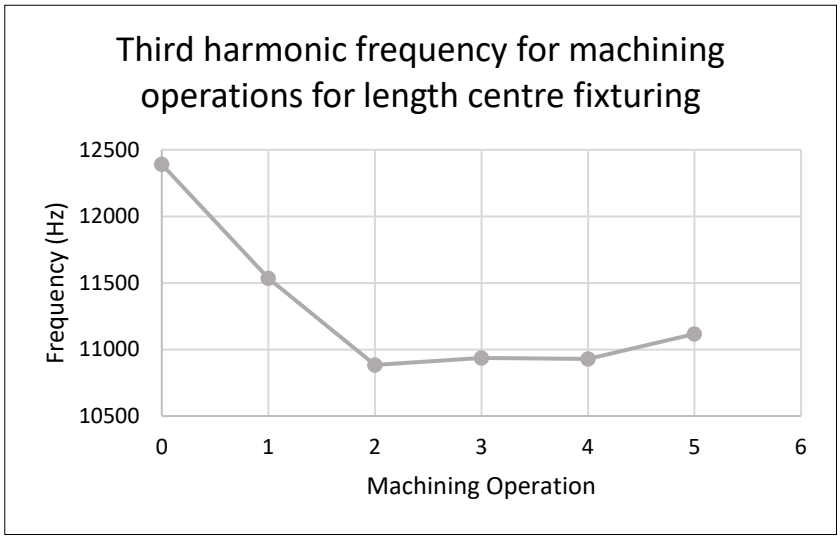

Figure 4.33 Natural Frequencies for Machining Operations for Length Centre Fixturing of Part 2

The third harmonic frequency for length-side fixturing, shown in figure 4.34, starts at 13022 Hz for the billet. The length-side-A fixturing, shown in blue, starts at 13974 Hz for operation 1 and then decreases to 12116 Hz for operation 2. Operation 3 decreases the frequency to 12059 after which the harmonic increases to 12644 Hz for operation 5. Length-side-B fixturing, shown in orange, increases from the billet frequency to 13061 Hz for operation 1. It then decreases through 12696 Hz at operation 2 to 12282 Hz for operation 5.

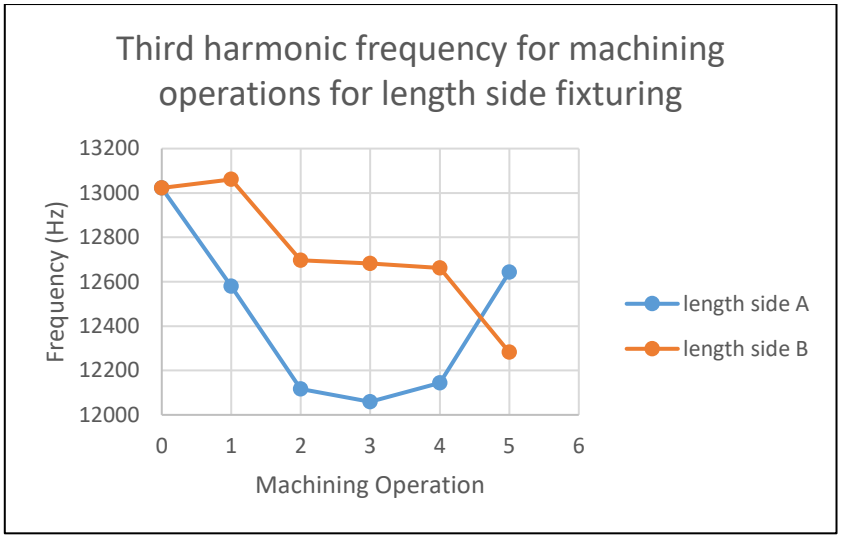

Figure 4.34 Natural Frequencies for Machining Operations for Length Side Fixturing of Part 2

4.5.2.4 Fourth Harmonic

The fourth harmonic frequency for breadth-centre fixturing, shown in figure 4.35, starts at 16150 Hz for the billet. It then decreases to 15382 Hz for operation 1 and 14860 Hz for operation 2. The three holes increase the frequency to 15080 Hz at operation 5.

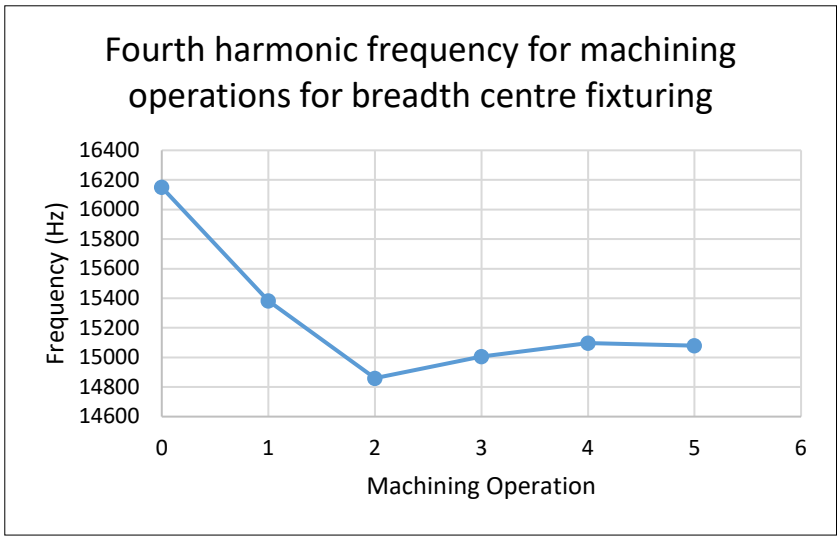

Figure 4.35 Natural Frequencies for Machining Operations for Breadth Centre Fixturing of Part 2

The fourth harmonic frequency for breadth-side fixturing, shown in figure 4.36, starts at 13883 Hz for the billet. The breadth-side-A fixturing, shown in blue, starts at 13563 Hz for operation 1. It then decreases to 13309 Hz for operation 2 and increases to 13580 at operation 4. Operation 5 decreases the harmonic to 13545 Hz. Breadth-side-B fixturing, shown in orange, starts at 13989 Hz for operation 1. It then decreases through 13825 Hz at operation 2, to 13773 Hz at operation 4, after which it increases to 13925 Hz for operation 5.

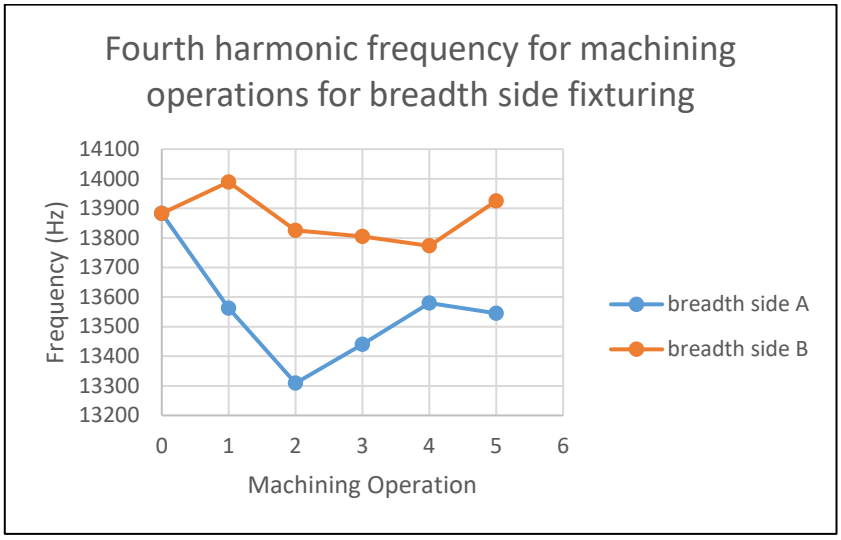

Figure 4.36 Natural Frequencies for Machining Operations for Breadth side Fixturing of part 2

The fourth harmonic frequency for length-centre fixturing, shown in figure 4.37, starts at 12533 Hz for the billet. It then decreases through 11679 Hz at operation 1, to 11313 Hz at operation 2. The three holes increase the frequency to 11628 Hz.

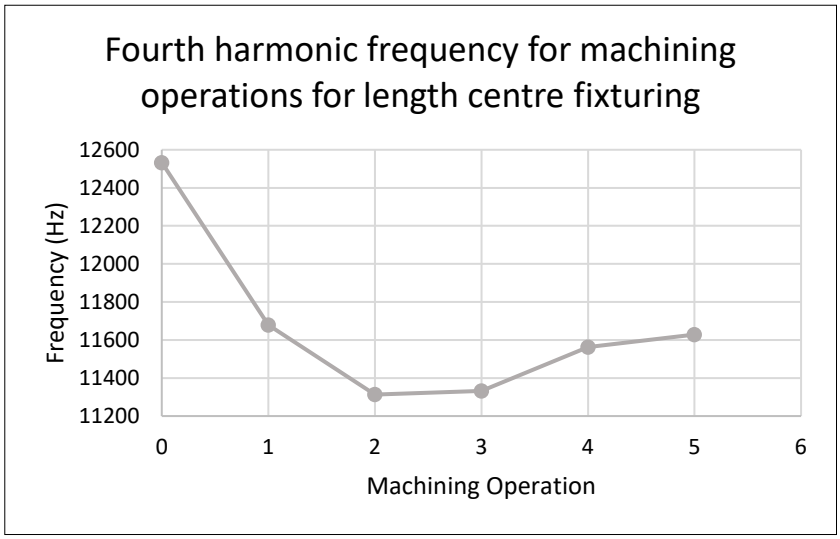

Figure 4.37 Natural Frequencies for Machining Operations for Length Centre Fixturing of Part 2

The fourth harmonic frequency for length-side fixturing, shown in figure 4.38, starts at 14652 Hz for the billet. The length-side-A fixturing, shown in blue, starts at 13974 Hz for operation 1. It then decreases to 13515 Hz for operation 2, and further to 13099 Hz for operation 5. Length-side-B fixturing, shown in orange, decreases from the billet frequency to 13970 Hz for operation 1. It decreases further to 13001 Hz for operation 2, and increases to 13511 Hz for operation 5.

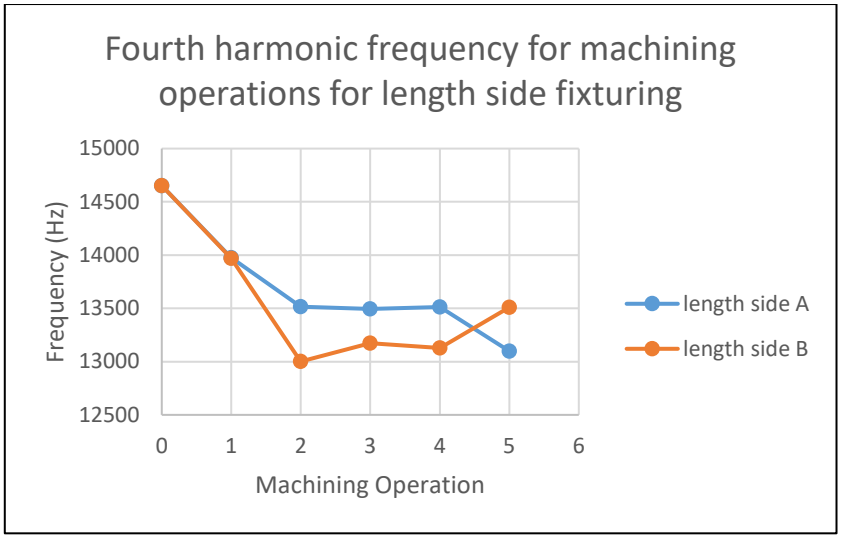

Figure 4.38 Natural Frequencies for Machining Operations for Length Side Fixturing of Part 2

4.5.2.5 Fifth Harmonic

The fifth harmonic frequency for breadth-centre fixturing, shown in figure 4.39, starts at 17802 Hz for the billet. It then increases to 18270 Hz for operation 1, and decreases to 17951 Hz for operation 2. The machining of the three holes brings the frequency to 17999 Hz at operation 5.

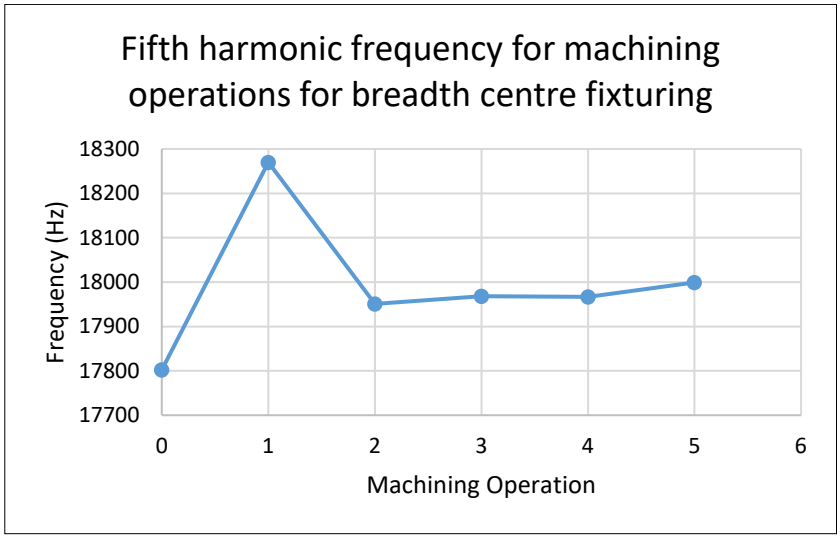

Figure 4.39 Natural Frequencies for Machining Operations for Breadth Centre Fixturing of Part 2

The fifth harmonic frequency for breadth-side fixturing, shown in figure 4.40, starts at 17629 Hz for the billet. The breadth-side-A fixturing, shown in blue, starts at 16715 Hz for operation 1. It then decreases to 17951 Hz for operation 2 and increases to 17999 Hz for operation 5. Breadth-side-B fixturing, shown in orange, starts at 15690 Hz for operation 1. It then decreases to 14531 Hz at operation 2, and increases to 14631 Hz for operation 5.

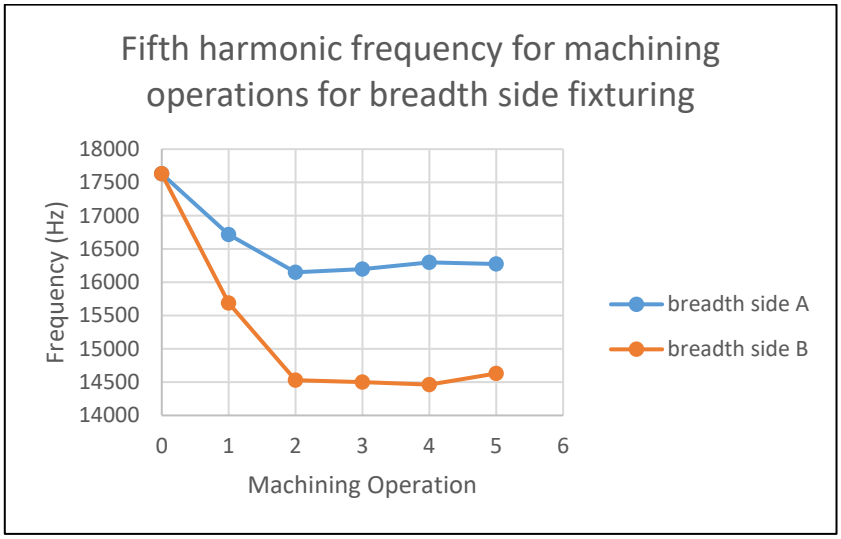

Figure 4.40 Natural Frequencies for Machining Operations for Breadth side Fixturing of part 2

The fifth harmonic frequency for length-centre fixturing, shown in figure 4.41, starts at 16371 Hz for the billet. It then decreases through 16243 Hz at operation 1, to 16125 Hz for operation 2. The machining of the three holes increases the frequency to 16326 Hz at operation 5.

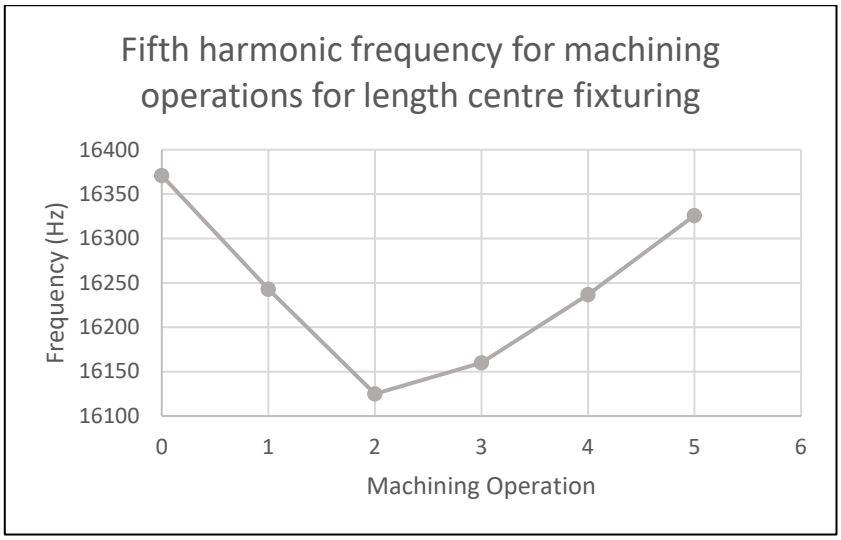

Figure 4.41 Natural Frequencies for Machining Operations for Length Centre Fixturing of Part 2

The fifth harmonic frequency for length-side fixturing, shown in figure 4.42, starts at 17267 Hz for the billet. The length-side-A fixturing, shown in blue, increases from the billet frequency to 17374 Hz for operation 1. It then decreases to 17152 Hz for operation 2, and further to 17079 Hz at operation 4. Operation 5 decreases the harmonic drastically to 15499 Hz. Length-side-B fixturing, shown in orange, increases from the billet frequency to 17310 Hz for operation 1, and decreases to 15607 Hz for operation 2. From operation 4 the harmonic increases greatly to 17136 Hz for operation 5.

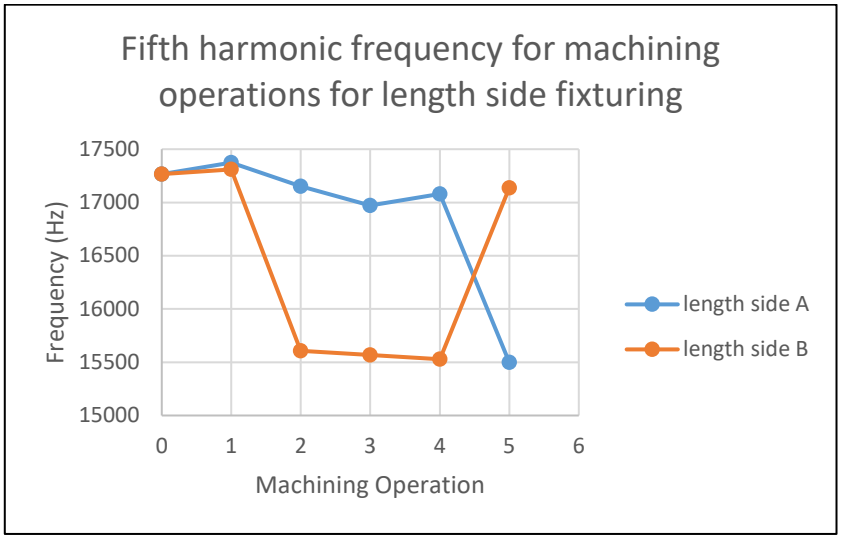

Figure 4.42 Natural Frequencies for Machining Operations for Length Side Fixturing of Part 2

4.6 Order of Part Feature Machining

This section presents the simulation results for changing the order of part features for part 1, such that the holes are machined before the slots. This investigation was a result of observations that in several instances the machining of the holes increased the natural frequency of part 1. The aim of the simulations is twofold; to determine if machining the holes (operations 3 to 6) before the slots (operations 1 and 2) improve the natural frequency response of part 1, and to determine if the effect of the operation on natural frequency are independent of each other. The new simulation data is plotted with the original machining-order simulation data, to illustrate the effect of the order change. In each graph the two simulations share the billet frequency and the final operation 6 frequency, which are the first and final states of both machining routes.

4.6.1 Graphs for Part 1

For each of the graphs: The blue data represents the original machining order, where the central slots are machined first as operations 1 and 2, and the holes are machined afterwards as operations 3 to 6. The orange data points represent the rearranged machining operations where the 4 holes are cut first as operations 1 to 4, and the 2 slots are machined last as operations 5 and 6. Simulations were performed for all fixture setups of Part 1 mode 1.

The two data sets for breadth-centre fixturing are featured in figure 4.43. The rearranged machining order, in blue, shows the four holes decreasing the natural frequency linearly, the same as in the original simulation. The machining of the first slot increases the frequency, after which the frequency decreases to 8009 Hz at operation 6.

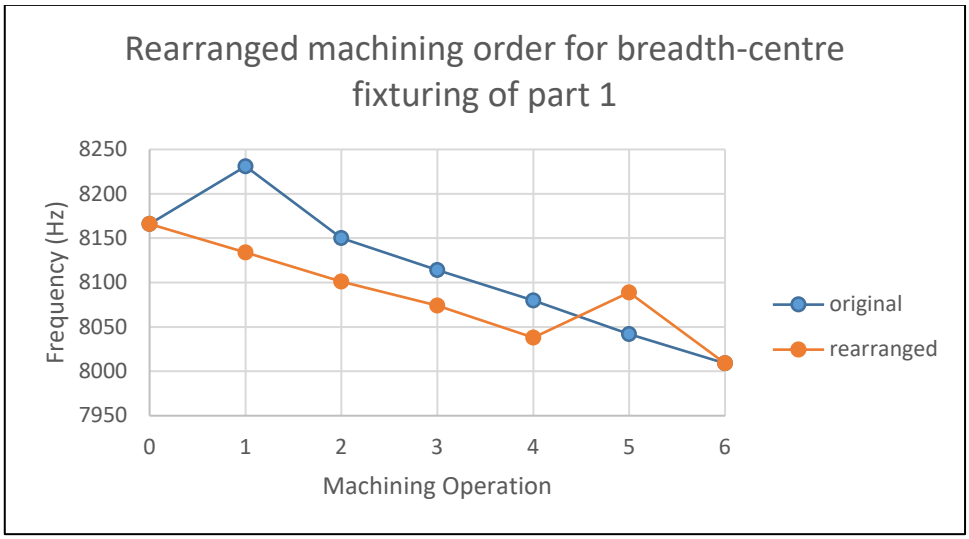

Figure 4.43 Rearranged machining order for first harmonic frequency for breadth centre fixturing

Figure 4.44 shows the first-harmonic frequencies for the rearranged machining order for breadth-side fixturing, plotted against the original frequencies. The first two holes increase the natural frequency to 7715 Hz, whereas holes 3 and 4 decrease the frequency to 7453 Hz. The machining of the slots further decreases the frequency, similar to the original machining order, to a final frequency of 6913 Hz at operation 6.

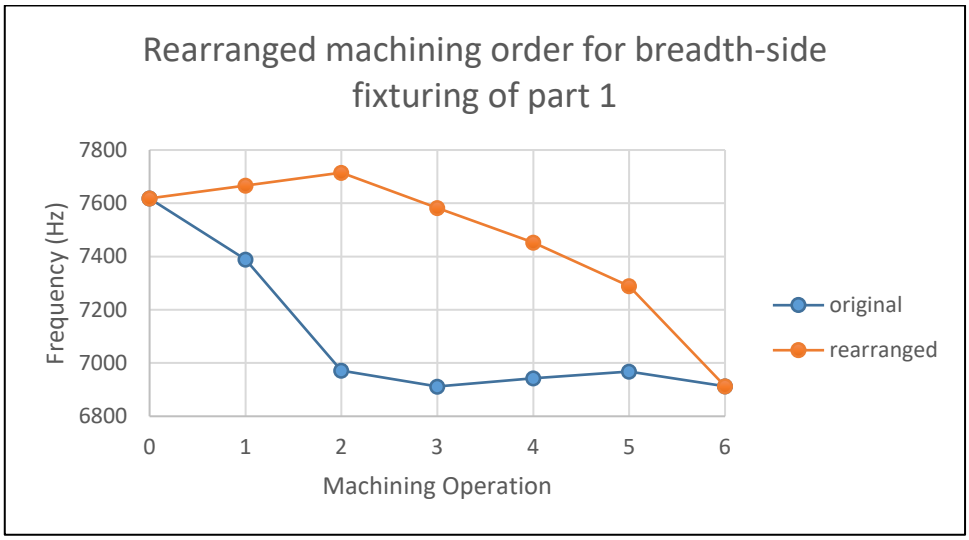

Figure 4.44 Rearranged machining order for first harmonic frequency for breadth side fixturing

The graph of the first-harmonic frequencies for the rearranged machining order for length-centre fixturing is shown in figure 4.45. The four holes increase the natural frequency linearly to 10851 Hz. The machining of the slots decreases the frequency, similar to the original machining order, to a final frequency of 9954 Hz at operation 6.

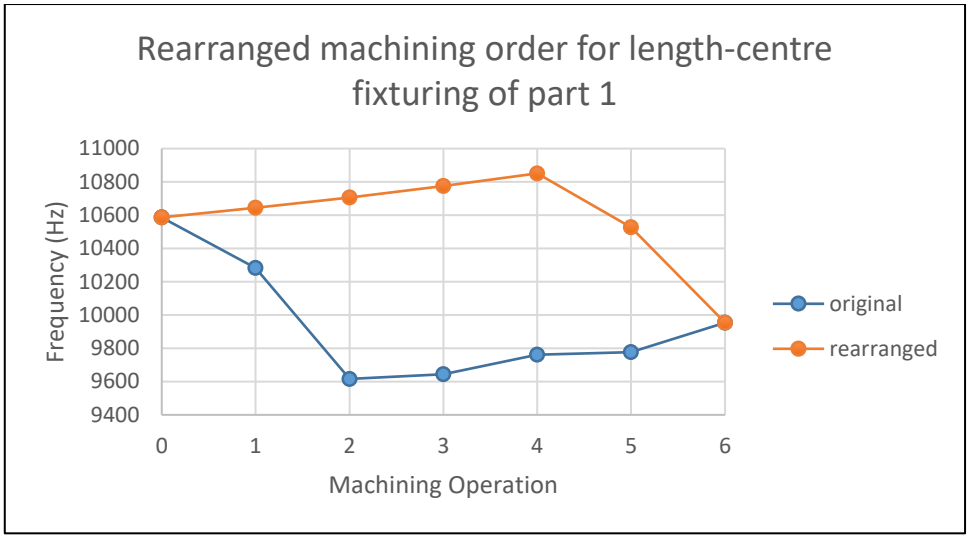

Figure 4.45 Rearranged machining order for first harmonic frequency for length centre fixturing

Figure 4.46 shows the graph of the first-harmonic frequencies of the rearranged machining order for length-side fixturing. The four holes increase the natural frequency slightly to 7063 Hz. The machining of the slots decreases the frequency, similar to the original machining order, to a final frequency of 5609 Hz at operation 6.

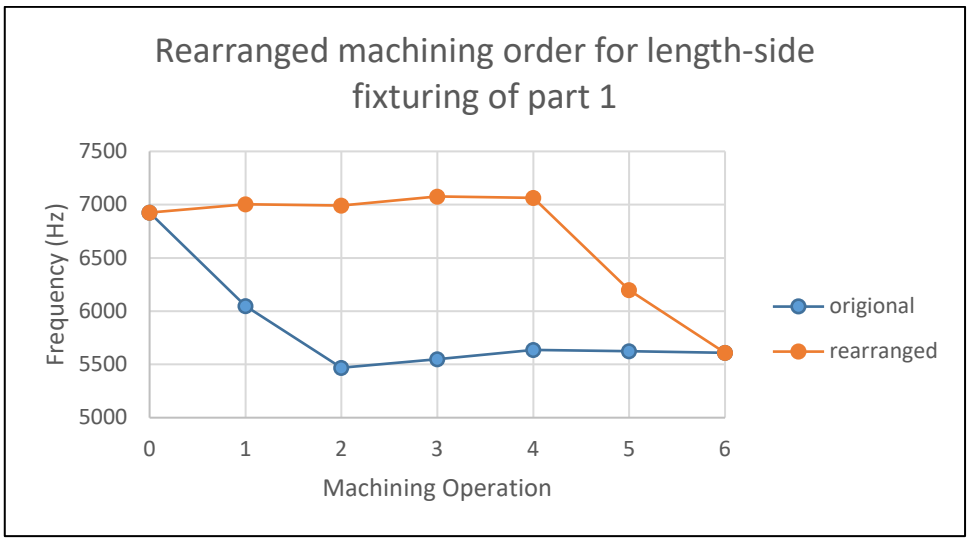

Figure 4.46 Rearranged machining order for first harmonic frequency for length side fixturing

4.7 Chapter Summary

Chapter 4 showed that mesh independence was reached with a mesh size of 1.5mm. The simulations revealed a strong correlation between the natural frequency of the part and both material removal and fixturing position. The results summarised in table 4.1 and table 4.2 illustrated the fixturing setups that produced the highest natural frequency for each operation, and revealed that the breadth-centre fixture setup performed best overall for both part 1 and part 2. The natural frequency graphs showed that similar trends exist in breadth-centre and length-centre fixturing for part 1 and 2. Simulation results for part 1 with the operation orders rearranged showed that the frequency response can be improved for certain fixture setups.

Chapter 5: Modal Frequency Verification

5.1 Chapter Introduction

This chapter presents the experimental analysis of the natural frequencies of the control parts as verification for the simulation results. The parts machined for experimental testing are specified, as well as all fixturing positions implemented. A load cell clamp assembly is outlined, followed by the vibration testing equipment used and the physical setup of the AFFS. The procedure employed in testing and the experimental results are then specified.

5.2 Parts for Testing

Material restrictions required the number of test parts to be minimized for the experimental analysis. It was anticipated that the dampening of the system would reduce the resolution of the resonant frequencies. The small changes in the resonant frequencies between the four holes would become immeasurable due to the dampening. Thus, the test parts included one part with all four holes machined. The billets that were machined for testing are illustrated in figure 5.1 and figure 5.2 for part 1 and 2 respectively. The parts shown in the figures are the first two machining operations for the initial bores, and the final machining operation with all holes machined.

Figure 5.1 Part 1 Workpieces

Figure 5.2 Part 2 Workpieces

5.3 Load Cell Assembly

The purpose of the load cell assembly was to provide a means of monitoring the clamping forces in order to keep them constant throughout the experimental testing. The clamping force is related to the dampening effect of the AFFS, therefore the force must remain constant to ensure the measurements integrity.

The pin matrix clamp did not function as desired due to design simplifications and manufacturing errors. The clamping arms were redesigned to incorporate load cells to measure the clamping force, keeping the original contact surface size of the pin matrix clamp. Figure 5.3 illustrates the components of the load cell assembly through a cad assembly. The assembly shows (a) the bracket that mounts the load cell to the existing mounts on the AFFS (b) the load cell and (c) the clamping surface mount. The CSM has a clamping surface equal in area to the pin matrix clamping surface. That CMS remains parallel with the part due to its rotary joint, keeping full surface contact with the part. The force sensors available were 20 kg cantilever wheat-stone bridge load cells. Any force greater than 20 kg exerted on the load cell will damage it. To avoid this from occurring during testing the clamping force was kept at 15 kg.

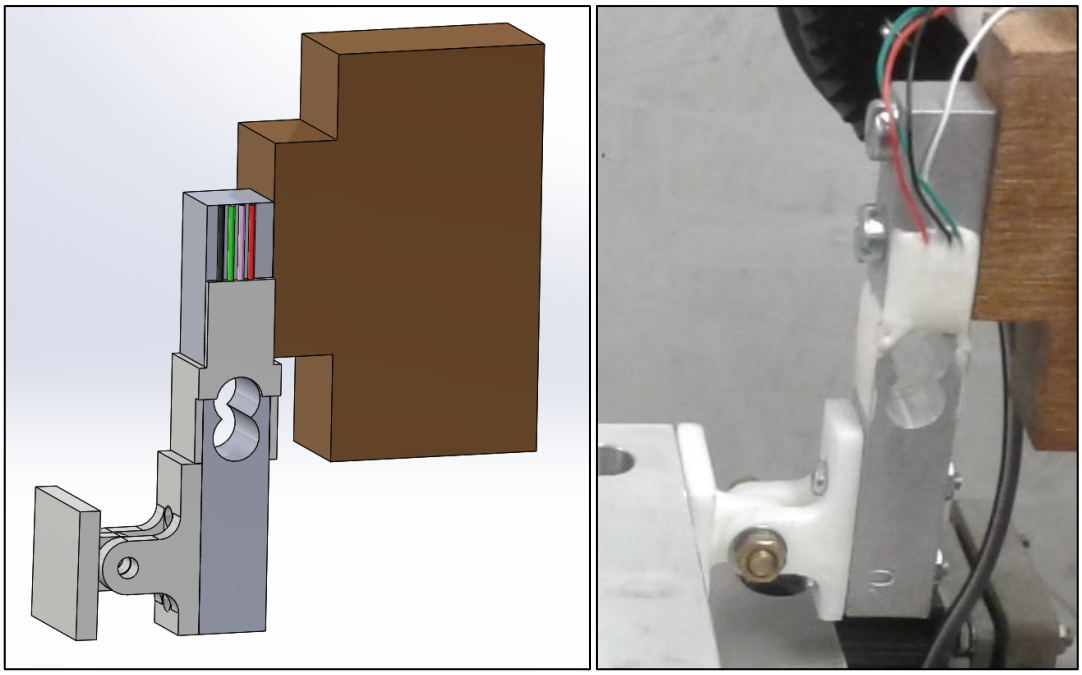

(a) (b)

Figure 5.3 (a) Load cell model (b) Load cell physical assembly

The three components used in to measure the clamping force are the Arduino Uno, load cell and HX711 amplifier, illustrated in figure 5.4. The Hx711 was required to amplify the load cell signal and convert it to a digital signal.

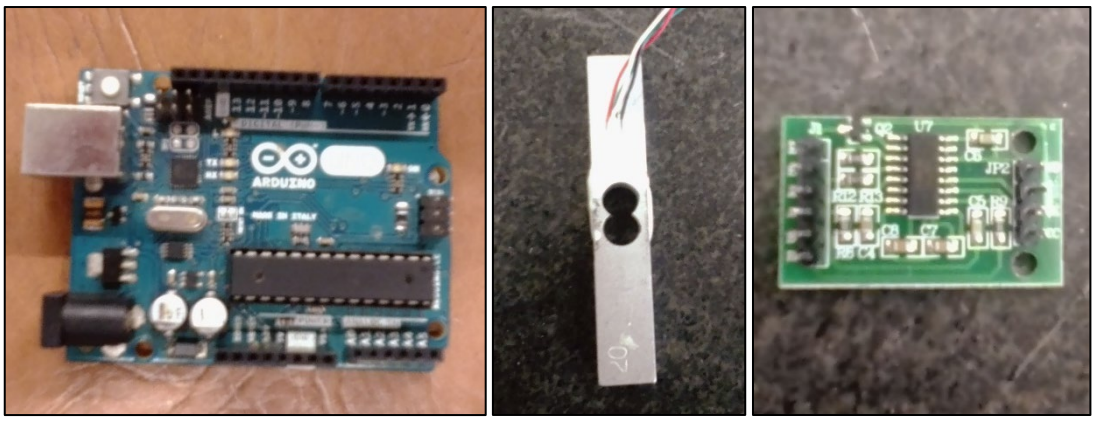

(a) (b) (c)

Figure 5.4 (a) Arduino uno (b) Load cell (c) HX711 amplifier

Figure 5.5 shows the wiring diagram for the load cells. The Arduino supplied power to the amplifiers which powered the load cells. The analogue load cell signals were retrieved from the amplifiers as digital signals and read from analogue pins 5 and 6 on the Arduino. The Arduino code used to calculate and display the two Force readings is shown in appendix.

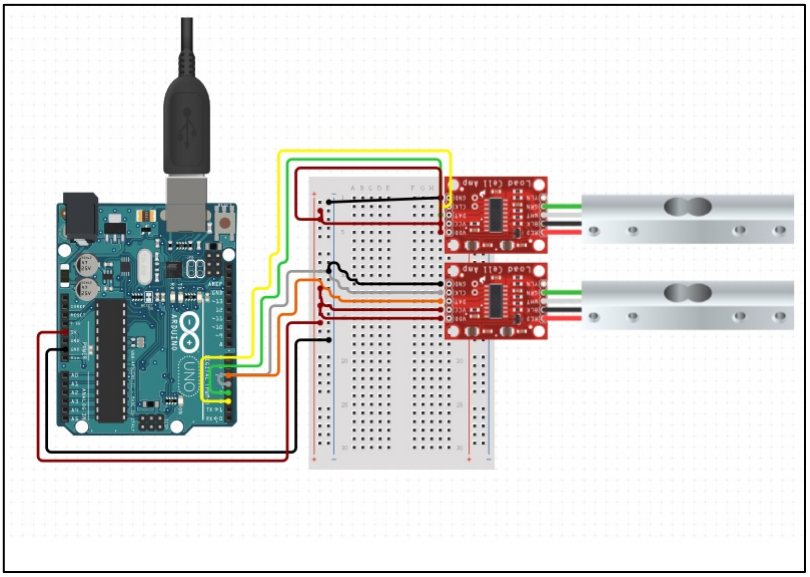

Figure 5.5 Load cell wiring diagram

The load cells were calibrated using weights illustrated in figure 5.6. The weights were added in increments to ensure that the load cell was measuring accurately across its range.

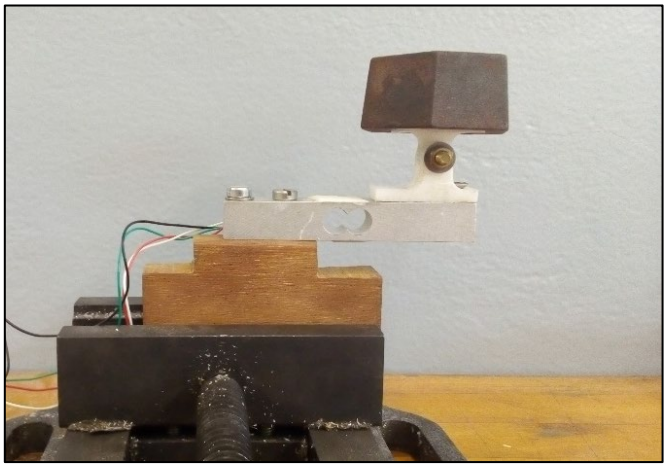

Figure 5.6 Load cell calibration setup with calibration weight

With no load applied the loadcell reading from the Arduino was 8385700. A mass of 200 grams gave a digital reading of 8406200 on the load cell. A mass of 500 grams gave a reading of 8436950 on the load cell. A simple calculation using the no load signal and the applied mass signal gave a calibration factor of 102.5. The equation below was formulated to give a reading in grams from the digital signal.

$$Mass = \frac{val - 8385700}{102.5} \tag{5.1}$$

The 'val' function in the equation represents the digital signal measured by the Arduino, the 8385700 value is the no load reading and 102.5 is the calibration factor.

5.4 Ni DAQ

The vibration signals were measured with National Instruments Data Acquisition (NI-DAQ) hardware, shown in figure 5.7 (a). The accelerometer used, shown in figure 5.7 (a), had a 1 – 20000 Hz frequency range and a sensitivity of 10 $mV/m.s^{-2}$. The accelerometer was tested using a Bruel & Kjaer accelerometer calibrator that vibrates at a constant frequency of 159.15 Hz. The accelerometer was held against the calibrator to test its accuracy and sensitivity. The measured frequency of the accelerometer was 159.15 Hz, confirming the accuracy of the accelerometer. The accelerometer was mounted to the parts using an adhesive. The adhesive technique allowed the accelerometer position to be adjusted without removing material from the part, which is required for a fixed mounting. An impact hammer, figure 5.7 (c), was used to excite the part in its clamped position for the frequency measurements. The analogue signal from the accelerometer was converted the frequency spectrum by applying a Fast Fourier Transform function in LabVIEW. The impact hammer signal was monitored to ensure all measurements were taken using the same impact force. Appendix B contains the LabVIEW code that was used to generate the frequency graphs.

(a) (b) (c)

Figure 5.7 (a) NI-DAQ (b) Accelerometer (c) Impact hammer

5.5 Final Experimental Assembly

The load assembly was fixed to the AFFS using the mounting points for the previously removed pin matrix clamp, illustrated in figure 5.9. Figure 5.8 illustrates the acceleromter attached to part 1, which is clamped in the AFFS.

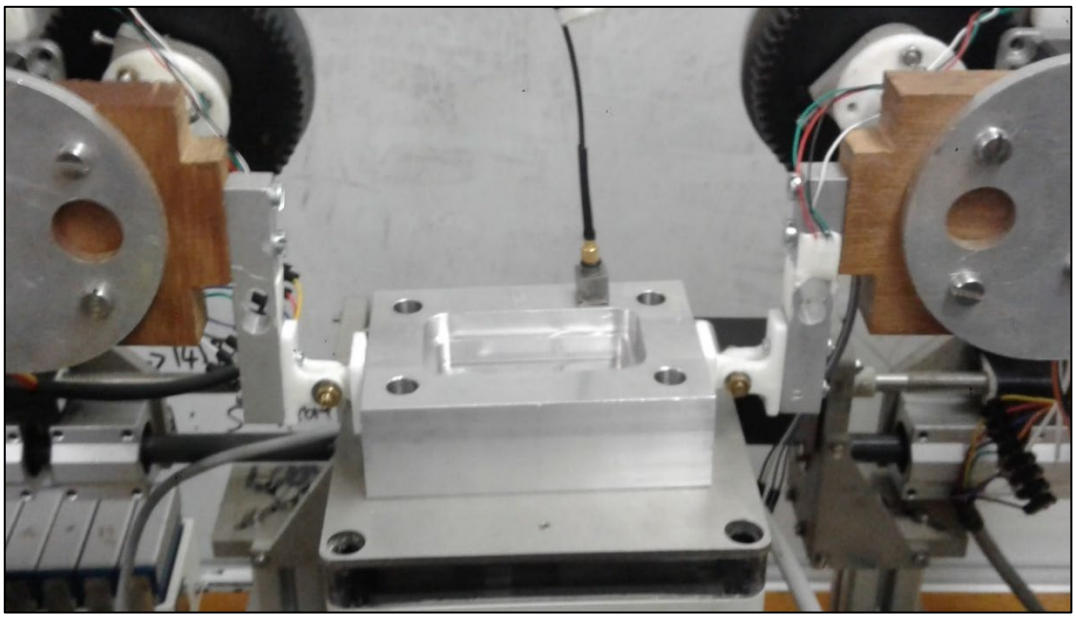

Figure 5.8 Part 1 fixtured on the fixture bed with accelerometer attached

The part was fixed between the load cells with a force of 150 N or 15000 grams measured from the Arduino. The fixture arms were moved in and out of position by controlling the stepper motors. The Parallel gripper was controlled using the servo motor.

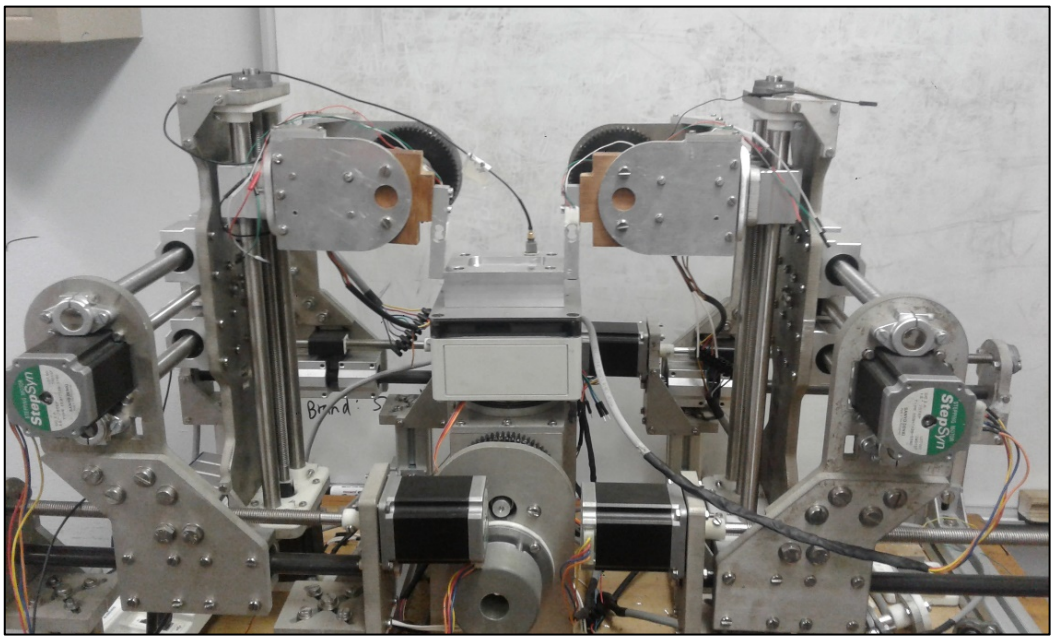

Figure 5.9 Part 1 fixtured in the AFFS

5.6 Frequency Response Experimental Procedure

5.6.1 Aim

The aim of the testing is to measure the acceleration of each control part under various fixturing positions to determine the parts natural frequency for that fixture setup.

5.6.2 Objectives

- Measure the acceleration of each part under all specified fixturing position
- Determine the natural frequencies of the part for each specific fixturing position

5.6.3 Procedure

- Place control part onto two-finger locater
- Tighten two-finger locater using servo motor
- Position clamping surfaces correctly relative to part for fixturing position
- Move clamping surfaces onto part until clamping force of 15kg is achieved
- Fasten accelerometer in position on part
- Induce vibration by exciting part with impact hammer until force of 5kg achieved
- Record z-axis acceleration with accelerometer
- Read the modal frequencies from the FFT LabVIEW frequency graph
- Repeat for each part

5.7 Frequency Response Results for Part 1

5.7.1 Part 1 Operation 1

Part 1 operation 1 is a symmetric part, with a single rectangular bore in its centre. It was fixed along its breadth on the side surface at both the centre and far corner, as well as along its length on the side surface at both the centre and far corner. The results of the frequency tests of this part for each fixturing setup are recorded and discussed in this section.

Figure 5.10 shows the frequency response of the knock test for part 1 operation 1 under breadth-centre fixturing. The natural frequencies for the first three modes visible in the graph are 85Hz, 165Hz, and 250Hz respectively.

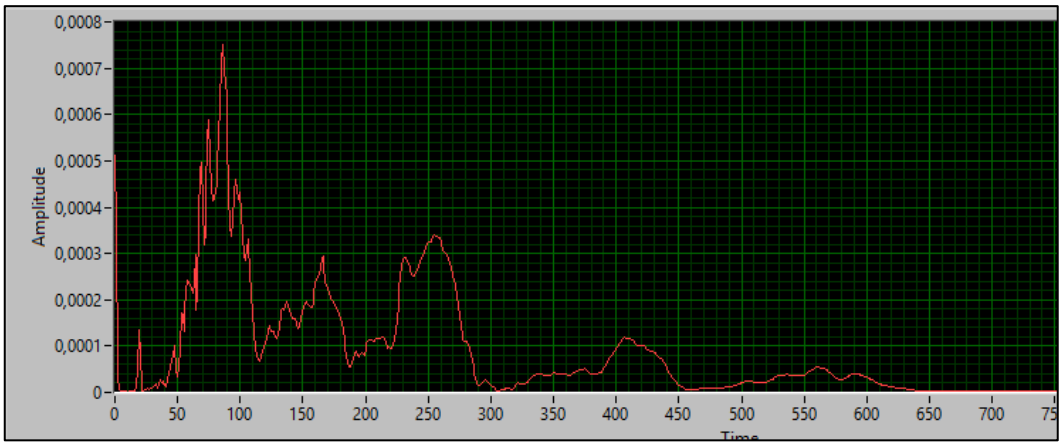

Figure 5.10 Natural Frequencies of Part 1 Operation 1 for Breadth-Centre Fixturing

Figure 5.11 shows the frequency response of the knock test for part 1 operation 1 under breadth-side fixturing. The natural frequencies for the first three modes visible in the graph are 60Hz, 120Hz, and 230Hz respectively.

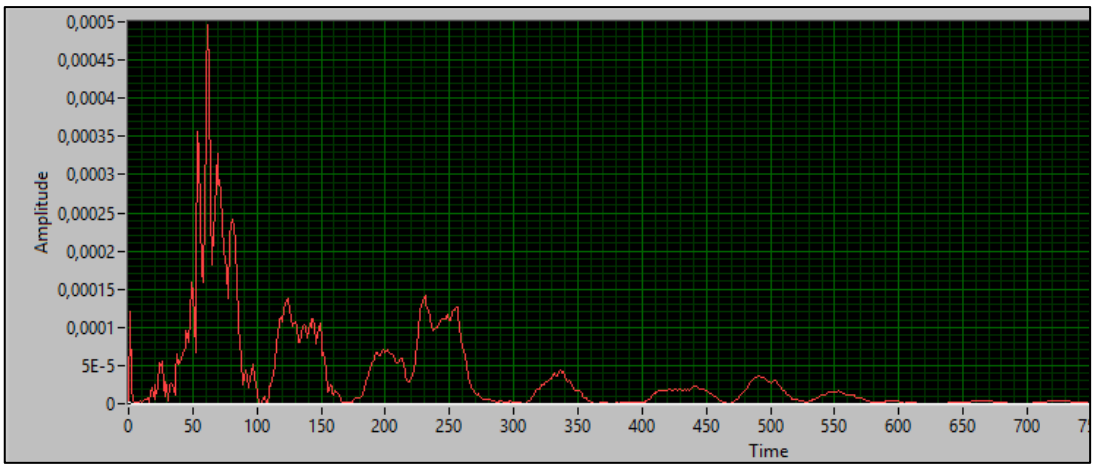

Figure 5.11 Natural Frequencies of Part 1 operation 1 for breadth side fixturing

Figure 5.12 shows the frequency response of the knock test for part 1 operation 1 under length-centre fixturing. The natural frequencies for the first three modes visible in the graph are 48Hz, 115Hz, and 168Hz respectively.

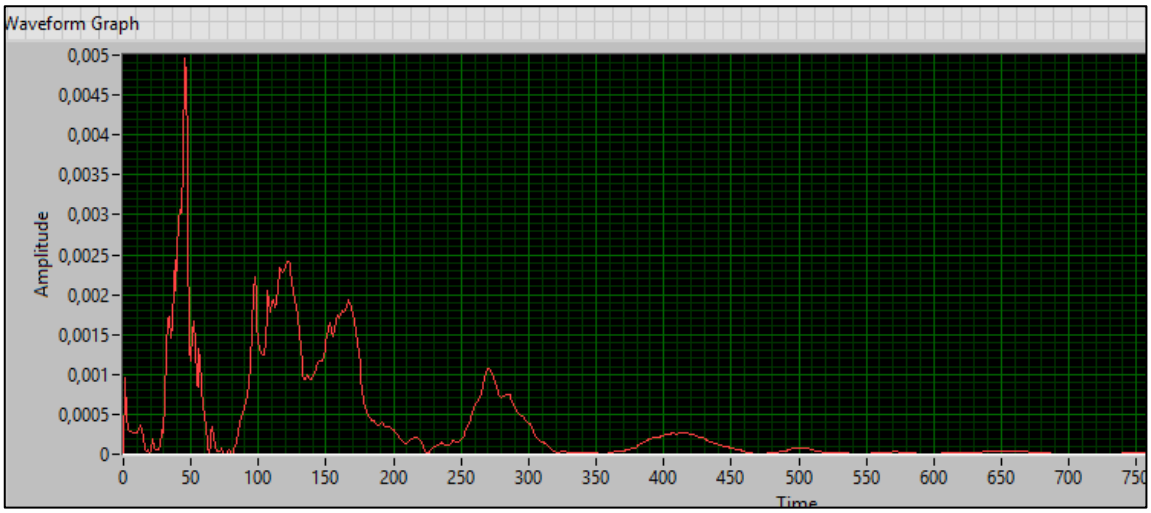

Figure 5.12 Natural Frequencies of Part 1 Operation 1 for Length-Centre Fixturing

Figure 5.13 shows the frequency response of the knock test for part 1 operation 1 under length-side fixturing. The natural frequencies for the first three modes visible in the graph are 40Hz, 85Hz, and 120Hz respectively.

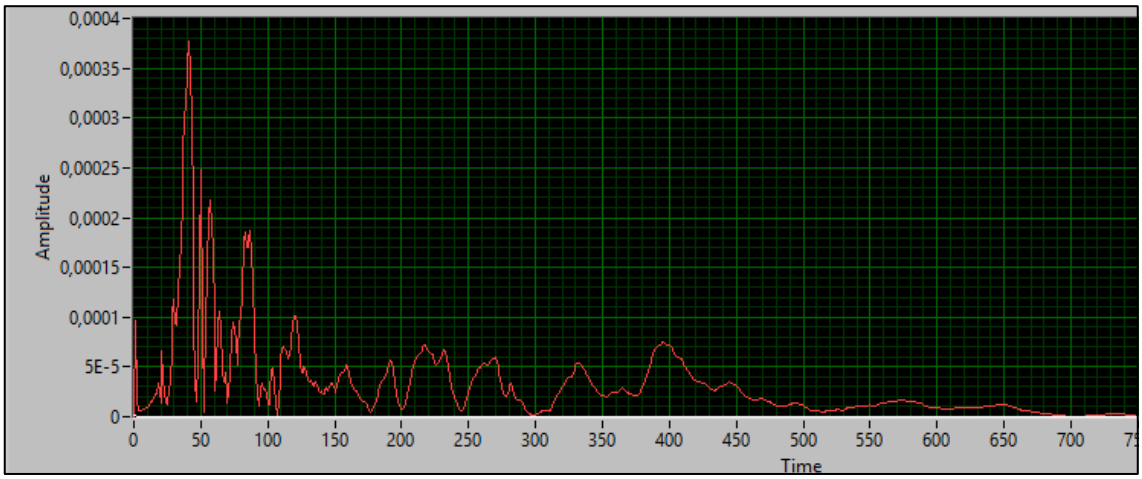

Figure 5.13 Natural Frequencies of Part 1 Operation 1 for Length-Side Fixturing

5.7.1.1 Analysis of Part 1 Operation 1 Results

The experimental results for part 1 operation 1 are organized in table 5.1.

Table 5.1 Natural frequencies for part 1 operation 1

Fixturing	Mode 1	Mode 2	Mode 3
Breadth centre	85	165	250
Breadth side	60	120	230
Length centre	48	115	168
Length side	40	85	120

5.7.2 Part 1 Operation 2

Part 1 operation 2 is a symmetric part, with two countersunk rectangular bores in its centre. It was fixed along its breadth on the side surface at both the centre and far corner, as well as along its length on the side surface at both the centre and far corner. The results of the frequency tests of this part for each fixturing setup are recorded and discussed in this section.

Figure 5.14 shows the frequency response of the knock test for part 1 operation 1 under breadth-centre fixturing. The natural frequencies for the first two modes visible in the graph are 110Hz, and 240Hz respectively. The third mode appears to be around 525hz, dismissing the peak at 330hz as an irregularity caused by the fixture. This frequency falls out of the spectrum of expected frequencies that could reasonable be the third mode, thus the final mode from the graph is indecisive.

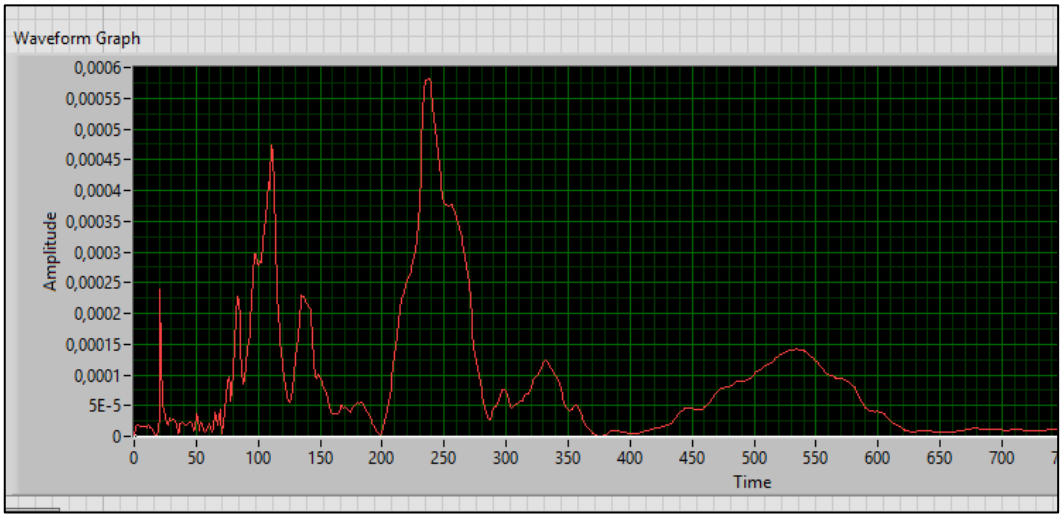

Figure 5.14 Natural Frequencies of Part 1 Operation 2 for Breadth-Centre Fixturing

Figure 5.15 shows the frequency response of the knock test for part 1 operation 1 under breadth-side fixturing. The natural frequencies for the first three modes visible in the graph are 110Hz, 150Hz, and 230Hz respectively.

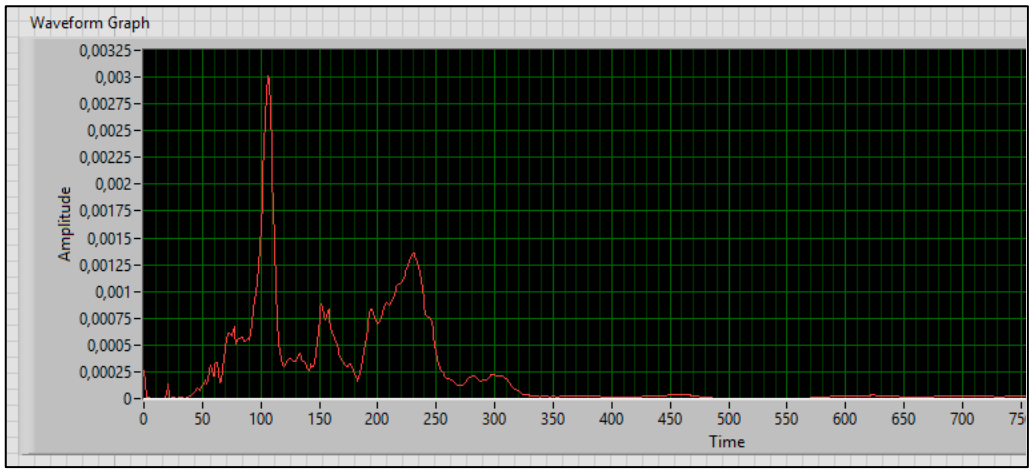

Figure 5.15 Natural Frequencies of Part1 Operation 2 for Breadth-Side Fixturing

Figure 5.16 shows the frequency response of the knock test for part 1 operation 1 under length-centre fixturing. The natural frequencies for the first three modes visible in the graph are 60Hz, 110Hz, and 175Hz respectively.

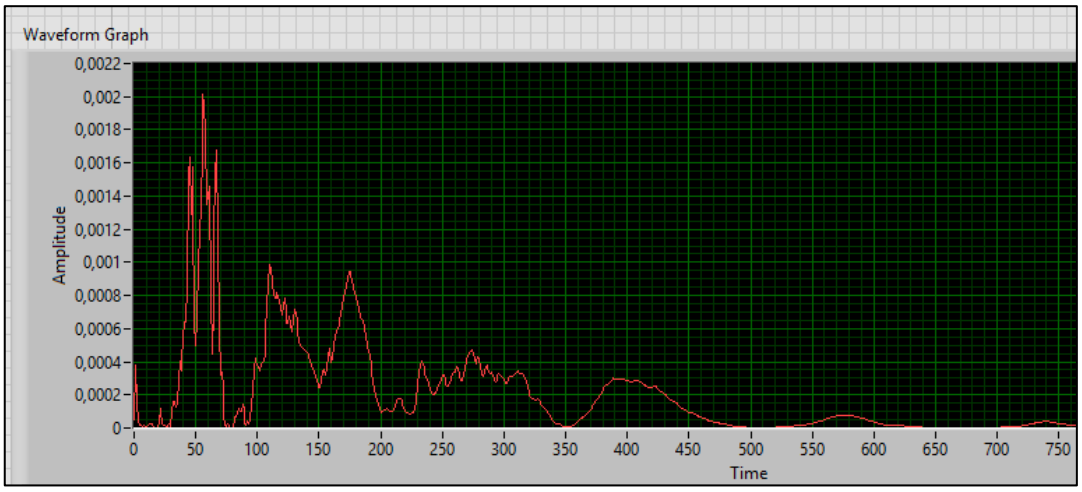

Figure 5.16 Natural Frequencies of Part 1 Operation 2 for Length-Centre Fixturing

Figure 5.17 shows the frequency response of the knock test for part 1 operation 1 under length-side fixturing. The natural frequencies for the first three modes visible in the graph are 40Hz, 60Hz, and 100Hz respectively.

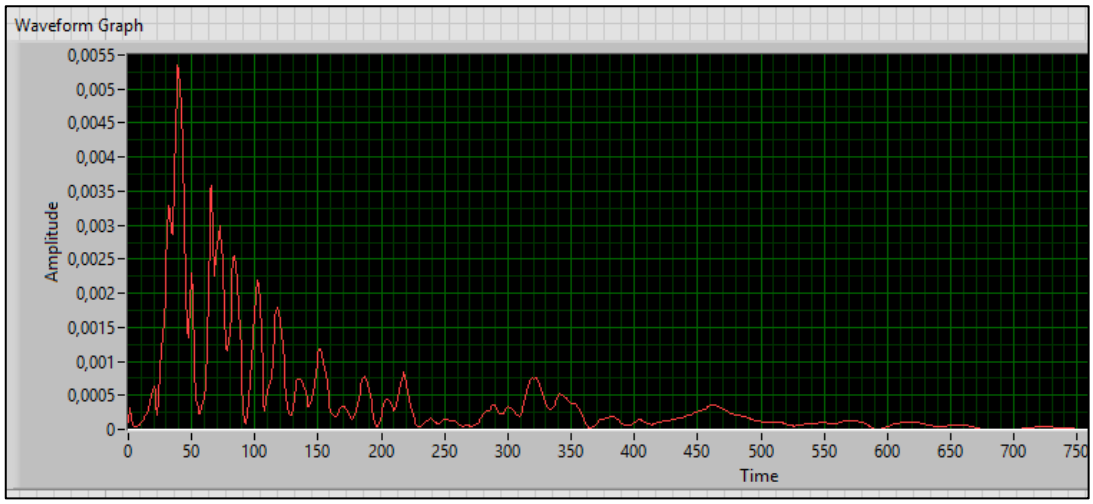

Figure 5.17 Natural Frequencies of Part 1 Operation 2 for Length-Side Fixturing

5.7.2.1 Analysis of Part 1 Operation 2 Results

The experimental results for part 1 operation 2 are organized in Table 5.2.

Table 5.2 Natural frequencies for part 1 operation 2

Fixturing	Mode 1	Mode 2	Mode 3
Breadth centre	110	240	-
Breadth side	100	150	230
Length centre	60	110	175
Length side	40	60	100

5.7.3 Part 1 Operation 6

Part 1 operation 6 is a symmetric part, with two countersunk rectangular bores in its centre and four holes drilled at each corner. It was fixed along its breadth on the side surface at both the centre and far corner, as well as along its length on the side surface at both the centre and far corner. The results of the frequency tests of this part for each fixturing setup are recorded and discussed in this section.

Figure 5.18 shows the frequency response of the knock test for part 1 operation 1 under breadth-centre fixturing. The natural frequencies for the first three modes visible in the graph are 100Hz, 220Hz, and 320Hz respectively.

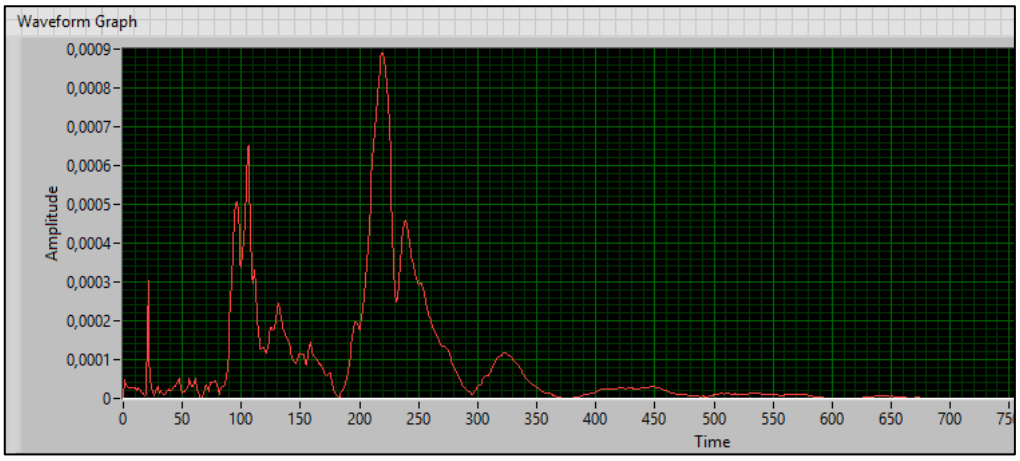

Figure 5.18 Natural Frequencies of Part 1 Operation 6 for Breadth-Centre Fixturing

Figure 5.19 shows the frequency response of the knock test for part 1 operation 1 under breadth-side fixturing. The natural frequencies for the first three modes visible in the graph are 100Hz, 210Hz, and 295Hz respectively.

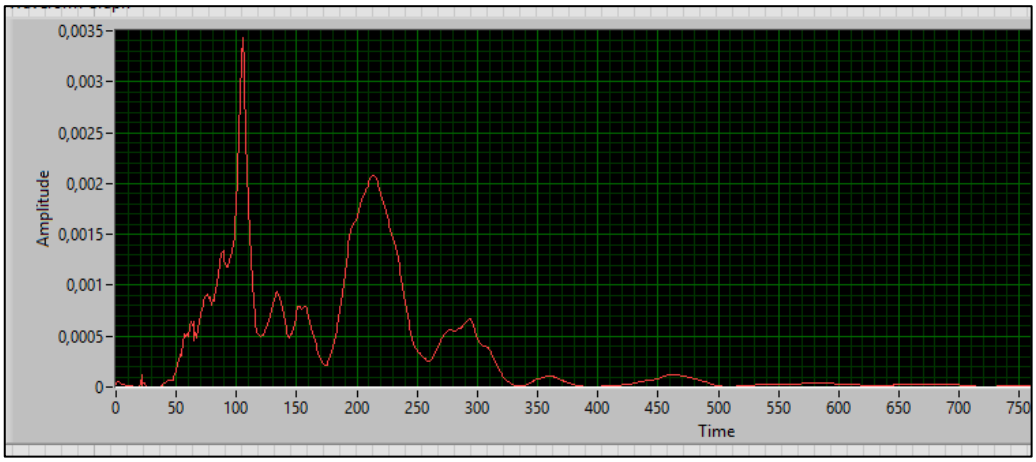

Figure 5.19 Natural Frequencies of Part 1 Operation 6 for Breadth-Side Fixturing

Figure 5.20 shows the frequency response of the knock test for part 1 operation 1 under length-centre fixturing. The natural frequencies for the first three modes visible in the graph are 70Hz, 140Hz, and 230Hz respectively.

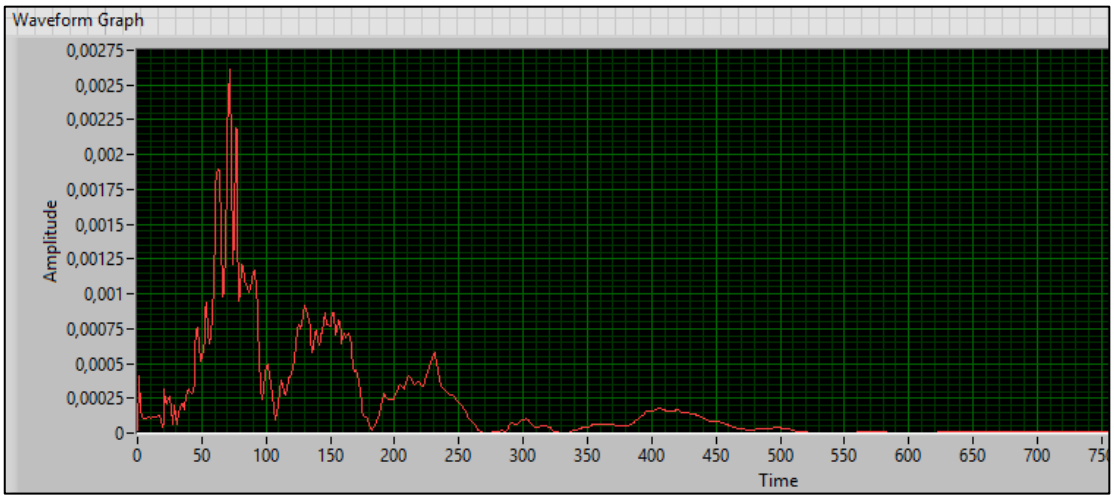

Figure 5.20 Natural Frequencies of Part 1 Operation 6 for Length-Centre Fixturing

Figure 5.21 shows the frequency response of the knock test for part 1 operation 1 under length-side fixturing. The natural frequencies for the first three modes visible in the graph are 25Hz, 70Hz, and 110Hz respectively.

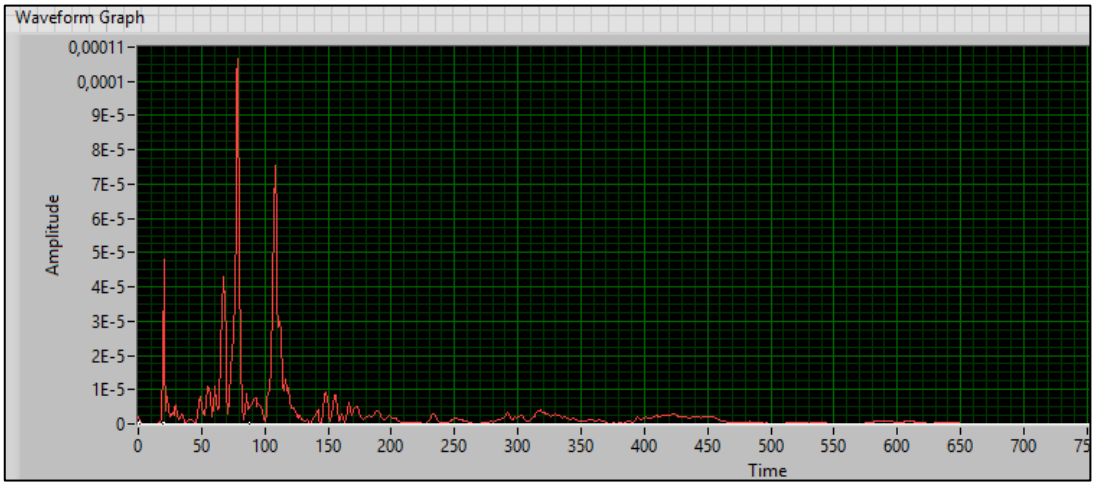

Figure 5.21 Natural Frequencies of Part 1 Operation 6 for Length-Side Fixturing

5.7.3.1 Analysis of Part 1 Operation 6 Results

The experimental results for part 1 operation 6 are organized in Table 5.3

Table 5.3 Natural frequencies for part 1 operation 6

Fixturing	Mode 1	Mode 2	Mode 3
Breadth centre	100	220	320
Breadth side	100	210	295
Length centre	70	140	230
Length side	25	70	110

5.8 Frequency Response Results for Part 2

5.8.1 Part 2 Operation 1

Part 2 operation 1 is a non-symmetric part, with a rectangular bore cut off-centred on its upper surface. It was fixed along its breadth on the side surface at both the centre and far corner, as well as along its length on the side surface at both the centre and far corner. The results of the frequency tests of this part for each fixturing setup are recorded and discussed in this section.

Figure 4.22 shows the frequency response of the knock test for part 1 operation 1 under breadth-centre fixturing. The natural frequencies for the first three modes visible in the graph are 110Hz, 180Hz, and 250Hz respectively.

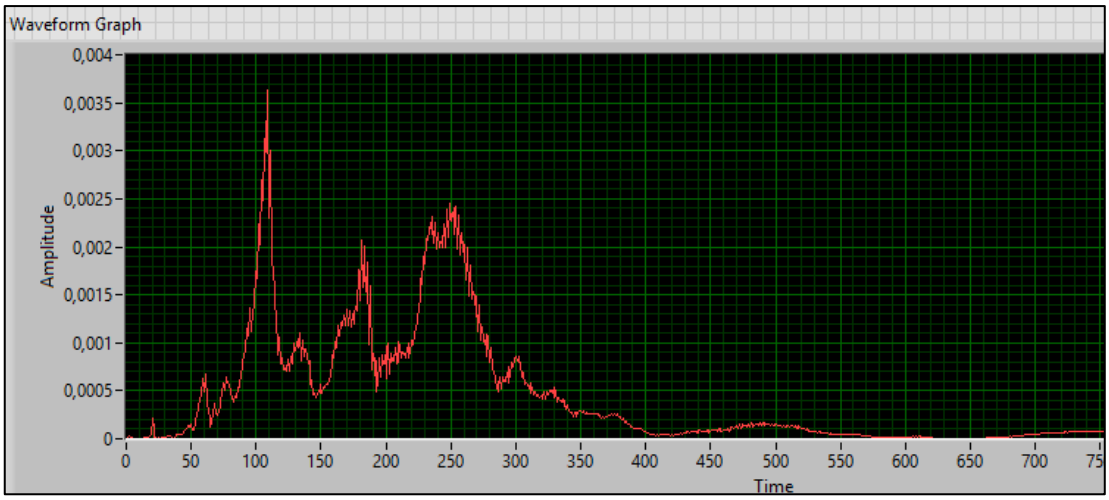

Figure 5.22 Natural Frequencies of Part 2 Operation 1 for Breadth-Centre Fixturing

Figure 4.23 shows the frequency response of the knock test for part 1 operation 1 under breadth-side-A fixturing. The natural frequencies for the first two modes visible in the graph are 100Hz, 190Hz. The Third mode is not captured in the graph.

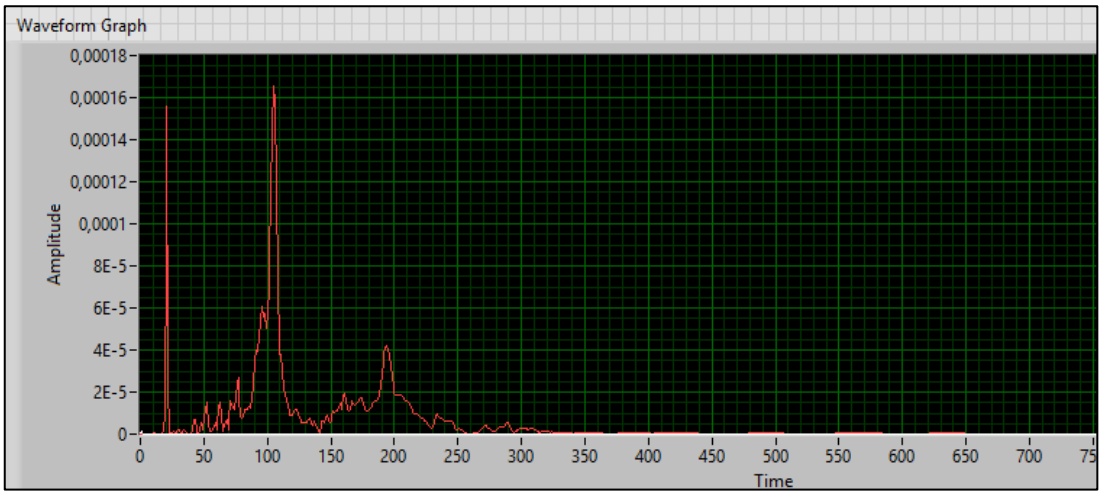

Figure 5.23 Natural Frequencies of Part 2 Operation 1 for Breadth-Side-A Fixturing

Figure 4.24 shows the frequency response of the knock test for part 1 operation 1 under breadth-side-B fixturing. The natural frequencies for the first three modes visible in the graph are 110Hz, 150Hz, and 240Hz respectively.

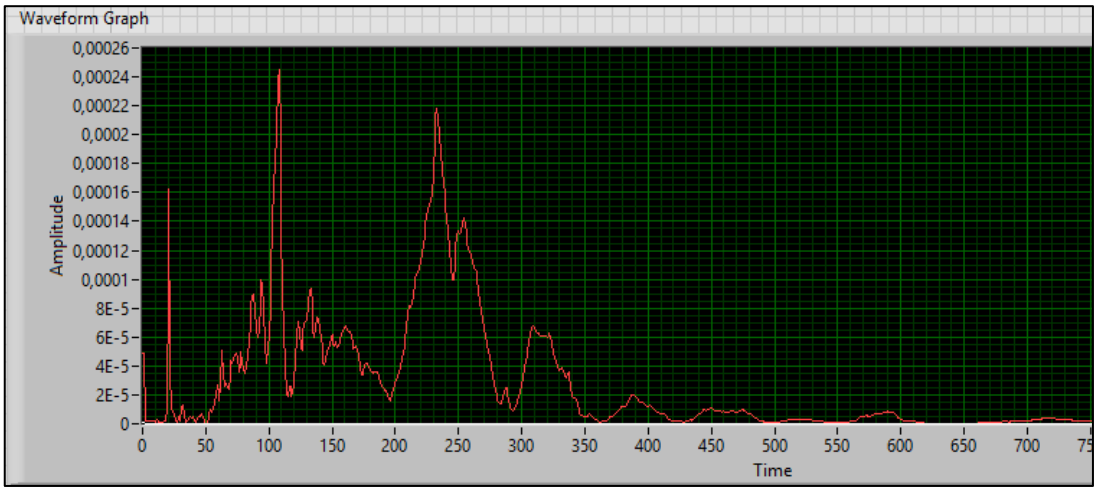

Figure 5.24 Natural Frequencies of Part 2 Operation 1 for Breadth-Side-B fixturing

Figure 4.25 shows the frequency response of the knock test for part 1 operation 1 under length-centre fixturing. The natural frequencies for the first three modes visible in the graph are 50Hz, 130Hz, and 200Hz respectively.

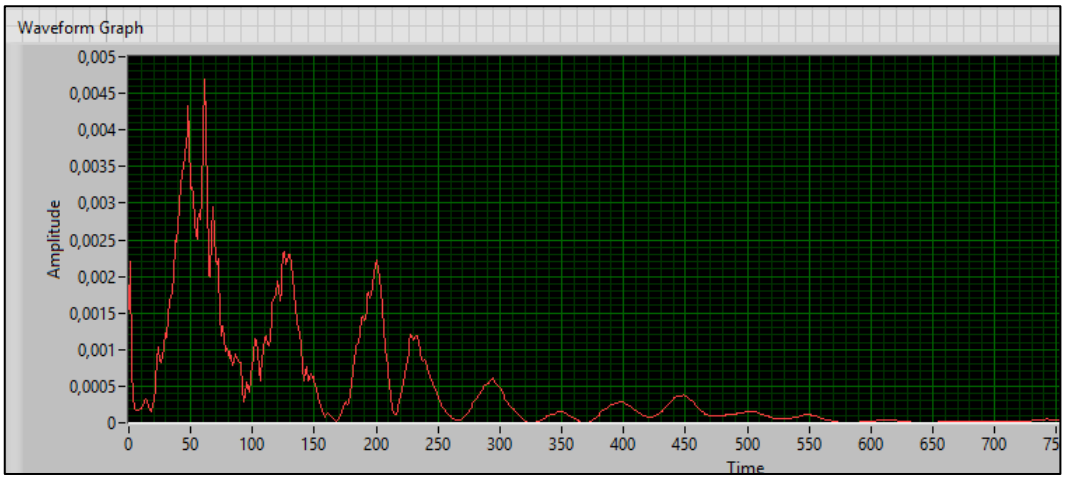

Figure 5.25 Natural Frequencies of Part 2 Operation 1 for Length-Centre Fixturing

Figure 4.26 shows the frequency response of the knock test for part 1 operation 1 under length-side-A fixturing. The natural frequencies for the first three modes visible in the graph are 40Hz, 80Hz, and 120Hz respectively.

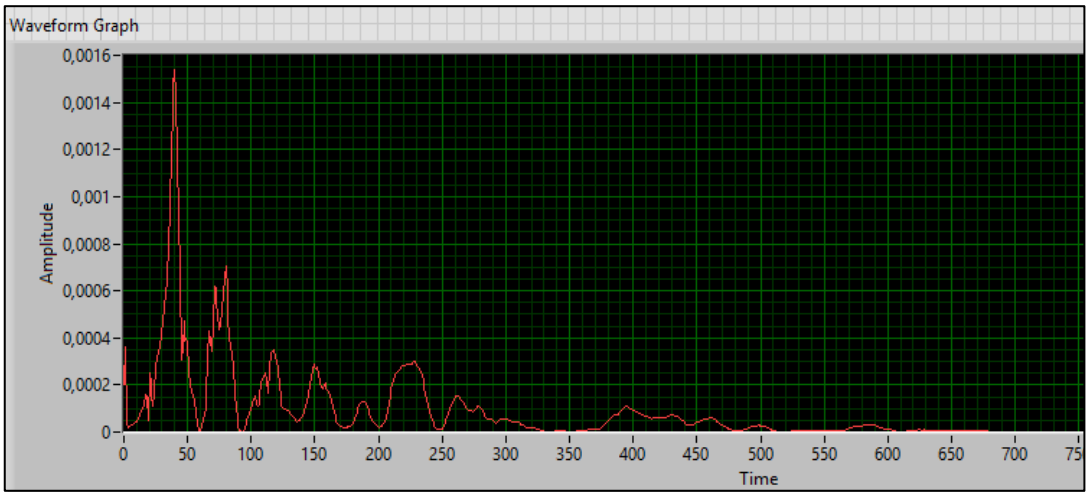

Figure 5.26 Natural Frequencies of Part 2 Operation 1 for Length-Side-A fixturing

Figure 4.27 shows the frequency response of the knock test for part 1 operation 1 under length-side-B fixturing. The natural frequencies for the first three modes visible in the graph are 50Hz, 70Hz, and 100Hz respectively.

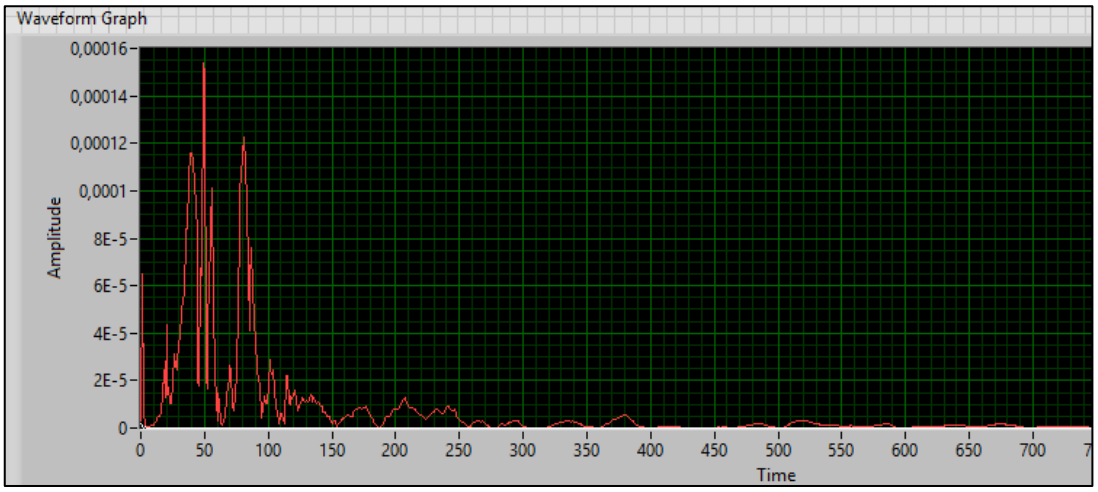

Figure 5.27 Natural Frequencies of Part 2 Operation 1 for Length-Side-B Fixturing

5.8.1.1 Analysis of Part 2 Operation 1 Results

The experimental results for part 2 operation 1 are organized in Table 5.4.

Table 5.4 Natural frequencies for part 2 operation 1

Fixturing	Mode 1	Mode 2	Mode 3
Breadth centre	110	180	250
Breadth side a	100	190	-
Breadth side b	110	150	240
Length centre	50	130	200
Length side a	40	80	120
Length side b	50	70	100

5.8.2 Part 2 Operation 2

Part 2 operation 2 is a non-symmetric part, with two countersunk rectangular bores cut off-centre on its upper surface. It was fixed along its breadth on the side surface at both the centre and far corner, as well as along its length on the side surface at both the centre and far corner. The results of the frequency tests of this part for each fixturing setup are recorded and discussed in this section.

Figure 5.28 shows the frequency response of the knock test for part 1 operation 1 under breadth-centre fixturing. The natural frequencies for the first three modes visible in the graph are 110Hz, 200Hz, and 320Hz respectively.

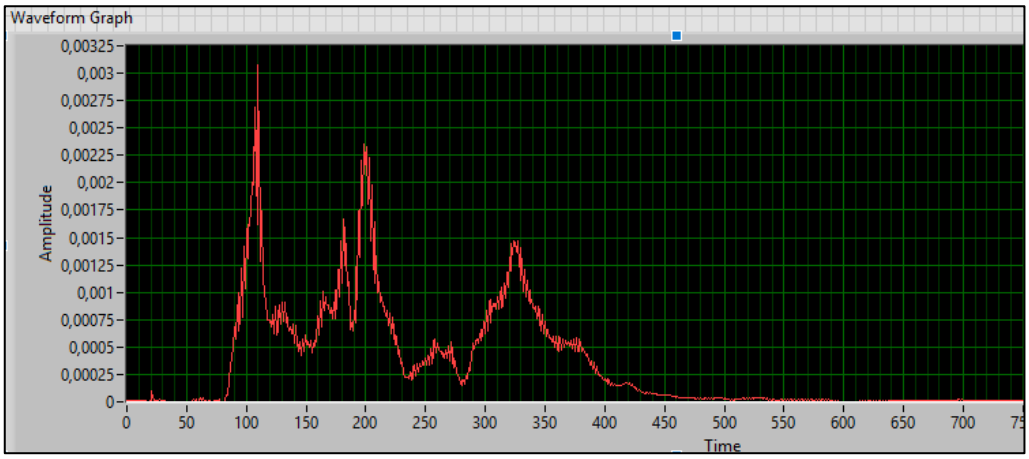

Figure 5.28 Natural Frequencies of Part 2 Operation 2 for Breadth-Centre Fixturing

Figure 5.29 shows the frequency response of the knock test for part 1 operation 1 under breadth-side-A fixturing. The natural frequencies for the first three modes visible in the graph are 100Hz, 160Hz, and 220Hz respectively.

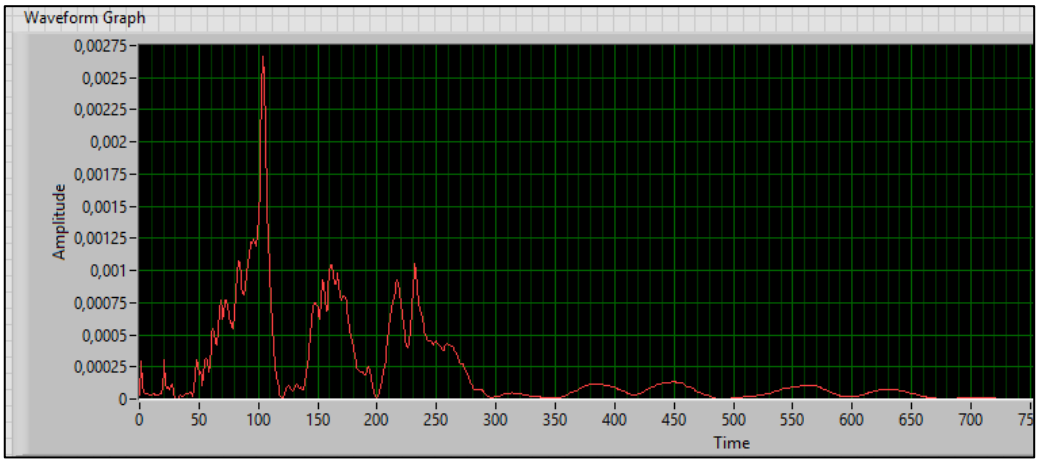

Figure 5.29 Natural Frequencies of Part 2 Operation 2 for Breadth-Side-A Fixturing

Figure 5.30 shows the frequency response of the knock test for part 1 operation 1 under breadth-side-B fixturing. The natural frequencies for the first three modes visible in the graph are 100Hz, 160Hz, and 230Hz respectively.

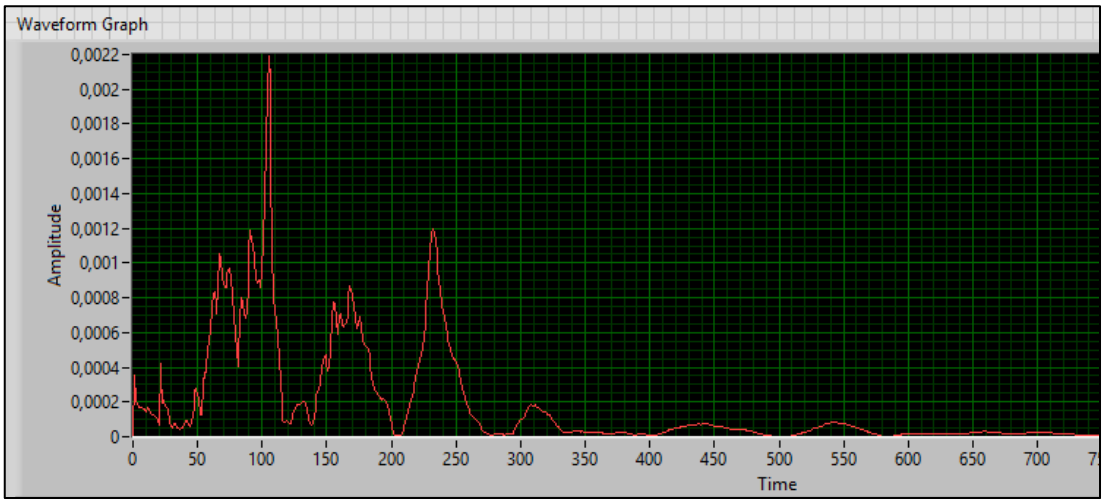

Figure 5.30 Natural Frequencies of Part 2 Operation 2 for Breadth-Side-B Fixturing

Figure 5.31 shows the frequency response of the knock test for part 1 operation 1 under length-centre fixturing. The natural frequencies for the first three modes visible in the graph are 48Hz, 120Hz, and 190Hz respectively.

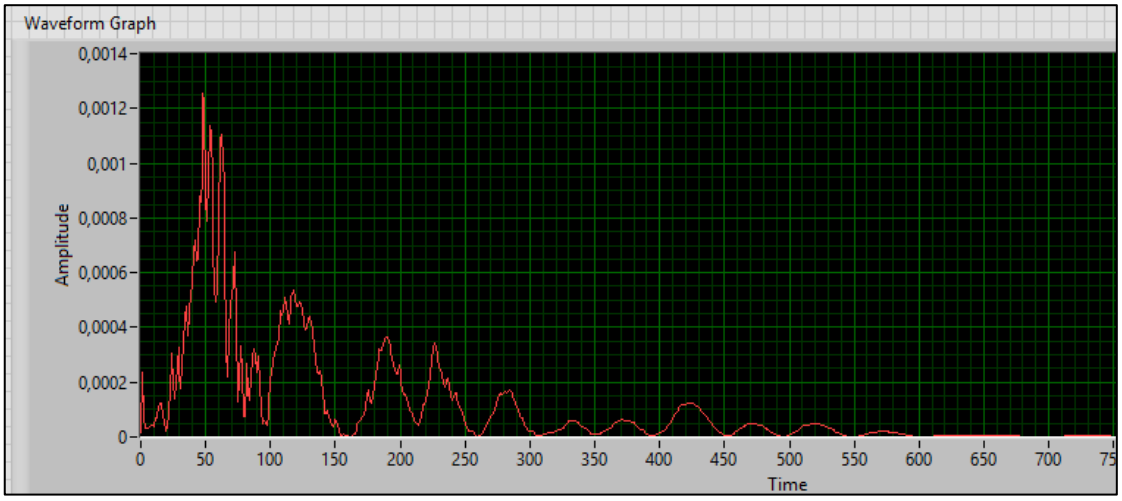

Figure 5.31 Natural Frequencies of Part 2 Operation 2 for Length-Centre Fixturing

Figure 5.32 shows the frequency response of the knock test for part 1 operation 1 under length-side-A fixturing. The natural frequencies for the first three modes visible in the graph are 40Hz, 65Hz, and 110Hz respectively.

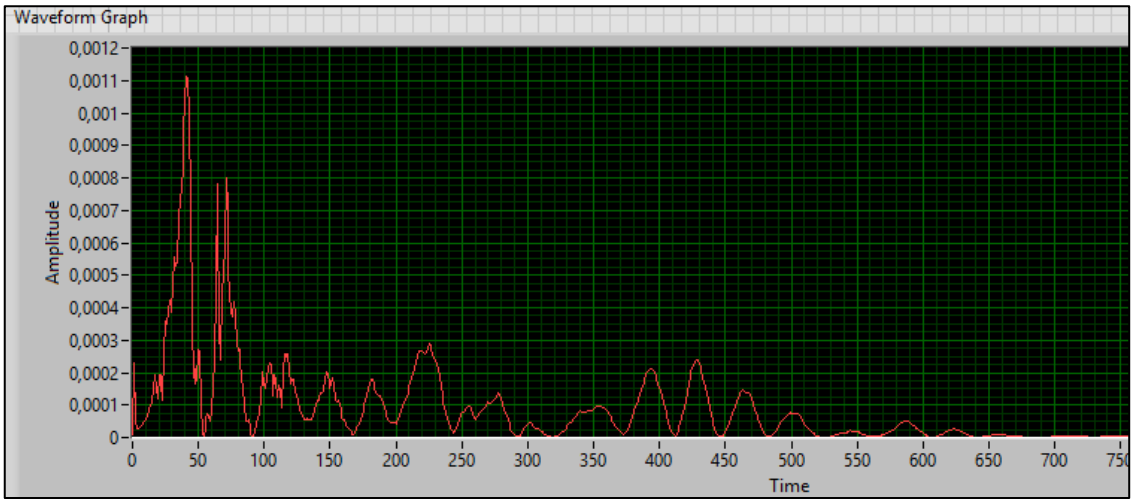

Figure 5.32 Natural Frequencies of Part 2 Operation 2 for Length-Side-A Fixturing

Figure 5.33 shows the frequency response of the knock test for part 1 operation 1 under length-side-B fixturing. The natural frequencies for the first three modes visible in the graph are 40Hz, 80Hz, and 120Hz respectively.

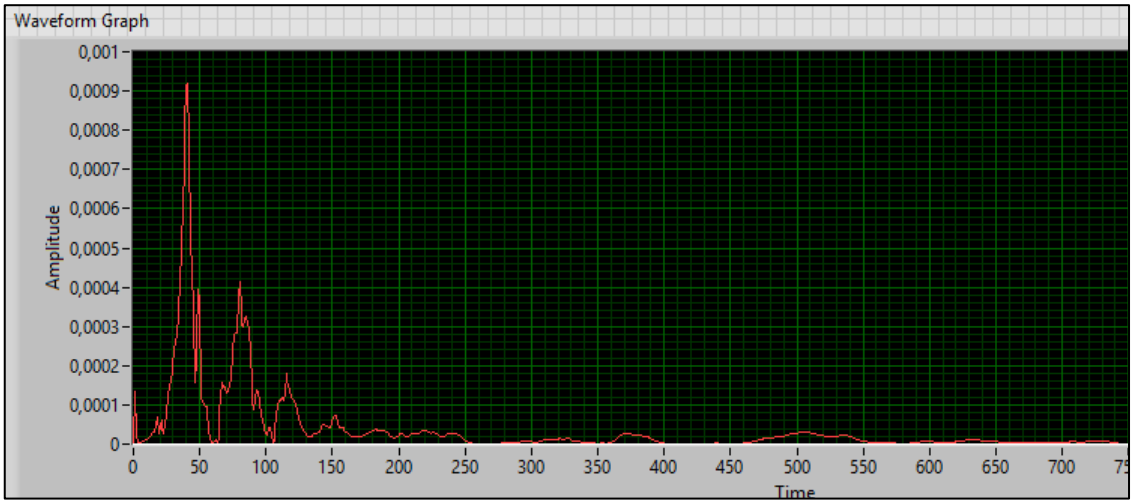

Figure 5.33 Natural Frequencies of Part 2 Operation 2 for Length-Side-B Fixturing

5.8.2.1 Analysis of Part 2 Operation 2 Results

The experimental results for part 2 operation 2 are organized in Table 5.5.

Table 5.5 Natural frequencies for part 2 operation 2

Fixturing	Mode 1	Mode 2	Mode 3
Breadth centre	110	200	320
Breadth side a	100	160	220
Breadth side b	100	160	230
Length centre	48	120	190
Length side a	40	65	110
Length side b	40	80	120

5.8.3 Part 2 Operation 6

Part 2 operation 6 is a non-symmetric part, with two countersunk rectangular bores cut off-centre on the upper surface with three holes drilled at each corner around the bore. It was fixed along its breadth on the side surface at both the centre and far corner, as well as along its length on the side surface at both the centre and far corner. The results of the frequency tests of this part for each fixturing setup are recorded and discussed in this section.

Figure 5.34 shows the frequency response of the knock test for part 1 operation 1 under breadth-centre fixturing. The natural frequencies for the first three modes visible in the graph are 106Hz, 200Hz, and 300Hz respectively.

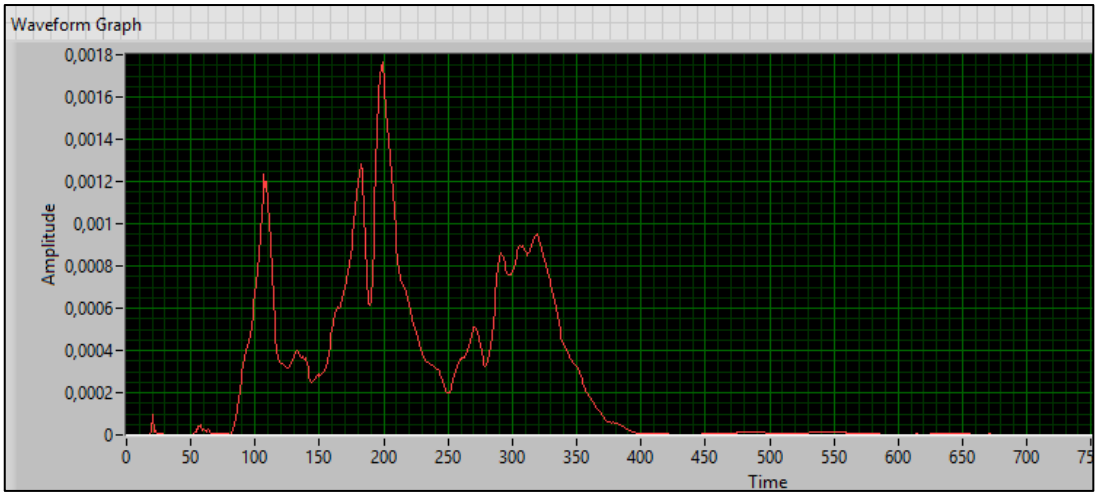

Figure 5.34 Natural Frequencies of Part 2 Operation 6 for Breadth-Centre Fixturing

Figure 5.35 shows the frequency response of the knock test for part 1 operation 1 under breadth-side-A fixturing. The natural frequencies for the first three modes visible in the graph are 80Hz, 160Hz, and 230Hz respectively.

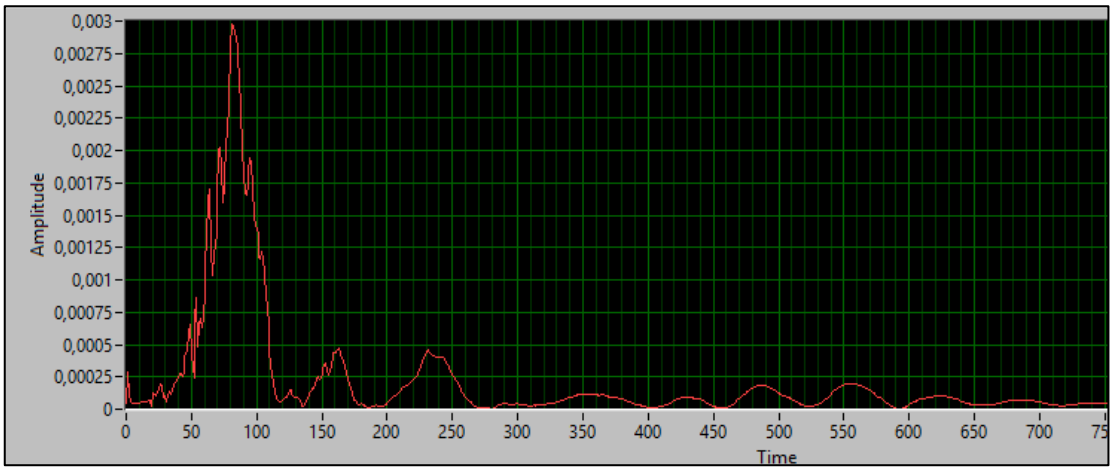

Figure 5.35 Natural Frequencies of Part 2 Operation 6 for Breadth-Side-A Fixturing

Figure 5.36 shows the frequency response of the knock test for part 1 operation 1 under breadth-side-B fixturing. The natural frequencies for the first three modes visible in the graph are 80Hz, 122Hz, and 215Hz respectively.

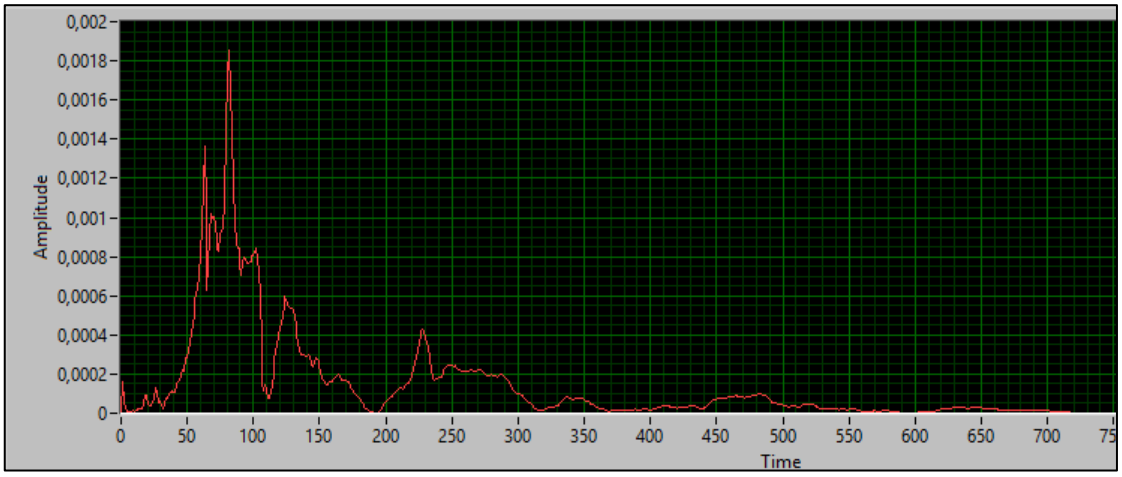

Figure 5.36 Natural Frequencies of Part 2 Operation 6 for Breadth-Side-B Fixturing

Figure 5.37 shows the frequency response of the knock test for part 1 operation 1 under length-centre fixturing. The natural frequencies for the first three modes visible in the graph are 70Hz, 130Hz, and 215Hz respectively.

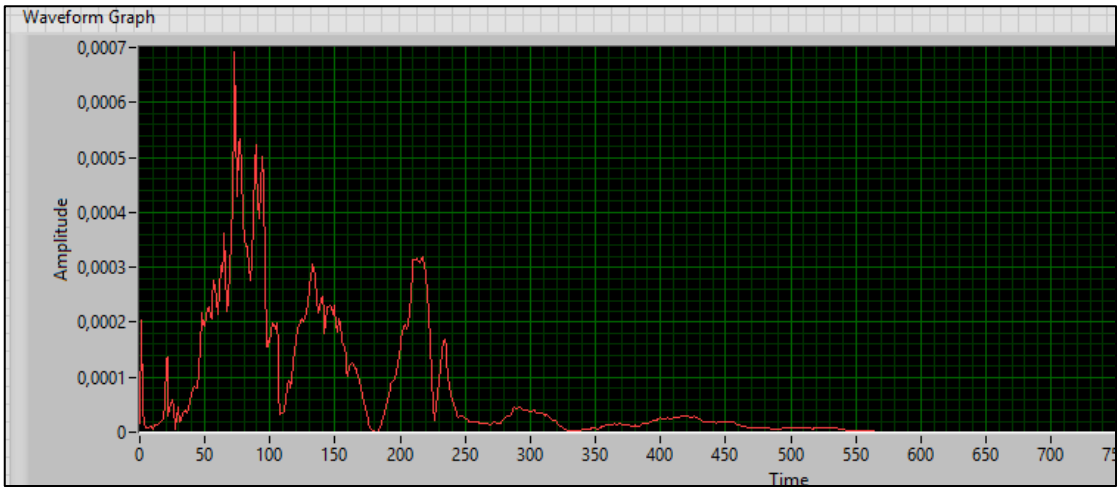

Figure 5.37 Natural Frequencies of Part 2 Operation 6 for Length-Centre Fixturing

Figure 5.38 shows the frequency response of the knock test for part 1 operation 1 under length-side-A fixturing. The natural frequencies for the first three modes visible in the graph are 40Hz, 80Hz, and 100Hz respectively.

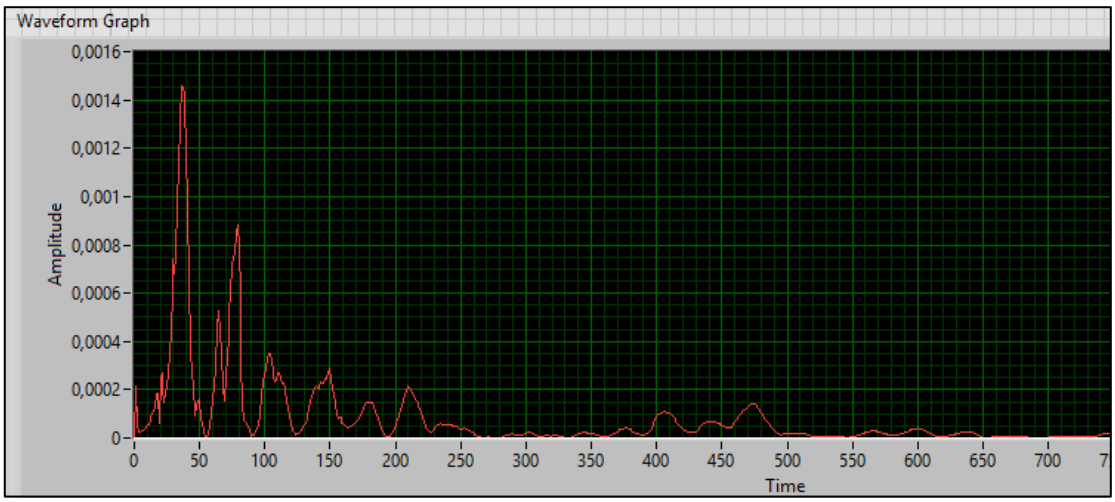

Figure 5.38 Natural Frequencies of Part 2 Operation 6 for Length-Side-A Fixturing

Figure 5.39 shows the frequency response of the impact test for part 1 operation 1 under length-side-B fixturing. The natural frequencies for the first three modes visible in the graph are 40Hz, 80Hz, and 98Hz respectively.

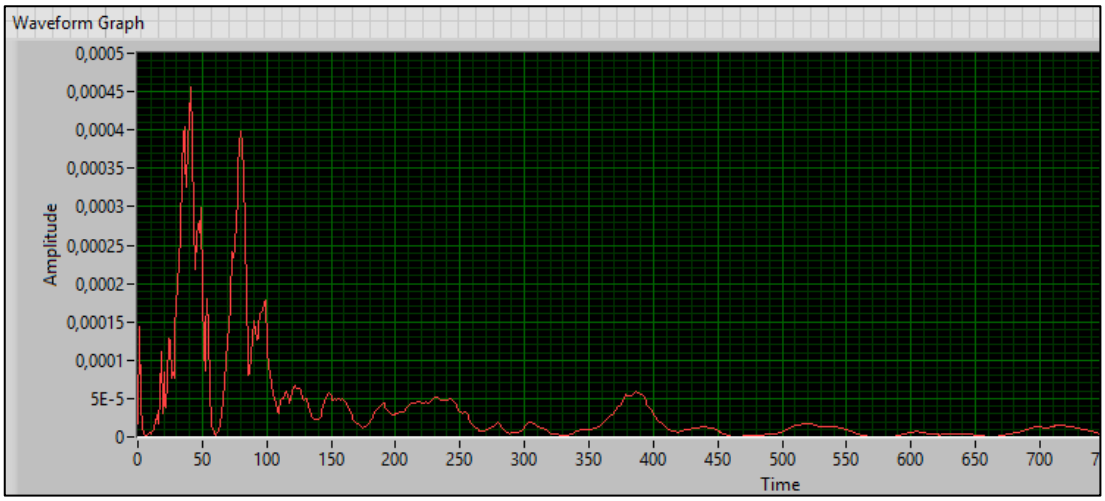

Figure 5.39 Natural Frequencies of Part 2 Operation 6 for Length-Side-B Fixturing

5.8.3.1 Analysis of Part 2 Operation 6 Results

The experimental results for part 2 operation 6 are organized in Table 5.6.

Table 5.6 Natural frequencies for part 2 operation 6

Fixturing	Mode 1	Mode 2	Mode 3
Breadth centre	106	200	300
Breadth side a	80	160	230
Breadth side b	80	122	215
Length Centre	70	130	215
Length side a	40	80	100
Length side b	40	80	98

5.9 Results Analysis

5.9.1 Part 1

Table 5.7 contains all the experimental frequency data for part 1, grouped together according to the fixturing scenario implemented. The data has been arranged according to mode and operation for each fixturing scenario to facilitate identifying trends in the frequency response, and to highlight differences between each fixturing setup.

For part 1 the prevalent trend is that breadth centre fixturing gives the best frequency response for all stages of material removal for all modes. The order of highest to lowest frequency response for the remainder of the fixturing setups are; breadth-side, length-centre, and length-side fixturing.

Table 5.7 Natural Frequencies for each Fixturing Scenario for Part 1

Part 1	Operation	Mode 1	Mode 2	Mode 3
Breadth centre	Op. 1	85	165	250
	Op. 2	110	240	-
	Op. 6	100	220	320
Breadth side	Op. 1	60	120	230
	Op. 2	100	150	230
	Op. 6	100	210	295
Length centre	Op. 1	48	115	168
	Op. 2	60	110	175
	Op. 6	70	140	230
Length side	Op. 1	40	85	120
	Op. 2	40	60	100
	Op. 6	25	70	110

For the breadth-centre, breadth-side, and length-centre fixturing setup the natural frequency tends to increase with each material removal operation. This is true for all three modes with a few exceptions, those being mode 1 and mode 2 of operation 6 for the breadth-centre fixturing, as well as mode 2 of operation 2 for length centre fixturing. For length-side fixturing, the natural frequencies tend to decrease for each new operation.

5.9.2 Part 2

Table 5.8 contains the experimental results for part 2. Similarly, to part 1, the breadth centre fixturing gives the highest natural frequency for all modes and operations. The only exception is for mode 2 operation 1, where breadth-side-a provides the highest natural frequency. The table illustrates that, in general, operation 6 reduces the natural frequency, with the exception of length-centre fixturing which causes natural frequency to increase.

Table 5.8 Natural Frequencies for each Fixturing Scenario for Part 2

Part 2	Operation	mode1	mode2	mode3
Breadth centre	Op. 1	110	180	250
	Op. 2	110	200	320
	Op. 6	106	200	300
Breadth side a	Op. 1	100	190	-
	Op. 2	100	160	220
	Op. 6	80	160	230
Breadth side b	Op. 1	110	150	240
	Op. 2	100	160	230
	Op. 6	80	122	215
Length centre	Op. 1	50	130	200
	Op. 2	48	120	190
	Op. 6	70	130	215
Length side a	Op. 1	40	80	120
	Op. 2	40	65	110
	Op. 6	40	80	100
Length side b	Op. 1	50	70	100
	Op. 2	40	80	120
	Op. 6	40	80	98

Breadth-centre fixturing yields the highest overall frequency response for both part 1 and 2. This may be a result of the breadth-centre fixturing setup holding the most material between the fixture surfaces compared with the other setups.

This explains why for both cases of fixturing along the length and breadth, the centre position yields a better response than the side. It also explains why fixturing along the breadth gives the highest frequency response, since fixturing along the breadth holds the largest volume of material between the fixture surfaces.

5.10 Chapter Summary

Chapter 5 outlined the equipment, methods and procedure used in the experimental analysis to ensure the integrity of the results. The vibration testing revealed a high level of dampening by the AFFS on the parts. The general trends in the natural frequencies follow similar trends to those discovered in the simulations. The results show that breadth-centre fixturing yields the highest overall frequencies for both part 1 and part 2.

Chapter 6: Discussion

6.1 Chapter Introduction

Chapter 6 discusses the research as a whole, focusing primarily on the correlation between the simulation and experimental results. The discrepancies between the simulation and experimental results are reviewed and analysed. The implications of the research for fixturing methods is explored, and methodologies are suggested. The weaknesses of the AFFS and the limitations of the experimental results are discussed, along with an explication of future improvements to both the hardware and methodology that could resolve those limitations.

6.2 Simulation Results

6.2.1 Part 1 Maximum Harmonic Response

The first observations for part 1 were in identifying the fixturing setup that resulted in the highest natural frequency for each machining operation. Table 6.1 summarises the best performing setups for each mode from the data in table 4.1. It revealed that for the first mode of vibration the length-centre fixture setup natural frequencies were largest for all machining operations. In the proceeding modes the breadth-centre fixture setup results in the highest frequency response with a few exceptions: mode 2 operation 6 as well as mode 3 operations 2 to 5, which had the highest frequency response with the Length-Side setup.

Table 6.1 Fixturing Setups for Highest Natural Frequency for Part 1

Mode number	Machining operations	Fixture setup
1	All	Length centre
2	Op 1, op2, op3, op4, op5	Breadth centre
	Op6	Length side
3	Op1, op6	Breadth centre
	Op2, op3, op4, op5	Length side
4	All	Breadth centre
5	All	Breadth centre

The two main observations with respect to the fixture setup that yields the highest natural frequency were:

1. The breadth-centre fixturing yields the highest overall frequency response.
2. The majority of the modes have a single fixturing setup that yields the highest frequencies for all the machining operations

6.2.2 Part 2 Maximum Harmonic Response

Table 6.2 contains a summary of the best performing fixture setups from the frequency results in table 4.2. The table reveals that the Length-centre fixturing resulted in the highest frequency for all operations for mode 1. For the higher order modes, 4 and 5, breadth-centre fixturing resulted in the highest frequency response. For operations 2 and 3, the highest frequency response was obtained through several different fixturing setups for the various machining operations. Thus, the breadth-centre setup was the best overall performing fixture setup.

Table 6.2 Fixturing Setups for Highest Natural Frequency for Part 2

Mode number	Machining operations	Fixture setup
1	All	Length centre
2	Op 1, op2, op3, op4	Breadth centre
	Op5	Length side
3	Op1	Breadth centre
	Op5	Length side a
	Op2, op3, op4	Length side b
4	All	Breadth centre
5	All	Breadth centre

6.2.3 Natural Frequency Graphs Part 1

The natural frequency data for part 1 was plotted in graph form, contained in Chapter 4.4, illustrating the relationship between natural frequency and machining operations for each mode. The graphs reveal that material removal either increases or decreases the natural frequency depending on geometry and fixturing. The optimal machining order is one where the features that increase natural frequency are machined first, followed by those that decrease natural frequency. If a feature requires a high amount of accuracy, that feature should be machined directly after those that increase the natural frequency.

For some fixturing setups, the default machining order is already optimum for a specific mode, for example the breadth-centre fixturing for mode 1 given in figure 4.3. The natural frequency increases for the first operation and thereafter decreases for each proceeding operation. This can be compared to length-centre fixturing for mode 1, illustrated in figure 4.5, where the natural frequency decrease for operations 1 and 2, thereafter increasing for operations 3 to 6. For breadth-centre fixturing the operations are already in the optimum order, operation 1 increases the natural frequency of the system, after which it decreases. The length-centre fixturing operation order is not optimised and should be rearranged so that operations 3 to 6 occur first, before operations 1 and 2 lower the natural frequency. If the order was rearranged

then operations 3 to 6 could be machined at a higher rate, and would increase the natural frequency for the next 2 operations; operation 1 and 2.

As a general rule, operations 1 and 2 lower the natural frequency, and operations 3 to 6 either all increase or decrease the frequency together. There are several unique cases where this general rule is broken. Observing the trend in figure 4.16, the fourth harmonic for breadth-side fixturing, the frequency decreases for operation 3 followed by an increase for both operation 4 and 5, and lastly decreasing for operation 6. The breadth-centre and length-side fixturing of part 1 for mode 5, graphed in figure 4.19 and figure 4.22 respectively, are the only cases of operations 1 or 2 increasing the natural frequency.

6.2.4 Natural Frequency Graphs Part 2

The graphs for part 2 show the rise and fall of the natural frequency as the part geometry is changed by the different machining operations. Similar to part 1, the default order of machining for part 2 was not always optimal for certain fixture setups.

The length-centre fixture setup that gave the highest harmonic response for mode 1, is graphed in figure 4.25. Operations 1 and 2 cause the natural frequency to decrease, and are arranged before operations 3 to 5. The optimal order would be to arrange operations 3, 4 and 5 first to take advantage of their effect of increasing the natural frequency.

6.2.5 Part Feature Order Simulations

The Simulation results verify that adjusting the machining order can improve the harmonic response of the part, and revealed that the trends of geometric features remained the same after the order was changed. There are two situations where rearranging the operation order could improve efficiency:

1. Arranging a feature that requires high accuracy directly after all features that increase natural frequency and stiffness
2. Selecting a machining order resulting in all features harmonic response improving by the arrangement, where all features require the same accuracy

Breadth-side fixturing from figure 4.44 is an example of the first case, where the holes are machined at a higher frequency but decrease the starting frequency for the slots. Length-centre and length-side fixturing, figure 4.45 and figure 4.46, are examples of the second case. In both fixture setups the holes are machined first at a higher frequency than the original, and increase the frequency for the slot operations. For breadth-centre fixturing, figure 4.43, the original machining order was already optimum. By changing the machining order, the holes natural frequencies stayed the same, while the slots natural frequency were decreased. The tendency

for each operation to increase or decrease natural frequency remained the same for both the original and rearranged operation orders.

6.2.6 Comparison Between Part 1 and Part 2

The frequency response for part 1 and part 2 are highly similar in several cases. For mode 1 the highest frequency response is obtained by length-centre fixturing for both parts. The graphs for length-centre fixturing are almost identical for both part 1 and part 2 for mode 1, illustrated in figure 4.5 and figure 4.25. This similarity also exists for breadth-centre fixturing, particularly for mode 2 illustrated in figure 4.7 and figure 4.27.

The similarities diminish when comparing the 'Side' fixturing setups. Part 1 is symmetrical for the majority of its length-side and breadth-side setups. Conversely, part 2 is asymmetrical for all of its length-side and breadth-side setups. Comparing the frequency response graphs for part 1 and part 2 show different trends for the same setups. An example of this is the length-side setup for mode 3. Part 1, graphed in figure 4.14, shows the natural frequency first decreasing for operations 1 and 2, increasing for operations 3 and 4, and finally decreasing to operation 6. Part 2, graphed in figure 4.34, Shows that length-side-b fixturing resulted in the highest overall frequencies, with a very different profile to part 1. For part 2, another observation is that the length-side-b fixturing shows a mirrored trend to length-side-a fixturing for operations 3 to 5.

When comparing the overall performance, using table 4.1 and table 4.2, it is evident that the breadth-centre setup achieves higher frequencies overall for both part 1 and part 2. Both part 1 and part 2 show similarities, for all modes, with respect to their best performing fixture setups.

6.2.7 Machining Speeds

Machining parameters are directly affected by the modes of vibration. The modal frequencies must be avoided when selecting parameters, as machining at the natural frequency of the part will cause regenerative vibrations. The input frequency of a machining operation is determined by the cutting speed and the number of teeth on the cutting tool, and will be referred to as the machining input frequency (MIF). Table 4.1 reveals that the first mode of vibration for operation 1 was 10283 Hz. This indicates that after the geometric feature of operation 1 has been machined part 1 will vibrate at 10283 Hz. Thus, the machining parameters for machining operation 1 should be chosen such that the MIF is either greater or smaller than 10283 Hz to avoid regenerative vibration. Similarly, the machining parameters for performing operation 2 should be chosen such that the MIF is either greater or smaller than 9616 Hz.

Examining a single operation across all modes reveals the allowable machining input frequencies, which are the frequencies between each mode. The natural frequency of part 1 is both a constraint on cutting parameters, and a measure of the effective rigidity of a fixturing setup.

6.3 Simulation and Experimental Results

In both the simulations and experiments, the breadth-centre fixture setup was shown to be the best overall performing setup. The experimental results showed that the breadth-centre fixture setup had the highest natural frequencies for each mode and operation, with only a few exceptions. This result implies that the overall billet shape has a greater effect on the optimum fixture setup than the part features. The breadth-centre setup holds the greatest volume of material between its fixture surfaces, for the billet shape, which may be the reason for its dominant natural frequencies.

The trends in the experimental natural frequencies with respect to material removal did not match those of the simulation results. The simulations showed that operations 1 and 2 decreased natural frequency, and operation 6 was always at a lower frequency compared to operation 1. The experimental frequencies for part 1, arranged in table 5.7, show that the material removal from operation 1 to operation 6 generally increases the natural frequency for all setups except length-side.

Upon initial inspection of the simulation results, the percentage difference in natural frequencies of part 1 and part 2 for a common mode and fixture setup is relatively small. In contrast, the experimental results show noticeable differences in the magnitudes of the natural frequencies for part 1 and part 2.

6.4 Deflection

The cause of a particular fixture setup to have a higher natural frequency compared to another setup may be related to the modal shape of the part. The modal shapes for length-centre and breadth-centre fixturing are illustrated in figures 6.1 (a) and (b) respectively. Although the area of deflection for length centre fixturing in (a) is far greater than that in (b) for breadth-centre fixturing, length-centre fixturing yielded a higher natural frequency. Table 6.3 shows that the length-centre fixture setup had a displacement of 2.99 mm compared to breadth-centres 3.17 mm.

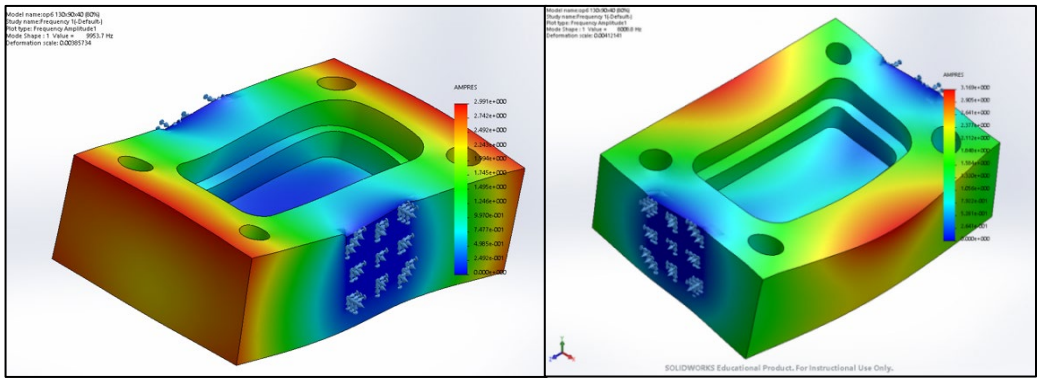

(a) (b)

Figure 6.1 Modal shapes of (a) length-centre and (b) breadth-centre fixturing setups for part 1 mode 1

Figure 6.2 illustrates the 5 modal shapes for part 1, starting with (a) the first harmonic through to (e) the fifth harmonic. The second modal shape shown in (b) is identical to the first harmonic shown in (a) but with slightly larger areas of displacement. The third and fourth modal shapes, pictured in (c) and (d) respectively, have 4 areas of high displacement situated at each corner of the part. The fourth mode has slightly larger areas of displacement compared to the third mode. The fifth mode, shown in (e), has an identical shape to the first and second harmonic, but with noticeably larger areas of displacement. Figure 6.2 infers that there are only 2 unique modal shapes for part 1 operation 6, which are repeated numerically with increasingly larger displacement areas. Inspecting all the modal shapes for operations 1 through 6 of part 1, for breadth-centre fixturing, reveals the same 2 modal shapes consistently throughout. Thus, a billet shape may only have a few unique modal shapes for a specific fixture setup regardless of the material removal.

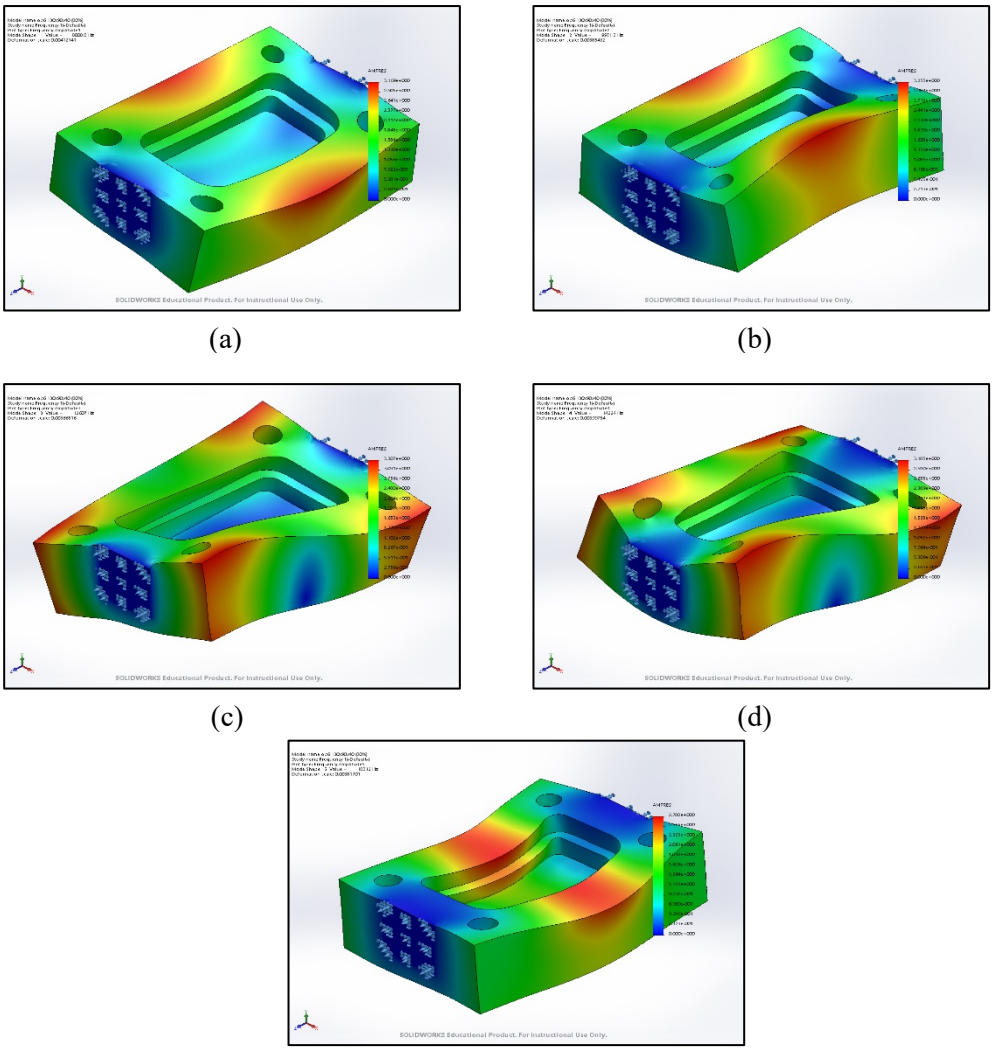

(a) (b) (c) (d) (e)

Figure 6.2 Part 1 operation 6 modal shapes under breadth-centre fixturing for (a) mode 1 (b) mode 2 (c) mode 3 (d) mode 4 (e) mode 5

Table 6.3 shows the deflection data for part 1. The deflections are arranged to illustrate the differences between each fixture setup for a particular mode and operation. Fixture setups that had the highest frequency, for each mode, are marked with a black dot next to the corresponding deflection. The fixture setups that achieved the lowest deflection as well as the highest natural frequency are marked with a blue highlighted dot. The table shows that for the higher modes and for most of operation 1, the fixture setup that produced the highest natural frequency and the lowest displacement was the breadth-centre setup. For part 2 only two cases appear where the highest natural frequency coincides with the smallest deflection. Thus, for higher order modes of symmetrical workpieces, the deflection may indicate the fixture setup with the highest natural frequency. Conversely, the table also illustrates that deflection is generally independent of harmonic response, as there is only a moderate correlation for the symmetric part 1 and almost no correlation with the asymmetric part 2. Measuring the

displacement experimentally to validate the simulations would be difficult due to the dependence of deflection on the location where the measurement is taken, as well as inexpedient due to the sensor expense and a lack of motivating simulation results.

Table 6.3 Simulated deflections for part 1 and part 2

		Part 1 deflections (mm)					Part 2 deflections (mm)				
	Mode:	1	2	3	4	5	1	2	3	4	5
Operation 1	Breadth centre	2,98	•2,84	•3,31	3,08	•2,19	•3,09	•3,43	4,74	3,95	•2,37
	Breadth side a	3,22	4,46	4,24	3,23	4,32	3,11	4,53	4,81	•3,18	4,29
	Breadth side b	-	-	-	-	-	3,31	5,59	•3,66	3,41	5,54
	Length centre	•2,84	3,63	3,65	2,9	3,17	4,27	5,61	5,27	5,14	3,65
	Length side a	3,94	3,78	3,87	3,12	3,09	3,79	4,09	3,93	3,52	3,77
	Length side b	-	-	-	-	-	4,26	4,64	5,06	4,12	4,51
Operation 2	Breadth centre	3,12	•3,22	3,2	•3,01	2,77	3,75	5,39	5,73	4,32	9,88
	Breadth side a	3,62	4,4	4,87	3,3	4,25	•3,39	4,46	7,01	•3,27	4,26
	Breadth side b	-	-	-	-	-	4,58	5,85	•3,77	4,49	5,52
	Length centre	•3,63	2,84	3,7	2,96	3,14	5,49	6,59	4,03	5,09	•3,64
	Length side a	4,04	3,73	•3,82	3,58	3,87	3,79	•4,38	3,81	4,57	4,17
	Length side b	-	-	-	-	-	4,91	4,93	6,62	4,21	5,92
Operation 3	Breadth centre	3,2	•3,27	3,25	•3,17	•2,78	3,68	5,46	5,8	4,47	9,89
	Breadth side a	3,59	4,46	4,84	3,32	4,27	•3,39	4,77	7,03	•3,34	4,59
	Breadth side b	3,68	4,59	4,87	3,42	4,67	4,51	5,93	•3,8	4,73	5,52
	Length centre	•4,4	4,74	4,43	5,39	3,31	5,58	6,46	4,28	5,11	•3,8
	Length side a	4,16	3,94	•3,99	3,66	4,15	3,79	•4,36	3,81	4,55	4,49
	Length side b	4,04	3,73	3,86	3,58	3,87	5,15	4,81	6,77	4,13	5,96
Operation 4	Breadth centre	3,15	•3,24	3,26	•3,13	•2,78	3,65	5,47	5,84	4,6	9,92
	Breadth side a	3,65	4,55	4,83	3,38	4,65	•3,46	4,75	7	•3,39	4,66
	Breadth side b	-	-	-	-	-	4,32	6,05	•3,75	4,7	5,56
	Length centre	•4,3	3,18	3,49	4,56	3,47	5,71	6,29	4,62	5,67	•3,73
	Length side a	4,16	3,87	•3,74	3,92	4,21	3,83	•4,36	3,81	4,57	4,66
	Length side b	4,03	3,72	3,79	3,59	3,88	5,14	4,81	6,7	4,11	5,96
Operation 5	Breadth centre	3,22	•3,29	3,33	•3,26	•2,77	3,72	5,43	5,89	4,61	10,14
	Breadth side a	3,72	4,63	4,83	3,43	4,57	•3,39	4,79	6,78	•3,39	4,65
	Breadth side b	3,62	4,6	4,79	3,41	4,66	4,51	5,98	•3,73	4,89	5,42
	Length centre	•5,17	4,65	4,75	4,57	3,39	5,71	6,73	4,37	5,29	•3,64
	Length side a	4,17	3,87	•3,71	4,07	4,22	5,13	4,79	6,66	4,17	5,94
	Length side b	4,15	3,93	3,94	3,68	4,15	3,93	•4,55	3,89	4,59	4,65
Operation 6	Breadth centre	3,17	3,26	•3,31	•3,19	•2,79	-	-	-	-	-
	Breadth side	3,68	4,59	4,79	3,41	4,56	-	-	-	-	-
	Length centre	•2,99	•3,84	3,14	3,88	3,24	-	-	-	-	-
	Length side	4,14	3,85	3,75	3,91	4,22	-	-	-	-	-

6.5 Centre of Volume and Mass

This section discusses the role that the centre of mass plays in the harmonic response of the part. If the material is assumed to be homogenous throughout then the location, and therefore equation, for the COM will be the same as that of the centre of volume (COV). Equation (6.1) was used to calculate the location of the COV for part 1 and 2:

$$COV\ position = \frac{\Sigma\ (\text{volume x Distance})}{\Sigma\ \text{Volume}} = COM\ position \quad (6.1)$$

Figure 6.3 shows the location of the COV as well as the individual geometric features for (a) part 1 and (b) part 2. In each case the COV of the billet is at the geometric centre. The x-y axis used for measuring the COV is positioned on the bottom left corner of the billet. The position of the COV on the billet before the machining operations is illustrated on figure 6.3 (a) and (b) as (x, y) = (36mm, 52mm).

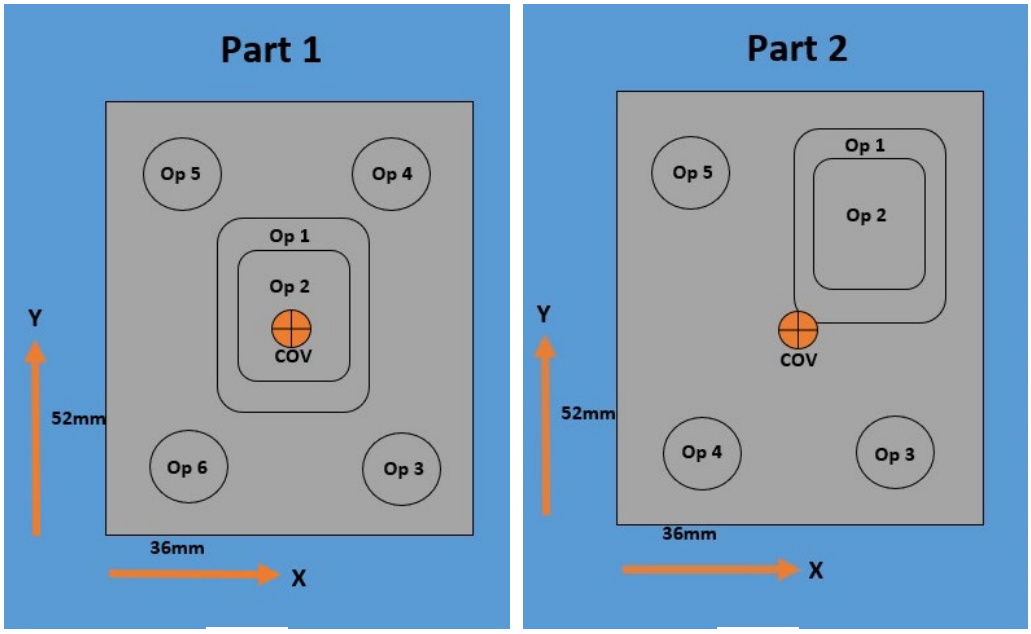

(a) (b)

Figure 6.3 Centre of volume position

Table 6.5 contains the COV positions calculated from equation (6.1). The COV calculations were used both to verify that there were no errors in the part CAD geometry, as well as investigating the relationship between fixture setups and the COV. The Z component of the COV has been neglected in the absence of z-direction changes to the fixture surfaces position. Operations 1 and 2 for part 1 do not influence the x and y COV position and have been omitted from the table. The results are displayed both as the position from the axis origin, as well as the change from billet position.

Table 6.4 Centre of volume positions for part 1 and part 2

Centre of volume position				
Part 1				
	x,y Position		Change from billet COV	
	x axis (mm)	y axis(mm)	x axis (mm)	y axis (mm)
Op. 3	35,79	52,34	-0,2	0,34
Op. 4	35,58	52,00	-0,41	0,00
Op. 5	35,79	51,66	-0,20	-0,34
Op. 6	36,00	52,00	0,00	0,00
Part 2				
	x,y Position		Change from billet COV	
	x axis (mm)	y axis (mm)	x axis (mm)	y axis (mm)
Op. 1	34,89	50,74	-1,11	-1,251
Op. 2	33,98	49,71	-2,01	-2,286
Op. 3	33,72	50,08	-2,27	-1,912
Op. 4	33,94	50,47	-2,05	-1,529
Op. 5	34,16	50,04	-1,83	-1,951

Figure 6.4 shows the COM position calculated from the CAD model of part 2 operation 5, using SolidWorks. The measured COM was (x, y) = (34.15mm, 50.04mm). The calculated COV position, read from Table 6.4, matches the measured position. The slight difference in the x-position values can be attributed to rounding-off errors in the hand calculations.

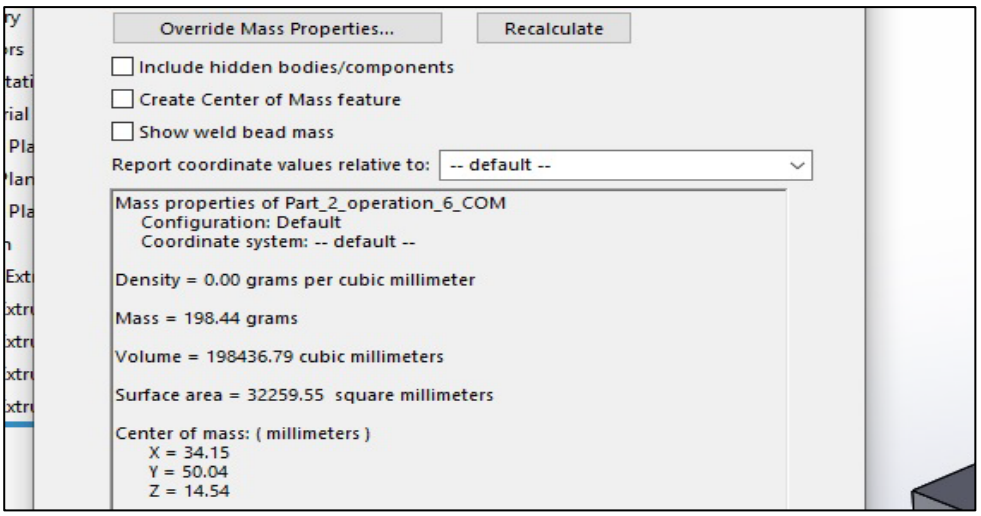

Figure 6.4 Centre of mass position calculated by SolidWorks

Several cases exist where the highest natural frequency, determined by simulation for a specific feature, is not produced by the breadth-centre fixture setup. For example, the fixturing of part 2 operation 5 for mode 3. The length-side-b fixture setup produces the highest natural frequency for monde 3, at 12644 Hz. The COV position had moved downwards, towards the length-side-b fixture surface, during the 5 operations. Thus, the position of the COV matches

the position of the best performing fixture setup. An examination of the connection between the COV and its relationship to the fixture setup for all the cases where a side fixture setup produced a maximum harmonic response revealed that in each case the COV moved towards the fixture surface.

Although a logical fixturing strategy might be to clamp the part towards the COM, the COM position changes were very small, having a maximum change from the billet location of 2.27mm. Observations of the COM corresponding to the best harmonic response may be a result of the geometry changes relating to the COM, rather than the position of the COM itself.

6.6 Expert System and Artificial Intelligence

An expert system is a program that uses artificial intelligence to simulate a human experts decision making to solve problems in a specific domain [49]. Expert systems consist of knowledge bases and inference engines [50]. The knowledge base consists of organized facts, generally represented as 'if-then' rules, about the domain. The inference engine is the 'intelligence' part of the expert system, which uses the knowledge base facts to make decisions. The purpose of an expert system for chatter control is to select fixturing strategies that achieve high-quality machined surfaces in the shortest amount of time possible. The machining time is minimized by maximizing stable cutting speeds and feed rates. The more rigidly a part is fixtured, the larger its natural frequency will be, which in turn allows machining to occur at higher cutting speeds. Thus, the strategy that maximizes rigidity while minimizing fixturing time is optimum. The two strategies considered for fixturing with the AFFS are:

1. Individual fixturing setups
2. The Inclusive fixturing setup

The individual fixturing setup strategy involves adjusting the fixture for each operation such that the machining of that operation occurs at its maximum harmonic frequency. The inclusive fixturing setup strategy uses a single fixture setup, that provides the best average frequency response for all the operations, for machining the entire part. The following steps are necessary in determining which of the two fixturing strategies to use:

1. Generation of fixturing setups
2. Selection of optimum fixture setup for each operation
3. Optimizing machining order
4. Time analysis of fixture strategies

Two types of parts must be accommodated by the fixture: parts that are similar to previous jobs and new parts. The generation of fixturing setups will create individual setups for 'new'

parts, after which the optimum fixture setup for each operation must be determined. For a part that is similar to previous jobs, the optimum setup can be selected form the expert systems knowledge base. The machining order is then optimized for the individual fixturing strategy, after which the time analysis and comparison for both the individual and inclusive strategies will occur. The time element of the individual strategy will be measured during machining, while the inclusive strategy time element will be calculated analytically. At the end of this process a fixturing strategy that minimizes chatter will be achieved.

6.6.1 Expert System Process Diagrams

The process of determining a parts optimum fixturing strategy was broken down into three parts: Fixture setup generation, fixture setup optimization and operation order optimization. Figure 6.5 shows the process algorithm for fixture setup generation. It consists of assigning fixture setups to a known part from the knowledge base, and for generating fixture setup possibilities for a new part type or new part features.

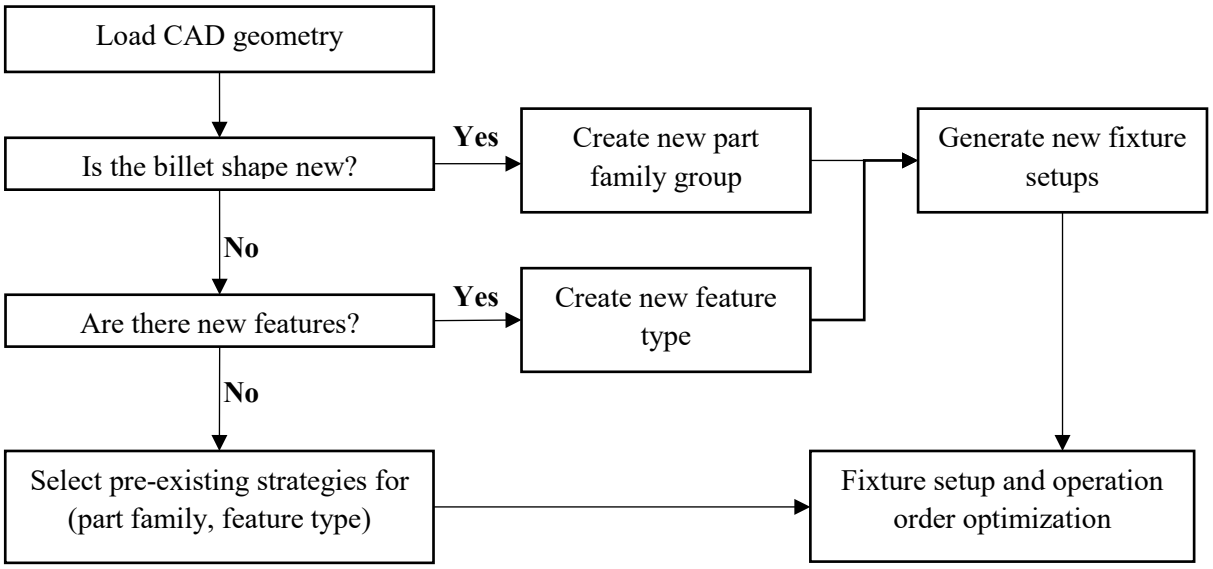

Figure 6.5 Expert system for fixture setup generation

The first step is the analysis of the CAD geometry of the part, comparing its billet shape and part features to the library. If the billet shape is new the expert system will assign the part to a new family group, and then generate the fixture setups for that part based on existing rules. If the part has new features the expert system will create new feature types for them, and generate fixture setups for those features. The process of generating new fixture setups will result in several possibilities for the new part. If the billet shape and features match existing part families and feature types, the expert system will assign a known fixture setup to each operation of that part. The ‘fixture setup and operation order optimization’ stage of the algorithm is a separate process whereby the best fixture setup for each operation of the new

part is determined though the experimental modal analysis. For a known part, this process will be used to determine the ideal machining order of the part features.

The process for verifying fixture setups for a known part, to optimize machining order, is shown in Figure 6.6. This is a result of the simulation results which revealed that changing the operation order can improve the overall harmonic response of the part by machining features that increase the natural frequency before those that decrease it. Although in most simulated cases the effect of a certain geometric feature on the natural frequency, whether frequency increases or decreases by the addition of that feature, is not affected by other geometric features, it is necessary to validate this for new feature arrangements. The process involves measuring the harmonic response of the part after each machining operation. Each measurement will be compared to those that preceded it, after which the corresponding operation will be placed in the appropriate order position. Once the first part has been completed all the individual machining operations that make up the part will be ordered from highest to lowest harmonic response. The new machining order will be implemented in the proceeding machining operations.

Figure 6.6 starts with loading the billet into the AFFS and performing a vibration test to determine the reference harmonic frequency of the part. This will require an input vibration signal from a vibration generator such as a sonic transducer. The first machining operation is performed and the vibrations are recorded, both during machining and statically. The frequency is compared to the other measured frequencies of the part. If it is smaller than the other frequencies it is placed at the end of the list. If it is larger than one of the frequencies it is placed before that machining operation. If there are machining operations remaining the cycle continues until the part is completed and removed from the AFFS.

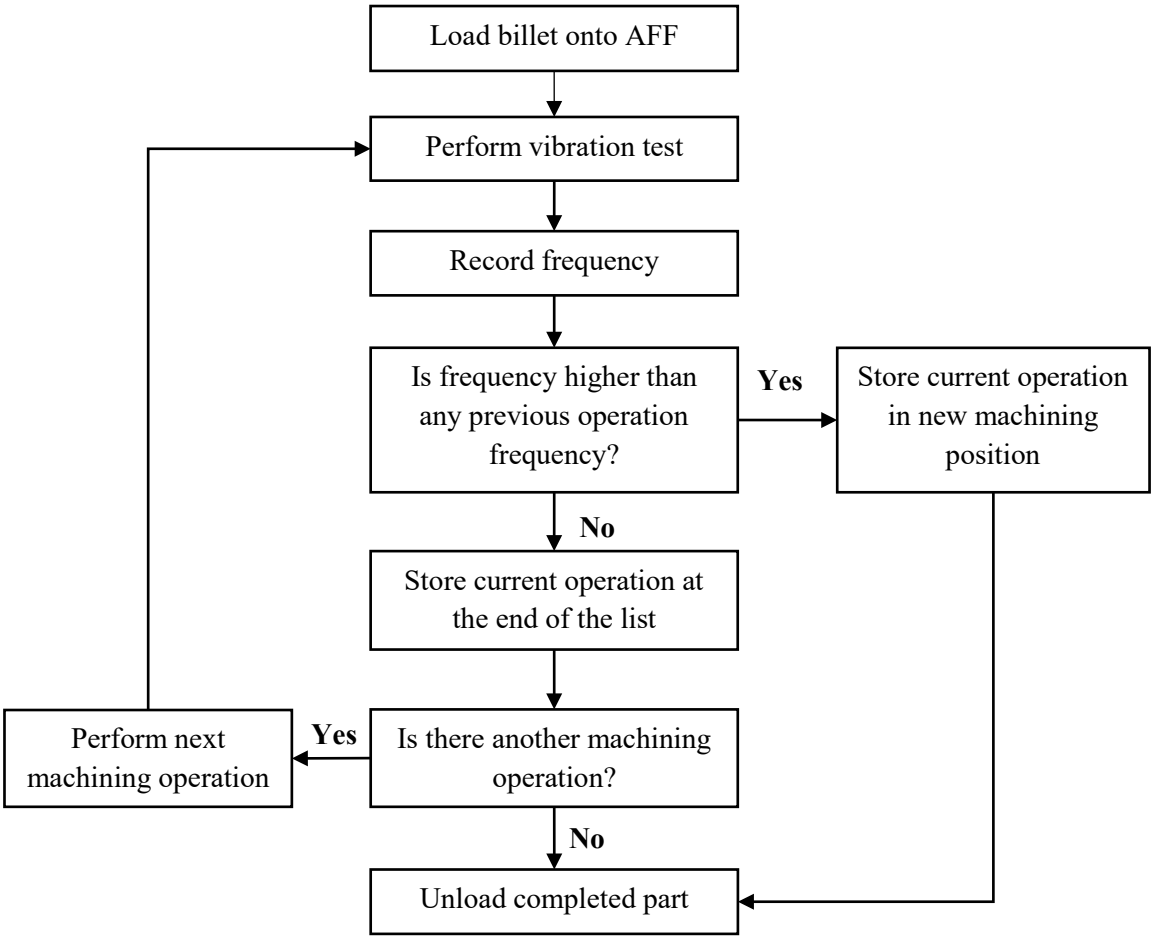

Figure 6.6 Expert system for determining operation machining order through vibration testing

Figure 6.7 shows the expert system process for 'verifying fixture setups' for a part from a new part family or one with new feature types. The process involves two unique stages: fixture setup optimization and operation order optimization.

Fixture setup optimization, grouped in the yellow box, is the process whereby the optimum fixture setup is determined from the setups generated by the expert system in Figure 6.5. The process begins by applying a fixture setup, for a single operation, to the part. A static vibration test is performed and its harmonic frequency is recorded. If there is another setup remaining the process is repeated, otherwise the optimum fixture setup is chosen based on the recorded harmonic frequencies.

Operation order optimization, grouped in the blue box, begins directly after the optimum fixture setup is determined. In this process the fixture setup is applied and its corresponding machining operation is performed. The frequency is recorded and used to place the current operation in its position, relative to the other operations, on the scale of highest to lowest frequency. After the position is established, the process returns to the beginning of the fixture setup optimization process for any remaining operations to be completed, otherwise the

completed part is unloaded from the AFFS. The final stage determines whether to continue with an individual fixture setup strategy, or to use an inclusive fixture setup strategy.

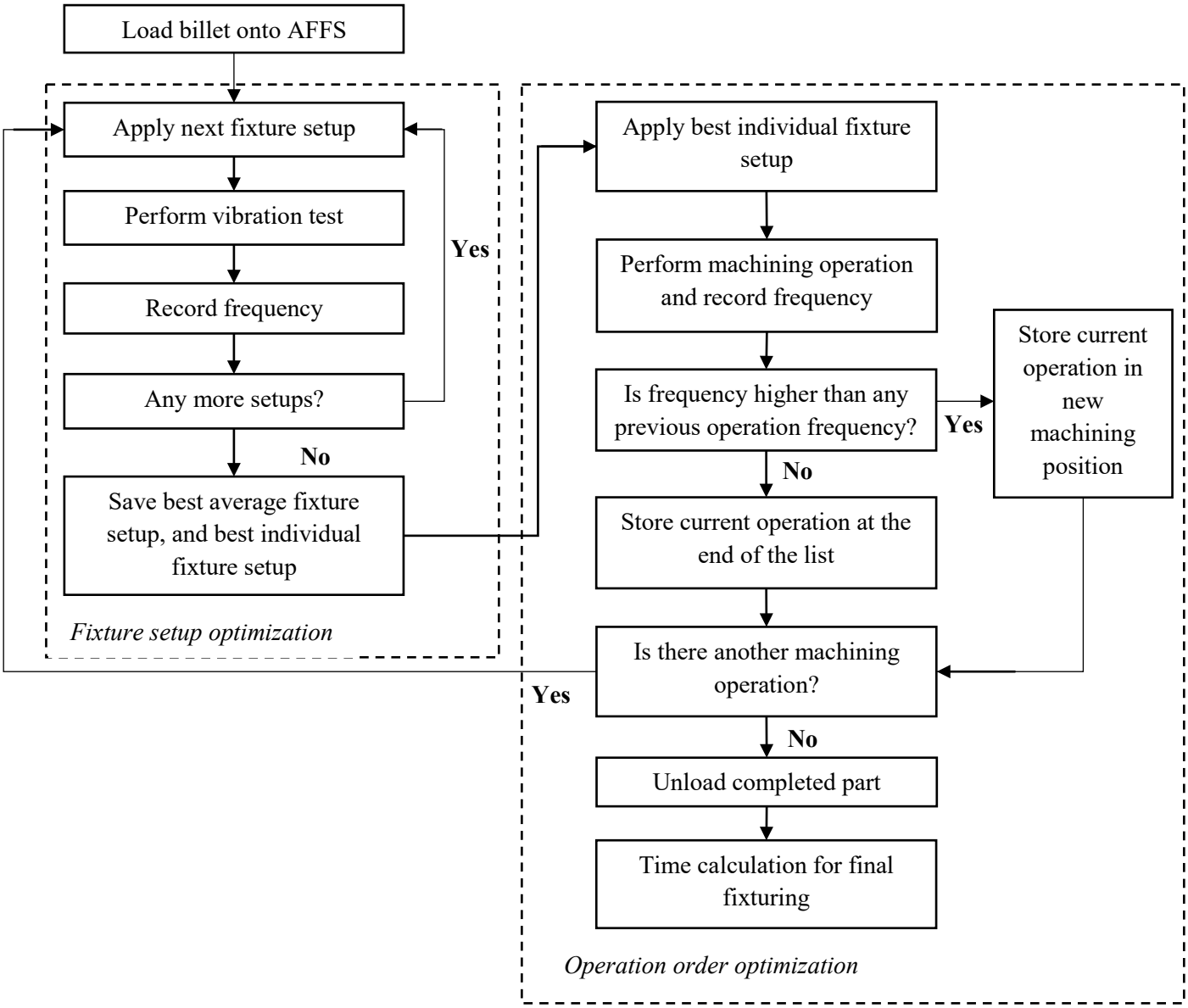

Figure 6.7 Expert system for determining fixture setup strategies for new part geometries

The two formulae for calculating the time required for each fixturing strategy to complete a part are given in equations 6.2 and 6.3. These two formulae are used in the final stage of operation order optimization (figure 6.7) to choose between the individual or inclusive fixturing strategies.

If the time taken to apply a single fixture setup can be denoted by T_{setup}, the time to machine a feature represented as $T_{Machine}$ and the number of features being X then equation 6.1 describes the total time required to machine a part using the inclusive fixturing strategy:

$$T_{Inclusivel} = T_{Setup} + \sum_{X}^{1} T_{Machine} \tag{6.2}$$

Considering the individual fixturing strategy, if the time taken to change the fixture setup from setup a to setup b can be denoted by $T_{setup\,ab}$ and the time to machine a feature can be represented as $T_{Machine}$, where X is the number of part features and the number of fixturing strategies to be implemented is Y, then the equation describing the total machining time can be written as:

$$T_{Individuall} = \sum_{Y}^{1} T_{Setup\,ab} + \sum_{X}^{1} T_{Machine} \tag{6.3}$$

Setup a and setup b represent any two adjacent fixture setups in the operation order. The number of fixture setups may be less than the number of machining operations. This would occur when operations that follow one another, in the machining order, share a common individual fixture setup.

6.7 The AFFS

The experimental analysis of the harmonics of the AFFS during fixturing exposed a high level of dampening when compared to the simulations results. The measured acceleration revealed the first 3 harmonics only, and contained a large amount of noise in the signal. These phenomena can be attributed to three factors; The load cells, plastic components, and the rigidity of the AFFS design. This section will explore the effect of each of these factors on the experimental results.

Load cells were used to keep clamping forces consistent across all the fixturing setups. The maximum allowable load of the load cells limited the clamping forces. This maximum allowable load before deterioration was 20 kg's. To limit the risk of overloading the load cells the clamping forces were 150 N or 15 kg's of load. The lower clamping forces limited the rigidity of the system and thus limited the amplitude of vibration.

Several plastic components were used in the AFFS, including the Fixture bed, Parallel gripper mounts, and the servo motor mounts. These components are part of the fixture bed assembly. The use of plastics over metals in the fixture bed resulted in its rigidity being decreased and an increase in its dampening effect.

The overall rigidity of the AFFS is affected by several design choices. The fixturing arms are cantilevered by a large bracket that allows the arms to actuate linearly up and down using a

lead screw and a steel runner. The bracket itself is mounted, at its base, to another lead screw with a steel runner that allows the bracket to move from side to side. This system produces a large amount of bending in the bracket during clamping, particularly when the fixture arm is at the upper position on the bracket. The fixture bed is attached to the AFFS base by two rotational joints. The joints have a measure of looseness to them from either wear or manufacture flaws. This looseness permeates to the fixture bed itself, causing it to rotate slightly when locked in place. Several 3d-printed components inside the fixture bed have poor tolerances in their fitment which also cause vibrational interference.

6.8 Industry 4.0 and the AFFS

Industry 4.0 is the emergence of the fourth industrial revolution, driven by internet of things (IoT) and is the vision of future manufacturing [51]. Manufacturing in industry 4.0 will focus on flexibility in customization and production volume [52], with the ultimate goal of creating individualized products in a batch size of one, while maintaining the efficiency of mass production [53]. The AFFS technology eliminates the costs involved in manufacturing custom fixtures, as well as optimizing the fixturing of workpieces to minimize chatter in machining. Thus, the AFFS is a technology essential to achieving the vision of customization in industry 4.0.

6.9 Chapter Summary

Chapter 6 contained a summary of the research findings, discussing the possible causes for the trends in the simulation and experimental results. The breadth-centre fixturing strategy had the best overall performance for both parts, due to its geometric advantage on minimizing deflection. Although there were shortfalls in the experimental testing due to the rigidity and plastic use in the gripper bed, the experimental results supported the simulations. An expert system methodology for fixture setup optimization was proposed, using vibration testing procedures to determine the optimum fixturing setup for the AFFS.

Chapter 7: Conclusion

7.1 Aim, Objectives and Research Findings

The aim of the research was to develop a methodology for fixture setup optimization for the AFFS as a means of chatter reduction. The literature review revealed that workpiece chatter occurs when the natural frequency of the billet matches that of the cutting tool. Thus, maximizing the natural frequency of the billet can allow higher cutting speeds with less risk of chatter occurring. The modal simulations and experimentation revealed that fixturing position has a significant effect on the natural frequency of a part. The order of machining of part features was also shown to play a significant role optimizing the natural frequency. The combination of selecting the appropriate machining order in conjunction with optimum fixturing strategy maximizes the natural frequency of the workpiece and thus minimizes the risk of chatter.

7.2 Results

The simulations for part 1 and part 2 showed a strong correlation between fixturing position and harmonic response. For both parts, the breadth-centre fixture resulted in the highest frequencies for the majority of part features and modes. This was attributed to the overall part shape having a greater effect on natural frequency than the individual part features. Part features either increased or decreased the natural frequency. Rearranging part features with those that increase natural frequency first was shown to optimize the harmonic response. Each part features effect to either decrease or increase natural frequency was independent of machining order.

The experimental testing results confirmed the simulation findings that breadth-centre fixturing produces the highest natural frequencies for the majority of modes and part features. The frequency signals measured were far smaller than the simulated frequencies, and contained a high level of noise. This was attributed to several weaknesses in the AFFS due to its proof-of-concept nature. This design weakness involved the use of cantilevered fixture arms without support structures to reduce deflection, and the reliance on several geared rotational mechanisms with poor rotational rigidity. The manufacturing weaknesses included the use of 3d-printed plastic components, the use of a plastic fixture bed structure, and a poorly assembled parallel pin locator mechanism.

7.3 Summary and Contribution

This research has shown that for two theoretical parts, the simulated natural frequency was affected both by fixture setup and geometry. The fixture setup allowing the highest overall natural frequencies was independent of geometry. The arrangement of part features was shown

to improve the overall harmonic response of the part. The experimental tests validated the simulation results, but were limited by the dampening and interference vibrations of the system. These effects were attributed to the use of plastic components in the fixture bed, flexion in the fixture arms and play in the rotational mechanisms. The results proved the existence of a relationship between fixturing and the harmonic response of a part, and showed how fixturing can be used to optimize harmonic response and thus minimize chatter.

This research contribution is that of an expert planning system for fixture setup generation and optimization, based on the static vibrational response of the fixture-part system. The expert system is able to determine the ideal fixture setup as well as influence machining operation order for chatter free machining conditions.

7.4 Further Development

The redesign of the AFFS incorporating stiffer joint mechanisms and fixture arm structures, and the replacement of all plastic components with a metal alternative, is imperative in improving the natural frequency of the system. This would better enable the simulation results for material removal to be validated through experimentation. The relationship between machining and natural frequency for different fixture setups should be investigated, focusing on the input frequency and cutting forces in relation to fixture position. The redesigned AFFS should be put to use in a CNC milling machine to capture vibration information for a large variety of parts and machining operations. This vibration information can be used to build a knowledge base for the development of the fixture-setup expert system for the AFFS.

References

[1] A. Merle, J. L. Chandon, E. Roux, and F. Alizon, "Perceived value of the mass-customized product and mass customization experience for individual consumers," *Production and Operations Management,* vol. 19, no. 5, pp. 503-514, 2010.

[2] Z. Bi and W. Zhang, "Flexible fixture design and automation: review, issues and future directions," *International Journal of Production Research,* vol. 39, no. 13, pp. 2867-2894, 2001.

[3] Y. Koren *et al.*, "Reconfigurable manufacturing systems," *CIRP annals,* vol. 48, no. 2, pp. 527-540, 1999.

[4] H. Wang, Y. K. Rong, H. Li, and P. Shaun, "Computer aided fixture design: Recent research and trends," *Computer-Aided Design,* vol. 42, no. 12, pp. 1085-1094, 2010.

[5] M. M. da Silva, G. S. Venter, P. S. Varoto, and R. T. Coelho, "Experimental results on chatter reduction in turning through embedded piezoelectric material and passive shunt circuits," *Mechatronics,* vol. 29, pp. 78-85, 2015.

[6] R. Harper. (2004, 22 April 2018). *Chatter Myths: Pieces of the Puzzle in Maximized Machining* [Article]. Available: https://www.moldmakingtechnology.com/articles/chatter-myths-pieces-of-the-puzzle-in-maximized-machining

[7] D. A. Stephenson and J. S. Agapiou, *Metal Cutting Theory and Practice*. Boca Raton: CRC Press, 2006, p. 848.

[8] D. A. Stephenson and J. S. Agapiou, *Metal cutting theory and practice*. CRC press, 2016.

[9] B. Warfield. (2011, 3 September). *Chatter in Machining: Milling & Lathe Vibration*. Available: https://www.cnccookbook.com/chatter-in-machining-milling-lathe-vibration/

[10] S. Smith, "The science of milling sounds," Accessed on: 25 September 2018Available: https://www.ctemag.com/news/articles/science-milling-sounds

[11] M. Wiercigroch and A. M. Krivtsov, "Frictional chatter in orthogonal metal cutting," *Philosophical Transactions of the Royal Society of London. Series A: Mathematical, Physical and Engineering Sciences,* vol. 359, no. 1781, pp. 713-738, 2001.

[12] M. S. Hajmohammadi and M. R. Movahhedy, "Investigation of Thermal Effects on Machining Chatter Using FEM Simulation of Chip Formation," *Procedia CIRP,* vol. 1, pp. 50-55, 2012/01/01/ 2012.

[13] B. Stone, *Chatter and Machine Tools*. Switzerland: Springer International Publishing, 2014, p. 260.

[14] L. Cen and S. N. Melkote, "CCT-based mode coupling chatter avoidance in robotic milling," *Journal of Manufacturing Processes,* vol. 29, pp. 50-61, 2017/10/01/ 2017.

[15] k. Klaver. (2012, 25 September). *How to Eliminate Chatter*. Available: https://www.moldmakingtechnology.com/articles/how-to-eliminate-chatter

[16] kennametal. *Reducing Chatter and Vibration in End Milling*. Available: https://www.kennametal.com/en/resources/tech-tips/milling/tech-tip-32.html

[17] Y. H. Kang and C. M. Zheng, "Mathematical modelling of chip thickness in micro-end- milling: A Fourier modelling," *Applied Mathematical Modelling,* vol. 37, no. 6, pp. 4208-4223, 2013/03/15/ 2013.

[18] I. Biró, T. Szalay, and N. Geier, "Effect of cutting parameters on section borders of the empirical specific cutting force model for cutting with micro-sized uncut chip thickness," *Procedia CIRP,* vol. 77, pp. 279-282, 2018/01/01/ 2018.

[19] B. Wu, X. Yan, M. Luo, and G. Gao, "Cutting force prediction for circular end milling process," *Chinese Journal of Aeronautics,* vol. 26, no. 4, pp. 1057-1063, 2013/08/01/ 2013.

[20] Y. Altintaş and P. Lee, "A General Mechanics and Dynamics Model for Helical End Mills," *CIRP Annals,* vol. 45, no. 1, pp. 59-64, 1996/01/01/ 1996.
[21] J. Tlusty and M. Polacek, *The stability of the machine tool against self-excited vibration in machining*. 1963, pp. 454-465.
[22] N. H. Hanna and S. A. Tobias, *A Theory of Nonlinear Regenerative Chatter*. 1974, p. 247.
[23] H. M. Shi and S. A. Tobias, "Theory of finite amplitude machine tool instability," *International Journal of Machine Tool Design and Research,* vol. 24, no. 1, pp. 45-69, 1984/01/01/ 1984.
[24] J. Tlusty and F. Ismail, *Basic Non-Linearity in Machining Chatter*. 1981, pp. 299-304.
[25] I. Minis, R. Yanushevsky, A. Tembo, and R. Hocken, *Analysis of Linear and Nonlinear Chatter in Milling*. 1990, pp. 459-462.
[26] Y. Altintas and E. Budak, *Analytical Prediction of Stability Lobes in Milling*. 1995, pp. 357-362.
[27] E. Budak and Y. Altintas, *Analytical Prediction of Chatter Stability in Milling—Part I: General Formulation*. 1998.
[28] Y. Altintas, S. Engin, and E. Budak, *Analytical Stability Prediction and Design of Variable Pitch Cutters*. 1999.
[29] M. Davies, J. Pratt, B. Dutterer, and T. Burns, *Stability Prediction for Low Radial Immersion Milling*. 2002, p. 217.
[30] E. Budak, *An Analytical Design Method for Milling Cutters With Nonconstant Pitch to Increase Stability, Part I: Theory*. 2003.
[31] A. Tekeli and E. Budak, *Maximization of chatter-free material removal rate in end milling using analytical methods*. 2005, pp. 147-167.
[32] B. Muhammad, M. Wan, J. Feng, and W. Zhang, *Dynamic damping of machining vibration: a review*. 2017, pp. 2935-2952.
[33] J. Yue, *Creating a Stability Lobe Diagram*. 2006, pp. 301-50.
[34] M. Wan, J. Feng, Y.-C. Ma, and W.-H. Zhang, "Identification of milling process damping using operational modal analysis," *International Journal of Machine Tools and Manufacture,* vol. 122, pp. 120-131, 2017/11/01/ 2017.
[35] V. Ostasevicius, R. Gaidys, R. Dauksevicius, and S. Mikuckyte, "Study of vibration milling for improving surface finish of difficult-to-cut materials," *Strojniški vestnik-Journal of Mechanical Engineering,* vol. 59, no. 6, pp. 351-357, 2013.
[36] M. U. Gaikwad and P. Kulkarni, "Static and Dynamic Analysis of End Mill Tool for Chatter Vibration Reduction."
[37] E. Uhlmann and K. Schauer, "Dynamic load and strain analysis for the optimization of micro end mills," *CIRP Annals-Manufacturing Technology,* vol. 54, no. 1, pp. 75-78, 2005.
[38] T. Özel and T. Altan, "Process simulation using finite element method—prediction of cutting forces, tool stresses and temperatures in high-speed flat end milling," *International Journal of Machine Tools and Manufacture,* vol. 40, no. 5, pp. 713-738, 2000.
[39] A. Özer, S. Eren Semercigil, R. Prasanth Kumar, and P. Yowat, "Delaying tool chatter in turning with a two-link robotic arm," *Journal of Sound and Vibration,* vol. 332, no. 6, pp. 1405-1417, 2013/03/18/ 2013.
[40] Y. Guo, H. Dong, G. Wang, and Y. Ke, "Vibration analysis and suppression in robotic boring process," *International Journal of Machine Tools and Manufacture,* vol. 101, pp. 102-110, 2016/02/01/ 2016.
[41] J. Pandremenos, C. Doukas, P. Stavropoulos, and G. Chryssolouris, "Machining with robots: a critical review," *Proceedings of DET2011,* pp. 1-9, 2011.

[42] Y. Lin, H. Zhao, and H. Ding, "Posture optimization methodology of 6R industrial robots for machining using performance evaluation indexes," *Robotics and Computer-Integrated Manufacturing,* vol. 48, pp. 59-72, 2017/12/01/ 2017.

[43] N. R. Slavkovic, D. S. Milutinovic, and M. M. Glavonjic, "A method for off-line compensation of cutting force-induced errors in robotic machining by tool path modification," *International Journal of Advanced Manufacturing Technology,* Article vol. 70, no. 9-12, pp. 2083-2096, 2014.

[44] U. Schneider, M. Ansaloni, M. Drust, F. Leali, and A. Verl, "Experimental investigation of sources of error in Robot Machining," in *Communications in Computer and Information Science* vol. 371, ed, 2013, pp. 14-26.

[45] G.-C. Vosniakos and E. Matsas, "Improving feasibility of robotic milling through robot placement optimisation," *Robotics and Computer-Integrated Manufacturing,* vol. 26, no. 5, pp. 517-525, 2010/10/01/ 2010.

[46] Y. Guo, H. Dong, and Y. Ke, "Stiffness-oriented posture optimization in robotic machining applications," *Robotics and Computer-Integrated Manufacturing,* vol. 35, pp. 69-76, 2015/10/01/ 2015.

[47] G. Xiong, Y. Ding, and L. Zhu, "Stiffness-based pose optimization of an industrial robot for five-axis milling," *Robotics and Computer-Integrated Manufacturing,* vol. 55, pp. 19-28, 2019/02/01/ 2019.

[48] A. Kumar, H. Jaiswal, R. Jain, and P. P. Patil, "Free Vibration and Material Mechanical Properties Influence Based Frequency and Mode Shape Analysis of Transmission Gearbox Casing," *Procedia Engineering,* vol. 97, pp. 1097-1106, 2014/01/01/ 2014.

[49] Y. Kumar, Y. J. I. J. o. C. Jain, and B. Research, "Research aspects of expert system," 2012.

[50] V. Zwass. (2016, October 07). *Expert system*. Available: https://www.britannica.com/technology/expert-system

[51] F. Shrouf, J. Ordieres, and G. Miragliotta, "Smart factories in Industry 4.0: A review of the concept and of energy management approached in production based on the Internet of Things paradigm," in *2014 IEEE International Conference on Industrial Engineering and Engineering Management*, 2014, pp. 697-701.

[52] M. M. Mabkhot, A. M. Al-Ahmari, B. Salah, and H. Alkhalefah, "Requirements of the Smart Factory System: A Survey and Perspective," vol. 6, no. 2, p. 23, 2018.

[53] H. Lasi, P. Fettke, H.-G. Kemper, T. Feld, M. J. B. Hoffmann, and I. S. Engineering, "Industry 4.0," journal article vol. 6, no. 4, pp. 239-242, August 01 2014.

Appendix A: Load Cell Code

```
#include "HX711.h" //using the HX11 library to read the Load Cell values

HX711 cell1(3, 2); //

HX711 cell2(5, 4); //

void setup() {

  Serial.begin(9600); //setting baud rate to 9600

}

long val1 = 0;

long val2 = 0;

float count = 0;

void loop() {


  count = count + 1;

  val1= 0.5 * val1    +   0.5 * cell1.read(); //take recent average (cell1.read is the HX711 load cell reading)

  val1 = cell1.read(); //most recent reading

  Serial.println( ( val1 - 8385700 ) / 102.5 ); //Scaling the reading to Kg's


Val2 = 0.5 * val2    +   0.5 * cell2.read(); //take recent average (cell2.read is the HX711 load cell reading)

  Val2= cell2.read(); //most recent reading

  Serial.println( ( val2 - 8385700 ) / 102.5 ); //Scaling the reading to Kg's


}
```

Appendix B: LabVIEW Code

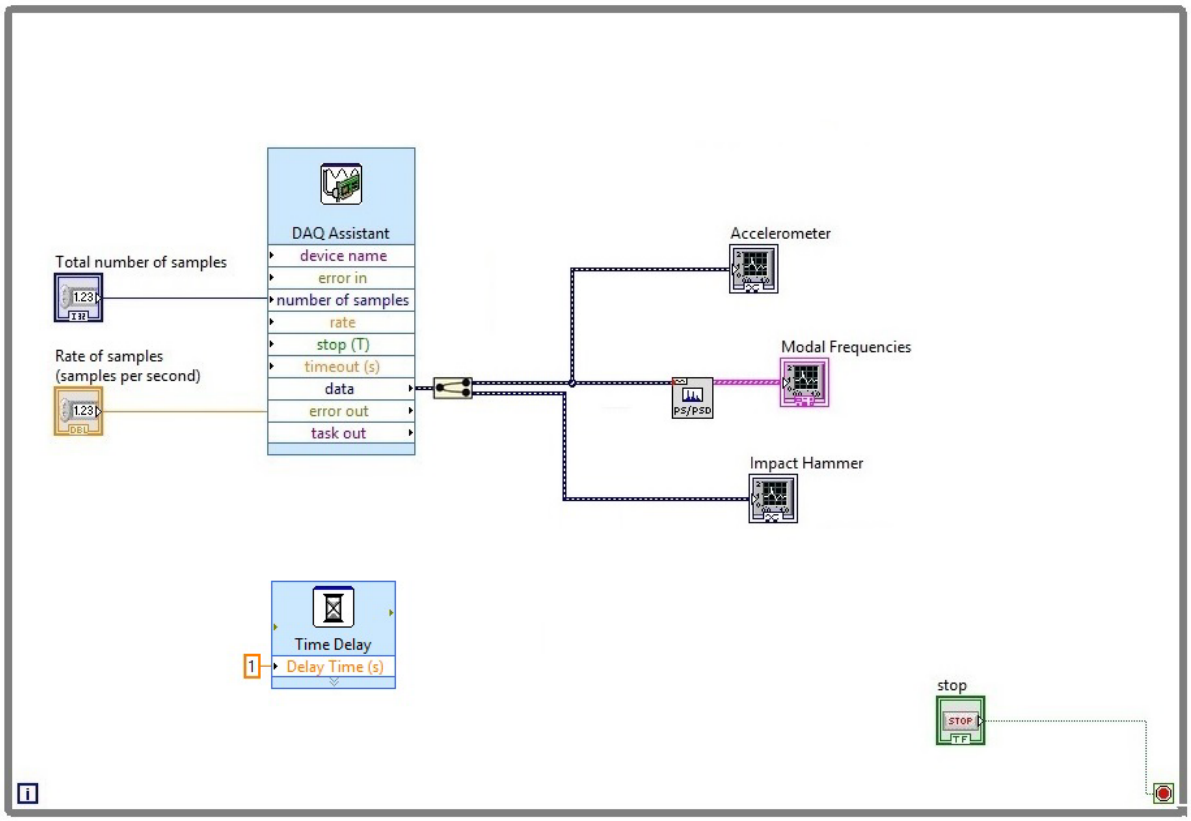

Appendix C: Machine Drawings